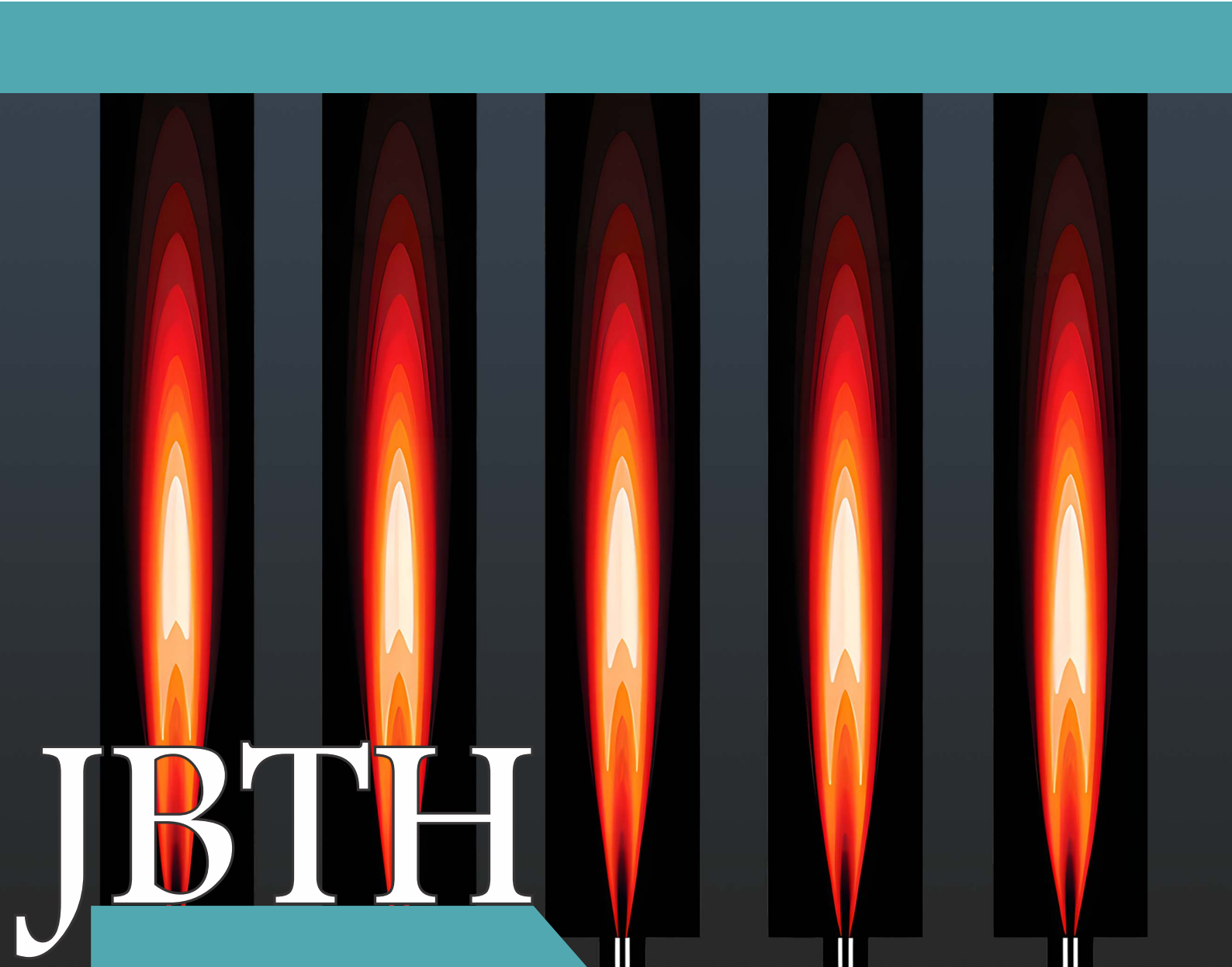
ISSN: 2764~5886 e~ISSN: 2764~622X



Journal of Bioengineering, Technologies and Health

An Official Publication of SENAI CIMATEC



Volume 8 • Number 4 • August 2025



JOURNAL OF BIOENGINEERING TECHNOLOGIES AND HEALTH

An Official Publication of SENAI CIMATEC

EDITOR-IN-CHIEF Leone Peter Andrade

PUBLISHED BY SENAI CIMATEC





August 2025 Printed in Brazil

JOURNAL OF BIOENGINEERING TECHNOLOGIES AND HEALTH

An Official Publication of SENAI CIMATEC

EDITOR-IN-CHIEF

Leone Peter Andrade

DEPUTY EDITOR

Roberto Badaró

ASSISTANT DEPUTY EDITORS

Alex Álisson Bandeira Santos (BR) Josiane Dantas Viana Barbosa (BR)

Lilian Lefol Nani Guarieiro (BR) Valéria Loureiro (BR)

ASSOCIATE EDITORS

Alan Grodzinsky (US)

Bruna Aparecida Souza Machado (BR)

Carlos Coimbra (US) Eduardo Mario Dias (BR) Frank Kirchner (DE)

Jorge Almeida Guimarães (BR)

Milena Soares (BR) Preston Mason (US) Sanjay Singh (US) Steven Reed (US)

Valter Estevão Beal (BR)

STATISTICAL ASSOCIATE EDITOR

Valter de Senna (BR)

EDITORIAL BOARD

Carlos Augusto Grabois Gadelha (BR)

Durvanei Augusto Maria (BR)

Eliane de Oliveira Silva (BR)

Erick Giovani Sperandio Nascimento (BR)

Fernando Pellegrini Pessoa (BR) Francisco Uchoa Passos (BR)

George Tynan (US) George Tynan (US)

Gilson Soares Feitosa (BR) Gisele Olímpio da Rocha (BR)

Hercules Pereira (BR)

Herman Augusto Lepikson (BR)

Hermano Krebs (US)

Idelfonso Bessa dos Reis Nogueira (NO)

Immanuel Lerner (IR) Ingrid Winkler (BR) James Chong (KR)

Jeancarlo Pereira dos Anjos (BR)

José Elias Matieli (BR) Joyce Batista Azevedo (BR)

Larissa da Silva Paes Cardoso (BR)

Lusiada Portugal (PT)

Luzia Aparecida Tofaneli (BR)

Maria Lídia Rebello Pinho Dias (BR)

Mario de Seixas Rocha (BR)

Maximilian Serguei Mesquita (BR)

Regina de Jesus Santos (BR) Renelson Ribeiro Sampaio (BR)

Roberto de Pinho (BR)

Rodrigo Santiago Coelho (BR)

Sanjay Mehta (US)

Vidal Augusto Zapparoli Castro Melo (BR)

Vilson Rosa de Almeida (BR)

PRODUCTION STAFF

Luciana Knop, Managing Editor

Valdir Barbosa, Submissions Manager

JOURNAL OF BIOENGINEERING TECHNOLOGIES AND HEALTH

SUMMARY

August 2025

Volume 8 • Number 4

| Original Articles | Roadmap for the Hydrogen Supply Network in |
|--|--|
| 6 | Brazil |
| Evaluation of the Potential of <i>Prosopis juliflora</i> Biomass for 2G Bioethanol Production: Chemical | Lucca R. S. A. Bastos, Leonardo O. S. Santana, Gerhard Ett |
| Characterization and Enzymatic Hydrolysis 317 Yuri Uriel Cerqueira Gil Braz Moreira, Geise Camila de Araujo Ribeiro, Lilian Lefol Nani Guarieiro, Carine Tondo Alves | Reproduction and Adaptation of Literature-Derived Modeling: Numerical Simulation of Methane/ Hydrogen Non-Premixed Combustion 352 Paulo Roberto Santana dos Reis, Felix Emile Martin, Turan |
| Evaluation of <i>Prosopis juliflora</i> for Bioethanol Production: Thermogravimetric Analysis and | Dias Oliveira, Luzia Aparecida Tofaneli, Alex Álisson |
| Structural Composition | Development of Coating to Mitigate Chromium Contamination from Bipolar Plates in a Metal-Supported Solide Oxide Fuel (MS-SOFC) 359 Ricardo Lima Travassos, Marcos Makoto Toyama, Fernando |
| Polyphenols and Antioxidant in Southwest Mexico <i>Agave</i> Leaves | Pellegrini Pessoa, Gerhard Ett |
| Misael Bermúdez Bazán, Mirna Estarrón Espinosa, Judith Esmeralda Urías Silvas, Javier Plácido Arrizon Gaviño, Anne Christine Gschaedler Mathis, Gustavo Adolfo Castillo Herrera | Computational Model to Optimize the Prediction of Fouling in the Deposition Process During Oil Pre-Processing in Heat Exchanger Networks Based on Machine Learning. |
| Study of Fuel Quality in the State of Maranhão Through Principal Component Analysis 333 Morgana Cristhya Silva dos Santos, Luciana Pereira Barbosa, | Machine Learning |
| Allan Kardec Duailibe Barros Filho | Thermal Analysis Algorithm for Oil and Gas Wells |
| The Importance of Conducting Tests to Ensure the Proper Functioning of Chemical Injection and Lift | João Victor Carvalho de Mattos, Márcio de Melo Araújo, José Fábio Abreu de Andrade |
| Gas Valves | Evaluation of the Degradation Process of Polyamide 12 Manufactured via Multi Jet Fusion: An FTIR |
| Hydrological Rainfall-Runoff Modeling Using the WRF-Hydro Model | Analysis |
| Antônio José da Silva Neto, Davidson Martins Moreira | Pinalina Lank Dataction Using Infrared Company |
| Gamification in Electrical Energy Monitoring347 Patrick Antonio Morelo, Jorge Anderson de Jesus Santos, Pericles Vinicius Cerqueira Marques, Rebeca Oliveira dos Santos, Paulo Henrique de Jesus Santana, Marcus Vinicius | Pipeline Leak Detection Using Infrared Cameras: A Convolutional Neural Network Approach 379 João Vitor S. Mendes, João Pedro Almeida, Rodrigo Dias Paolillo, Alexandre Adonai Silva, Rodrigo F. Bastos, Herman A. Lepikson |
| Mendes | |

Systematic Reviews / Literature Reviews

3D Printing of PCL/HA Composite Scaffolds for Bone Tissue Regeneration: A Brief Review .. 385 Melissa de Souza Gomes dos Santos, Henrique Cesar Santos de Jesus, Joanne Graziela Andrade Mendes, Imarally Vitor de Souza Ribeiro Nascimento, Josiane Dantas Viana

Instructions for Authors

Statement of Editorial Policy

Checklist for Submitted Manuscripts

The Journal of Bioengineering, Technologies and Health (JBTH) is an official publication of the SENAI CIMATEC University (Serviço Nacional de Aprendizagem Industrial - Universidade Centro Integrado de Manufatura e Tecnologia). It is published bimonthly (February - April - June - August - October - December) in English by SENAI CIMATEC University – Avenida Orlando Gomes, 1845, Piatã, Zip Code: 41650-010, Salvador-Bahia-Brazil; phone: (55 71) 3879-5501. The editorial offices are at SENAI CIMATEC University.

Editorial Office

Correspondence concerning subscriptions, advertisements, claims for missing issues, changes of address, and communications to the editors should be addressed to the Deputy Editor, Dr. Roberto Badaró, SENAI CIMATEC University (Journal of Bioengineering, Technologies and Health – JBTH) – Avenida Orlando Gomes, 1845, Piatã, Zip code: 41650-010, Salvador-Bahia-Brazil; phone: (55 71) 3879-5501; or sent by e-mail: jbth@fieb.org.br/jbth.cimatec@gmail.com.

Permissions

The permissions should be asked to the Ediot in Chief of the Journal of Bioengineering, Technologies and Health and SENAI CIMATEC University. All rights reserved. Except as authorized in the accompanying statement, no part of the JBTH may be reproduced in any form or by any electronic or mechanic means, including information storage and retrieval systems, without the publisher's written

COVER: Figure 3. Temperature contours. Reproduction and Adaptation of Literature-Derived Modeling: Numerical Simulation of Methane/Hydrogen Non-Premixed Combustion by Paulo Roberto Santana dos Reis et al. J Bioeng. Tech. Health 2025;8(4):355.

permission. Authorization to photocopy items for internal or personal use, or the internal or personal use by specific clients is granted by the Journal of Bioengineering, Technologies and Health and SENAI CIMATEC University for libraries and other users. This authorization does not extend to other kinds of copying such as copying for general distribution, for advertising or promotional purposes, for creating new collective works, or for resale.

Postmaster

Send address changes to JBTH, Avenida Orlando Gomes, 1845, Piatã, Zip Code: 41650-010, Salvador-Bahia-Brazil.

Information by JBTH-SENAI CIMATEC University

Address: Avenida Orlando Gomes, 1845, Piatã, Zip

Code: 41650-010, Salvador-Bahia-Brazil

Home-page: www.jbth.com.br

E-mail: jbth@fieb.org.br / jbth.cimatec@gmail.com Phone: (55 71) 3879-5501 / 3879-5500 / 3879-9500

DOI:10.34178



ISSN: 2764-5886 / e-ISSN 2764-622X

Copyright

© 2025 by Journal of Bioengineering, Technologies and Health SENAI CIMATEC All rights reserved.

Evaluation of the Potential of *Prosopis juliflora* **Biomass for 2G Bioethanol Production: Chemical Characterization and Enzymatic Hydrolysis**

Yuri Uriel Cerqueira Gil Braz Moreira^{1*}, Geise Camila de Araujo Ribeiro², Lilian Lefol Nani Guarieiro², Carine Tondo Alves³

¹Master's student in Industrial Management and Technology; PRH – ANP Master's Scholarship Holder; ²SENAI CIMATEC University; Salvador, Bahia; ³Federal University of Recôncavo da Bahia; Feira de Santana, Bahia, Brazil

This study aims to characterize different parts of the plant *Prosopis juliflora* (Algaroba) and to evaluate the potential of its biomass for second-generation (2G) bioethanol production. Different parts of the plant (*Prosopis juliflora in natura*) were evaluated for cellulose, hemicellulose, lignin, moisture, and ash content, in addition to the yield of reducing sugars in enzymatic hydrolysis with cellulase from *Trichoderma reesei*. The results indicated that the stem bark, rich in cellulose (38.71%) and hemicellulose (21.68%), showed the highest saccharification yield (2.74 mg/mL in 24 h). In contrast, fractions with a high lignin content, such as the pod with seed (45.91%), require pretreatments to make enzymatic conversion feasible. The strategic selection of the biomass fraction and the use of appropriate methods are crucial for optimizing the recovery of fermentable sugars, enabling the use of Algaroba in biofuel production.

Keywords: Cellulase. Glucose. Physicochemical Characterization. Saccharification.

Ethanol has emerged as a viable and complementary energy option to fossil fuels in the transportation sector, stimulating research focused on improving biofuels derived from renewable sources [1]. In this context, lignocellulosic biomass stands out as a promising feedstock due to its wide availability, low cost, and the absence of direct competition with food production [2-4].

Lignocellulosic biomass is composed of cellulose (40–50%), hemicellulose (20–30%), and lignin (10–25%), in addition to smaller amounts of ash, pectin, proteins, non-structural carbohydrates, and extractives. Its chemical composition varies according to the source and cultivation conditions, making initial characterization essential to define efficient strategies for producing biofuels and bioproducts. Hydrolysis of the biomass, following pretreatment, is the second most important step in bioethanol production, as it determines the efficiency of generating the desired product.

Received on 10 May 2025; revised 15 July 2025. Address for correspondence: Yuri Uriel Cerqueira Gil Braz Moreira. Av. Orlando Gomes, 1845, Piatã, Salvador, Bahia, Brazil. Zipcode: 41650-010. E-mail: yuri-braz@hotmail.com. Original extended abstract presented at SAPCT 2025.

J Bioeng. Tech. Health 2025;8(4):317-320 © 2025 by SENAI CIMATEC University. All rights reserved.

Hydrolysis converts cellulose and hemicellulose polymers into fermentable sugars through either acid or enzymatic processes [1,5,6].

The plant species *Prosopis juliflora*, commonly known as Algaroba, has garnered attention due to its characteristics: it is a small to medium-sized tree with high resistance to adverse environmental conditions, such as arid, saline, and high-pH soils, and is considered invasive in semi-arid regions [7-10].

The use of *P. juliflora* as a feedstock for bioethanol production is a promising strategy to contain its spread in ecosystems where it is invasive, combining both environmental and economic benefits. In this context, this study aims to characterize the different parts of *P. juliflora in natura* and to evaluate the properties of its hydrolysate, thereby understanding its potential for biotechnological applications and its relevance as a raw material in industrial processes.

Materials and Methods

To chemically characterize Algaroba biomass *in natura* (stem bark, woody stem, pod bark, pod with seed, pulp without seed, and seed), this procedure evaluated moisture and ash content, as well as cellulose, hemicellulose, and lignin fractions.

The determination of total solids and moisture followed the protocol described by Sluiter and colleagues [11], the sample was weighed before and after drying at 105°C. Ash content was quantified by calcination in a muffle furnace, following the method by Sluiter and colleagues [12]. Lignin quantification, adapted from Silwadi and colleagues [13] and Sluiter and colleagues [14], involved acid hydrolysis to separate the insoluble fraction (AIL) and allowed quantification of the soluble fraction (ASL) by spectrophotometry. Cellulose determination was performed as described by Asgher and colleagues [15], Bauer and Ibánez [16], Updegraff [17], and adapted from Ribeiro and Assis [18], using hydrolysis with nitric acid and acetic acid, followed by colorimetric analysis with the anthrone reagent. Hemicellulose content was estimated according to Kapoor and colleagues [19], by alkaline extraction and final precipitation induced by sulfuric acid and ethanol.

For enzymatic hydrolysis, commercial cellulase from Trichoderma reesei ATCC 26921 (Sigma-Aldrich©, Merck KGaA, Darmstadt, Germany) was used. Biomass was suspended in citrate-phosphate buffer (100 mmol/L, pH 5) at a concentration of 5% (w/v) [20-24]. The mixture was maintained at 50°C and 150 rpm for 2 hours, followed by the addition of the enzyme (10 U/g dry biomass). Two controls were used: one without substrate (enzyme only) and one without enzyme (substrate only). After 24 hours, reducing sugars were quantified using the DNS reagent, as described by Miller [25], with absorbance measured at 540 nm using a UV/Vis spectrophotometer.

Results and Discussion

The data in Table 1 show marked contrasts in the composition of different parts of *P. juliflora*, which can directly influence biotechnological utilization routes. The stem bark presented high levels of cellulose (38.71%) and hemicellulose (21.68%), totaling 60.39% holocellulose. This profile suggests potential for processes based on fermentable sugars due to the high proportion of easily hydrolyzable components.

The woody stem, although similar in cellulose content (38.24%), had lower hemicellulose content (16.46%), resulting in a slightly lower holocellulose content (54.71%). Still, both fractions show promise for biochemical conversion.

The pod bark showed a low cellulose content (6.85%) but a higher hemicellulose content (21.06%). Its high ash (5.66%) and moisture (20.87%) suggest the need for additional preprocessing steps to avoid yield losses. The pod with seed had high cellulose (39.33%) and the highest lignin (45.91%), requiring more intensive pretreatments to reduce lignin recalcitrance and enable efficient sugar release. However, this fraction also had the highest holocellulose (61.68%), indicating significant potential once lignin barriers are overcome.

The pulp without seeds, with moderate cellulose (23.56%), hemicellulose (21.13%), and lignin (20.52%), presented a balanced composition, indicating moderate potential for enzymatic hydrolysis. In contrast, the seed contained very low levels of fibrous constituents (7.12% cellulose and 10.57% hemicellulose), making it less suitable for sugar-focused bioconversion.

Comparing results with the literature, partial agreement was observed. [22,24,26,27] analyzed woody fractions of *P. juliflora* and reported cellulose contents between 45–49.4%, hemicellulose 18–25%, and lignin 18-29.1%, values close to those in this study (38.24%, 16.46%, and 22.65%, respectively). For stem bark, holocellulose (60.39%) and lignin (28.06%) aligned with Gupta, Sharma and Kuhad [21]. For the pod (or pod with seed), Gayathri and Uppuluri [28] reported 26% cellulose, 30% hemicellulose, and 4% lignin, showing partial convergence but divergence in lignin content. These differences, especially in seed and pulp fractions, reinforce the need for specific evaluations, considering lignin's barrier role in hydrolysis and holocellulose's importance for fermentation.

Table 2 presents the reducing sugar yields from the enzymatic saccharification of *P. juliflora in natura* over 24 hours and 48 hours. The stem bark showed the best performance, reaching 2.74 mg/mL (13.23%) at 24 h, and then decreasing to 2.56 mg/mL (10.77%) at 48 h, likely due to enzyme

Table 1. Chemical composition of biomass samples.

| Sample | Moisture (%) | Ash (%) | Cellulose (%) | Hemicellulose (%) | Total Lignin (%) | Holocellulose (%) |
|-------------------|--------------|---------|---------------|-------------------|------------------|-------------------|
| Stem bark | 7.76 | 3.83 | 38.71 | 21.68 | 28.06 | 60.39 |
| Woody stem | 2.81 | 0.64 | 38.24 | 16.46 | 22.65 | 54.71 |
| Pod husk | 20.87 | 5.66 | 6.85 | 21.06 | 16.87 | 27.92 |
| Pod with seed | 17.99 | 5.31 | 39.33 | 22.35 | 45.91 | 61.68 |
| Pulp without seed | 21.11 | 5.70 | 23.56 | 21.13 | 20.52 | 44.69 |
| Seed | 5.40 | 2.49 | 7.12 | 10.57 | 11.47 | 17.69 |

Values in % g/100 g of dry biomass.

Table 2. Enzymatic hydrolysis of raw Algaroba biomass.

| Sample | Enzymatic hydrolysis after 24 h reaction (mg/mL) (%) | Enzymatic hydrolysis after 48 h reaction (mg/mL) (%) |
|---------------|--|--|
| Stem bark | 2.74 (13.23%) | 2.56 (10.77%) |
| Woody stem | 0.03 (0.11%) | 0.30 (1.22%) |
| Pod with seed | 1.38 (7.43%) | 1.44 (6.69%) |

Values expressed in mg/mL and %.

inhibition by by-products or active site saturation. Woody stem had modest values at 24 h (0.03 mg/mL, 0.11%), increasing slightly at 48 h (0.30 mg/mL, 1.22%). The pod with seed reached 1.38 mg/mL (7.43%) at 24 h and 1.44 mg/mL (6.69%) at 48 h, indicating intermediate yields.

Other authors observed that specific pretreatments resulted in higher yields. Deswal and colleagues [20] and Naseeruddin and colleagues [29] reported 3.9 mg/mL/g sugar yields from woody *P. juliflora*. Gupta, Khasa and Kuhad [21] in 2009 achieved 18.45 mg/mL after lignin removal, and, in 2011 the same authors reported 33% yield using *T. reesei* cellulase supplemented with *A. niger* β-glucosidase (Novozyme 188) [22].

Conclusion

The results demonstrate that the composition of different *P. juliflora* fractions directly

influence fermentable sugar yields. The stem bark, with higher cellulose and hemicellulose, stood out in enzymatic hydrolysis. Fractions with high lignin content, such as those with seeds, require pretreatments for efficient conversion.

Previous studies confirm the importance of lignin removal and enzyme supplementation (notably β -glucosidase) to increase hydrolysis efficiency. Thus, careful selection of biomass fraction, combined with efficient pretreatments and optimized enzyme cocktails, emerges as a decisive strategy to enhance sustainable sugar and biofuel production from *P. juliflora*.

Acknowledgements

We thank SENAI CIMATEC University and FINEP, through the PRH 27.1 Program of ANP, for financial support.

References

- Hemansi R, Srivastava N, et al. Second generation bioethanol production: the state of art. In: Srivastava N, et al, editors. Sustainable approaches for biofuels production technologies. Cham: Springer International Publishing; 2019. p. 121-146. (Biofuel and Biorefinery Technologies; vol. 7).
- Koupaie E, et al. Enzymatic pretreatment of lignocellulosic biomass for enhanced biomethane production: a review. J Environ Manage. 2019;233:774-84.
- 3. Sajith S, et al. An overview on fungal cellulases with an industrial perspective. J Nutr Food Sci. 2016;6(1).
- Shahzadi T, et al. Advances in lignocellulosic biotechnology: a brief review on lignocellulosic biomass and cellulases. Adv Biosci Biotechnol. 2014;5(3):246-51.
- Bajpai P. Global production of bioethanol. In: Bajpai P. Developments in bioethanol. Singapore: Springer Singapore; 2021. p. 177-96. (Green Energy and Technology).
- Devi A, et al. A panoramic view of technological landscape for bioethanol production from various generations of feedstocks. Bioengineered. 2023;14(1):81-112.
- Damasceno GADB, Ferrari M, Giordani RB. Prosopis juliflora (SW) DC, an invasive specie at the Brazilian Caatinga: phytochemical, pharmacological, toxicological and technological overview. Phytochem Rev. 2017;16(2):309-31.
- González-Montemayor ÁM, et al. *Prosopis* spp functional activities and its applications in bakery products. Trends Food Sci Technol. 2019;94:12-9.
- 9. Henciya S, et al. Biopharmaceutical potentials of *Prosopis* spp (Mimosaceae, Leguminosa). J Food Drug Anal. 2017;25(1):187-96.
- Ramírez V, et al. Chromium hyper-tolerant *Bacillus* sp MH778713 assists phytoremediation of heavy metals by mesquite trees (*Prosopis laevigata*). Front Microbiol. 2019;10:1833.
- Sluiter A, et al. Determination of total solids in biomass and total dissolved solids in liquid process samples: laboratory analytical procedure (LAP). Technical Report. 2008.
- 12. Sluiter A, et al. Determination of ash in biomass: laboratory analytical procedure (LAP). Technical Report. 2005.
- 13. Sluiter A, et al. Determination of structural carbohydrates and lignin in biomass. Technical Report. 2012.
- 14. Silwadi M, et al. Pretreatment and acid hydrolysis of Omani *Prosopis juliflora* wood. J King Saud Univ Eng Sci. 2023;35(6):359-65.
- 15. Asgher M, Ahmad Z, Iqbal HMN. Alkali and enzymatic delignification of sugarcane bagasse to expose cellulose polymers for saccharification and bio-ethanol production.

- Ind Crops Prod. 2013;44:488-95.
- 16. Bauer S, Ibáñez AB. Rapid determination of cellulose. Biotechnol Bioeng. 2014;111(11):2355-7.
- 17. Updegraff DM. Semimicro determination of cellulose in biological materials. Anal Biochem. 1969;32(3):420-4.
- 18. Ribeiro GCA, Assis SA. β-glucosidases from Saccharomyces cerevisiae: production, protein precipitation, characterization, and application in the enzymatic hydrolysis of delignified sugarcane bagasse. Prep Biochem Biotechnol. 2024;54(3):317-27
- 19. Kapoor K, et al. Study the effect of gamma radiation pretreatment of sugarcane bagasse on its physicochemical morphological and structural properties. Radiat Phys Chem. 2017;141:190-5.
- 20. Deswal D, Gupta R, Kuhad RC. Enhanced exoglucanase production by brown rot fungus *Fomitopsis* sp RCK2010 and its application for cellulose saccharification. Appl Biochem Biotechnol. 2012;168(7):2004-16.
- 21. Gupta R, Sharma KK, Kuhad RC. Separate hydrolysis and fermentation (SHF) of *Prosopis juliflora*, a woody substrate, for the production of cellulosic ethanol by *Saccharomyces cerevisiae* and *Pichia stipitis* NCIM 3498. Bioresour Technol. 2009;100(3):1214-20.
- 22. Gupta R, Khasa YP, Kuhad RC. Evaluation of pretreatment methods in improving the enzymatic saccharification of cellulosic materials. Carbohydr Polym. 2011;84(3):1103-9.
- 23. Gupta R, et al. Kinetic study of batch and fed-batch enzymatic saccharification of pretreated substrate and subsequent fermentation to ethanol. Biotechnol Biofuels. 2012;5(1):16.
- 24. Sivarathnakumar S, et al. Bioethanol production from woody stem *Prosopis juliflora* using thermo tolerant yeast *Kluyveromyces marxianus* and its kinetics studies. Bioresour Technol. 2019;293:122060.
- 25. Miller GL. Use of dinitrosalicylic acid reagent for determination of reducing sugar. Anal Chem. 1959;31(3):426-8.
- 26. Naseeruddin S, et al. Selection of the best chemical pretreatment for lignocellulosic substrate *Prosopis juliflora*. Bioresour Technol. 2013;136:542-9.
- 27. Thanarasu A, et al. Anaerobic codigestion of alkalipretreated *Prosopis juliflora* biomass with sewage sludge for biomethane production. Energy Fuels. 2019;33(8):7357-65.
- 28. Gayathri G, Uppuluri KB. Hybrid hydrolysis and fermentation optimization of *Prosopis juliflora* pods for the enhanced biohydrogen production by dark fermentation. Biomass Convers Biorefin. 2024;14(12):12877-93.
- 29. Naseeruddin S, Desai S, Venkateswar Rao L. Ethanol production from lignocellulosic substrate *Prosopis juliflora*. Renew Energy. 2017;103:701-7.

Evaluation of *Prosopis juliflora* **for Bioethanol Production: Thermogravimetric Analysis and Structural Composition**

Clara Rodrigues Pereira^{1*}, Carine Tondo Alves², Yuri Uriel Cerqueira Gil Braz Moreira³, Geise Camila de Araujo Ribeiro³, Tatiana Oliveira do Vale³, Lilian Lefol Nani Guarieiro³

¹ PhD student in Industrial Management and Technology, CAPES Scholarship Holder; ²Department of Energy Engineering, Federal University of Recôncavo da Bahia; Feira de Santana, Bahia; ³ SENAI CIMATEC University Center; Salvador, Bahia. Brazil

Prosopis juliflora (P. juliflora), known as Algaroba, presents great potential for bioethanol production due to its cellulose- and hemicellulose-rich composition. This study analyzed its biomass through thermogravimetric techniques and structural characterization to assess its energy viability. Samples of woody stem, stem bark, and pods were subjected to thermal and chemical composition analyses, which identified different thermal degradation profiles and structural carbohydrate contents. Results indicated that stem bark presented the highest levels of glucose and cellulose, while lignin showed significant concentration, suggesting the need for pretreatments to optimize bioenergy conversion. Thus, P. juliflora demonstrates potential as a feedstock for biofuels, provided that challenges related to lignin and economic feasibility are overcome. Keywords: Prosopis juliflora. Biomass. Energy Viability.

Prosopis juliflora (P. juliflora), commonly known as Algaroba, is notable for its high adaptability, serving as both a valuable resource and an ecological threat in various ecosystems. Its presence can cause significant environmental impacts, such as alterations to biodiversity and depletion of water resources, making it the subject of numerous studies [1].

In this context, in addition to being an invasive species, *P. juliflora* presents high potential as a feedstock for biofuels due to its lignocellulosic composition, which is rich in cellulose and hemicellulose, characteristics that make it promising for second-generation ethanol production [2].

Its high carbohydrate content enables efficient use in biorefineries, provided that processes such as pretreatment, hydrolysis, and fermentation are optimized. However, challenges such as high lignin concentration, economic feasibility,

Received on 3 May 2025; revised 21 July 2025. Address for correspondence: Clara Rodrigues Pereira. Av. Orlando Gomes, 1845, Piatã, Salvador, Bahia, Brazil. Zipcode: 41650-010. E-mail: clara.r.pereira@gmail.com. Original extended abstract presented at SAPCT 2025.

J Bioeng. Tech. Health 2025;8(4):321-324 © 2025 by SENAI CIMATEC University. All rights reserved.

and environmental impacts of production still need to be addressed. Advancing research to improve conversion techniques and sustainable management is therefore essential to transform this invasive species into a high-value energy resource [2].

This study aimed to evaluate the thermogravimetric profile and the structural carbohydrate and lignin composition of woody stem, stem bark, and pods of *P. juliflora*, in order to assess the bioenergy potential of this biomass.

Materials and Methods

This study was conducted at the Energy and Bioproducts Research Institute of Aston University, Birmingham, England, through an institutional partnership with SENAI CIMATEC University, within the scope of the CAPES Sandwich PhD program. This collaboration provided access to suitable infrastructure for the required analyses.

The methodological stage involved analyzing woody stem, stem bark, and pods from *P. juliflora* biomass using thermogravimetric analysis, structural compound determination, and acid hydrolysis of the untreated sample. Thermogravimetric analysis was performed using

a Mettler Toledo TGA/DSC 2 STARe system, where 3 mg samples (in triplicate) were heated from 40°C to 900°C at 10°C/min under N₂ flow (30 mL/min), allowing characterization of thermal properties and degradation through mass variation.

Additionally, structural carbohydrate and lignin characterization followed the NREL method [3], where 150 mg of woody stem, bark, and pods were weighed and mixed with H₂SO₄ (72%) and deionized water. After 1 h in a water bath at 30°C and another 1 h in an autoclave at 121°C, the solution was vacuum filtered, neutralized with CaCO₃, and analyzed by HPLC to identify glucose, xylose, and arabinose. Thus, the hemicellulose, cellulose, and lignin contents were determined according to the NREL protocol, enabling an assessment of the sustainable biotechnological and industrial potential of *P. juliflora*.

Results and Discussion

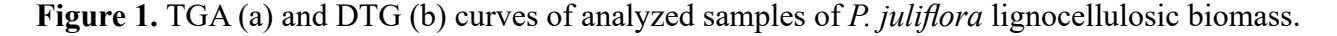
Thermal analyses using the Mettler Toledo TGA/DSC 2 STARe system provided a detailed overview of the thermal degradation of woody stems, bark, and pods of *P. juliflora*. The steps of moisture removal and degradation of hemicellulose, cellulose, and lignin were

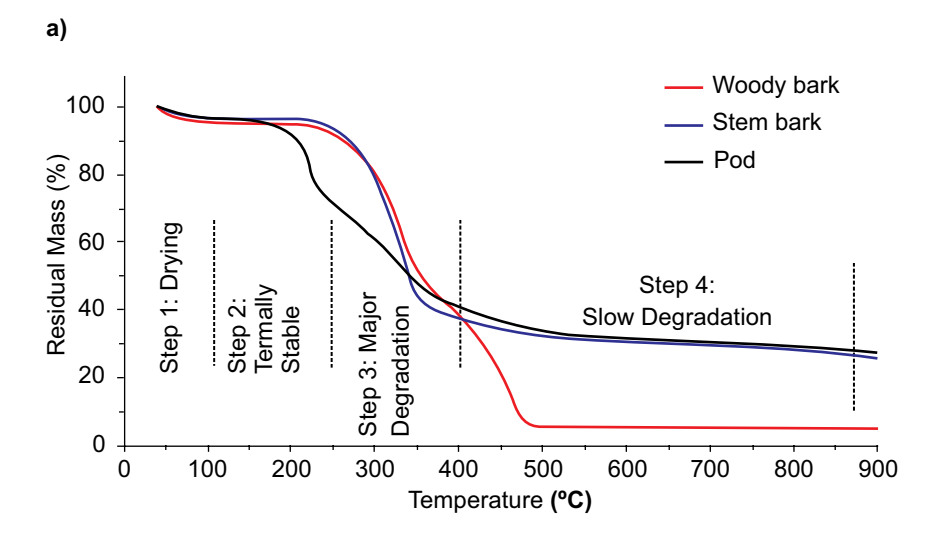
identified, characterizing thermal behavior and energy potential of the samples.

The results were represented by TGA curves (representing the variation in residual mass with temperature) and DTG curves (the derivative of the TGA curve) (Figure 1).

The DTG curve highlighted the maximum decomposition peaks of each component. The TGA and DTG curves indicated moisture between 40°C and 100°C. loss of lignocellulosic biomass, followed hemicellulose degradation between 202.5°C and 295.3°C, with the pods showing the most pronounced degradation, indicating a higher sugar content. Cellulose degraded between 329°C and 375°C, with greater intensity in woody stem and bark, suggesting a composition favorable to decomposition in this range. Lignin degradation occurred between 425.5°C and 633°C, with a more intense reaction in the woody stem due to its highly cross-linked polymeric structure.

These results confirm previous studies on the thermogravimetric profile of *P. juliflora*, which reported similar degradation ranges for biomass constituents [4-6]. Beyond the thermogravimetric profiles, the lignocellulosic constituents were analyzed, including lignin, glucose, xylose, arabinose, cellulose, and hemicellulose (Figure 2).





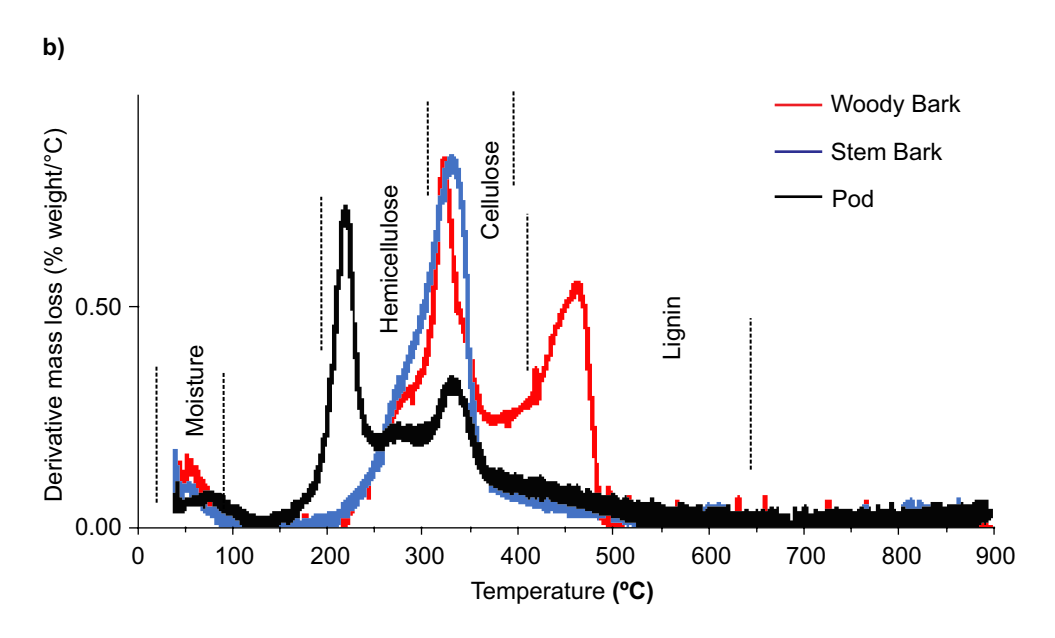
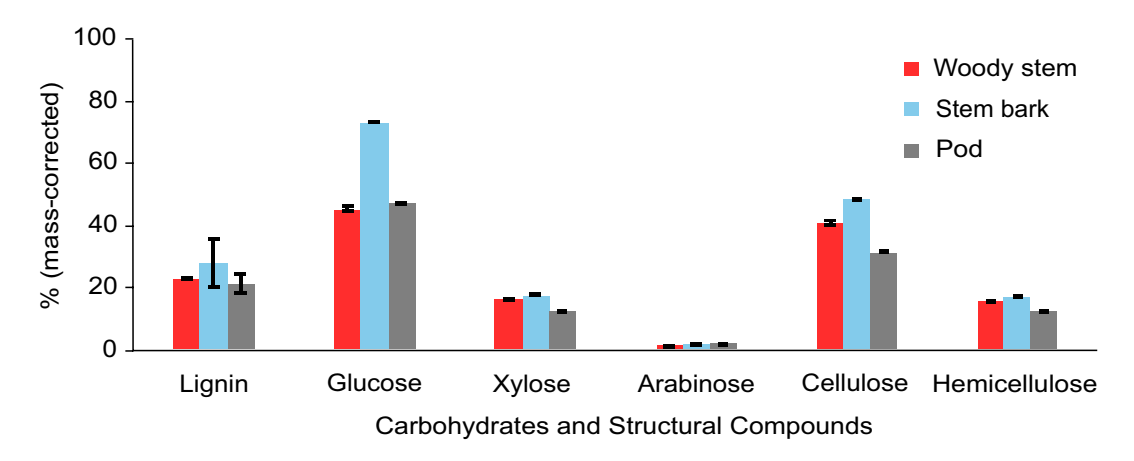


Figure 2. Structural carbohydrate and lignin characterization in woody stem, stem bark, and pods of *P. juliflora*.



The data showed that the stem bark had the highest glucose (73%) and cellulose (48%) contents, indicating strong potential for bioenergy conversion. The woody stem showed intermediate glucose (45%) and cellulose (41%) values, while the pods had slightly lower values (47% and 31%). Hemicellulose was also prominent in stem bark, reinforcing its importance in lignocellulosic biomass, as noted in previous studies [7].

The lignin content was highest in stem bark (28%), followed by woody stem (23%) and pods (19%), indicating a likely need for pretreatments to increase cellulose accessibility in raw biomass.

Woody stem values (41% cellulose, 16% hemicellulose, and 23% lignin) align with previous studies, which reported 66% total carbohydrates, whereas this study identified 57%. These results reinforce the viability of *P. juliflora* as a source of biomass for energy production.

Conclusion

The results indicated that *P. juliflora* has strong potential for bioethanol production, particularly from its stem bark, which is rich in cellulose and glucose. Thermogravimetric analysis confirmed its energy viability; however, the high lignin

content requires pretreatments to optimize conversion. Thus, *P. juliflora* can be considered a sustainable alternative for biofuels, provided that future studies improve conversion processes and economic feasibility.

Acknowledgements

The author thanks the Coordination for the Improvement of Higher Education Personnel (CAPES) for funding her PhD scholarship.

References

- 1. Hosseinzadeh J, et al. Evaluation of biomass and vegetative characteristics of mesquite (*Prosopis juliflora*) afforestation in arid area of Iran. 2024.
- 2. Gayathri G, Uppuluri KB. The comprehensive characterization of *Prosopis juliflora* pods as a potential bioenergy feedstock. Sci Rep. 2022;12(1):18586.

- 3. Sluiter A, et al. Determination of structural carbohydrates and lignin in biomass. Lab Anal Proced. 2008;1617(1):1-16.
- 4. Arun J, et al. Hydrothermal liquefaction of *Prosopis juliflora* biomass for the production of ferulic acid and bio-oil. Bioresour Technol. 2021;319:124116.
- 5. Carneiro-Junior JAM, et al. Valorization of Prosopis juliflora woody biomass in northeast Brazilian through dry torrefaction. Energies. 2021;14(12):3465.
- 6. Thanarasu A, et al. Anaerobic codigestion of alkalipretreated *Prosopis juliflora* biomass with sewage sludge for biomethane production. Energy Fuels. 2019;33(8):7357-65.
- 7. Zhu JY, Pan XJ. Woody biomass pretreatment for cellulosic ethanol production: technology and energy consumption evaluation. Bioresour Technol. 2010;101(13):4992-5002.
- 8. Palled V, et al. *Prosopis juliflora*—A potential problematic weed for lignocellulosic ethanol production. In: Energy and Environment: Select Proceedings of ICWEES-2016. Singapore: Springer; 2018. p. 191-206.

Polyphenols and Antioxidant in Southwest Mexico Agave Leaves

Misael Bermúdez Bazán¹, Mirna Estarrón Espinosa¹, Judith Esmeralda Urías Silvas¹, Javier Plácido Arrizon Gaviño², Anne Christine Gschaedler Mathis², Gustavo Adolfo Castillo Herrera¹*

Food Technology, CIATEJ; Industrial Biotechnology, CIATEJ; A.C. Zapopan, Jalisco, México

Currently, the revalorization of the agave leaves produced by the mezcal industry has increased since various studies confirmed the presence of secondary metabolites in this agro-waste. These phytochemicals have shown potential applications in the pharmaceutical and food industries. Therefore, this research aimed to determine and compare the phenolic content and antioxidant activity of different agave leaf species. Leaves from the Agave species angustifolia, americana, cupreata, karwinskii, and potatorum were macerated in methanol. The extracts were concentrated and characterized by their total phenolic content (TPC: Folin-Ciocalteau) and total flavonoid content (TFC: AlCl3), antioxidant activity (AA), and phenolic profile. The results evaluated by ANOVA and post hoc Tukey analysis showed that the species and geographical origin significantly influenced the total phenolic content (p<0.05). The extracts of A. americana and A. cupreata showed high phenolic and flavonoid content within a range of 7.12±1.08-3.19±0.13 and 3.01±0.10- 0.72±0.16 mg GAE/g dry leaf, respectively. Similarly, the AA was influenced by these factors (p<0.05), within ranges from 13.02±0.60-4.86±0.95; 7.84±1.30-3.52±0.97, 15.72±3.27-4.74±0.17 µmol ET/g dry leaf for the ABTS, DPPH, and FRAP assays, respectively. The extracts with the central AA were A. americana (Chiapas); A. angustifolia (Oaxaca), and A. cupreata (Guerrero). In addition, the phenolic profile of these species showed a high content of catechin and (-)-epicatechin, two flavonoids with potent antioxidant and biological activities. The leaves of mezcal agaves are a potential source of diverse secondary metabolites of industrial interest, and they can be exploited for the development of new industrial applications.

Keywords: Agave. Antioxidant Activity. Polyphenols. Byproducts; Extraction.

Agaves are perennial plants that belong to the large family of plants known as *Asparagaceae*. Within the *Agavoideae* subfamily, it is endemic to the American continent and comprises 9 different genera [1]. The Agave genus is the largest, comprising 251 species of plants, which are primarily distributed in Mexico. Therefore, Mexico is the primary country with a diversity of these plants, boasting 177 endemic species distributed throughout the country [1].

The production of alcoholic beverages, such as mezcal, is one of the largest industrial applications of the agave plant. According to the Mexican Mezcal Quality Regulatory Council [2], the production in 2022 totaled 14,165,505 liters, with 81.08% of the production using *Agave angustifolia*,

Received on 17 May 2025; revised 30 July 2025. Address for correspondence: Gustavo Adolfo Castillo Herrera. Av. Orlando Gomes, 1845, Piatã, Salvador, Bahia, Brazil. Zipcode: 41650-010. E-mail: gcastillo@ciatej.mx.

J Bioeng. Tech. Health 2025;8(4):325-332 © 2025 by SENAI CIMATEC University. All rights reserved.

also known as maguey espadín. Additionally, 1.43% and 1.98% came from the species Agave karwinskii (maguey cuishe) and Agave potatorum (maguey tobalá), respectively. Other species used in the production of mezcal are the cupreata and americana Agaves, for which data on their use in mezcal production in 2022 were not reported [2].

The high demand for mezcal has contributed to the growth of agroindustrial waste, which poses an environmental concern [3]. Agave leaves are the primary agricultural waste produced by this industry, as they are discarded without any environmental processing. Approximately 50-60% of the total weight of an agave corresponds to the leaves [4], so its waste translates into economic losses. The production of mezcalero agaves was 393,604.65 tons, generating 196,802.32 tons of leaves [5].

Recently, there has been interest in utilizing agave leaves for industrial purposes, as various studies have reported the presence of secondary metabolites in different species of agaves. These phytochemical compounds have been of interest

to the pharmaceutical and food industries due to their potential as antioxidants, anti-inflammatory agents, anticancer agents, immunomodulators, and hypolipidemic agents, among others [6-9].

The most studied secondary metabolites from agaves, with their biological potential, are saponins and fructans in commercial agave species used for the production of tequila and mezcal [10,11]. Despite the sufficient research on the characterization of phenolic compounds from Agave (angustifolia, potatorum, karwinskii, cupreata, and americana) leaves, their antioxidant activity, and phenolic profile need more research about these characteristics. Thus, this research aimed to determine and compare the phenolic content, total flavonoids, as well as the antioxidant activity and phenolic profile of extracts from mezcal agave leaves in the Southwestern region of Mexico, and to provide an overview of the potential uses of these leaves as agrowaste from the mezcal industry.

Materials and Methods

Collection of Plant Material

The origin of the agaves used to obtain extracts is described in Table 1, in which the identification code based on the species and geographical origin of each plant is shown.

Conditioning of Plant Material

Fresh leaves of each plant material were washed and cut into small pieces for subsequent drying at 50°C in a convection oven for 21 h. The dried plant material was milled. The fiber and powder obtained were further reduced in a blender and subsequently sieved using a 40 mesh. Powder was stored at room temperature in plastic bags protected from light until it was used.

Preparation of the Extracts

For the extraction of phenolic compounds, powder of each plant material was defatted with n-hexane for 24 h in a 1:10 ratio (mass/volume). The defatted material was recovered, dried, and extracted by maceration using methanol in two stages. Maceration was carried out in a 1:5 ratio (m/v) for 24 h. The crude extracts from both extractions were vacuum-filtered, combined, and concentrated using a rotary evaporator. Subsequently, extracts were kept at -18°C and protected from light until use.

Determination of Total Phenolic Content

The determination of total phenols was carried out using the methodology described in Rover & Brown [12] with some modifications, employing the Folin-Ciocalteu reagent. Gallic acid was used at a concentration of 0.5 g/L as a standard solution, with a quantification range of 5-300 mg/L. Aliquots of 20 μL of diluted plant extract were taken in triplicate and reacted with 100 μL of 10% (v/v) Folin's reagent for 5 minutes in the dark. Subsequently, 7.5% (v/v) Na₂CO₃ was added for 90 minutes in the dark at 30°C. The measurements were performed using a UV-VIS spectrophotometer at a wavelength of 765 nm. The results were expressed in milligrams of gallic acid equivalents per gram of dry leaf.

Determination of Total Flavonoid Content

The determination of total flavonoid content was carried out using the procedure as in Dewanto and colleagues [13] with some modifications. Measurements were carried out in duplicate by taking aliquots of diluted plant extract (225 μL) from each plant material, which were reacted with 5% NaNO₂ (70 μL) and 10% AlCl₃·6H₂O (150 μL) for 5 minutes. The reaction was terminated by adding 0.5 mL of 1 M NaOH and incubating for 10 min in the dark. To quantify the total flavonoid content, quercetin was used as a standard (1 mg/ml), and it was quantified in a range of 5-600 μg/ml in a UV-VIS spectrophotometer at 415 nm. The results were expressed as mg quercetin equivalents/g dry leaf.

Table 1. Geographic origin and extracts codification from agave species by region.

| Species | Region | Code |
|----------------------------|--|----------------|
| Agave angustifolia Haw. | Atetetla, Huitzuco, Guerrero Lodo Grande, Chilapa de Álvarez, Guerrero | AAHG ACCHG1 |
| Agave cupreata Trel & Berg | Los Amates, Chilapa de Álvarez, Guerrero Mazatlán, Chilpancingo, Guerrero. | ACCHG2 ACMG |
| Agave americana 1 | | AACH1 |
| Agave americana 2 | Comitán, Chiapas | AACH2 |
| Agave americana 3 | | AACH3 |
| Agave karwinskii Zucc. | San Juan del Río | AK |
| Agave potatorum Zucc. | Tlacoluca, Oaxaca | AP |
| Agave angustifolia Haw. | San Francisco Sola, Oaxaca | AASO |

Evaluation of Antioxidant Activity by the ABTS⁺ Radical Assay

The ABTS⁺⁺ reactive radical was prepared by using the procedure described by Lopez-Romero and colleagues [9]. The ABTS⁺⁺ radical solution was initially adjusted to an absorbance of 0.7 \pm 0.02 in a UV-VIS spectrophotometer at 734 nm.Measurements were carried out in triplicate, taking aliquots of diluted plant extract from each sample (20 μ L), which were reacted with adjusted ABTS⁺⁺ (180 μ L) for 5 minutes. Trolox 1M was used as a standard solution with a quantification range of 5-400 μ M. The results were expressed as μ M trolox equivalents/g dry leaf.

Evaluation of Antioxidant Activity by the DPPH Radical Assay

The DPPH reactive radical was prepared using the procedure described by Lopez-Romero and colleagues [9]. The DPPH radical solution was initially adjusted to an absorbance of 0.7 ± 0.02 at 515 nm in a spectrophotometer. Measurements were carried out in triplicate by taking aliquots of diluted plant extract from each sample (20 μ L), which were reacted with adjusted DPPH+ (180 μ L) for 30

minutes. 1M Trolox was used as a standard solution with a quantification range of 5-400 μ M. The results were expressed as μ M trolox equivalents/g dry leaf.

Iron Reducing Antioxidant Power (FRAP) Assay

The FRAP reagent was prepared according to the procedure described in Zhang and colleagues [14]. Aliquots of diluted plant extract (20 μ L) were taken from each plant material, and the FRAP solution (150 μ L) was reacted for 30 minutes in the dark. The measurements were carried out in triplicate, and 1M Trolox was used as a standard solution with a quantification range of 5-400 μ M. Measurements were performed using a UV-VIS spectrophotometer at a wavelength of 593 nm. The results were expressed as μ M trolox equivalents/g dry leaf.

HPLC-DAD-UV Phenolic Profile Auantification

Thirteen standards of different compounds were used (Sigma-Aldrich®, purities 90- 99.8%), among which there were 4 phenols (gallic acid, 3,4-dihydroxy-benzoic acid, vinylic acid, and ferulic acid) and 9 flavonoids. (myricetin, rutin, quercetin, pueranin, kaempferol, rosmarinic acid,

(+)-catechin, (-)-epicatechin, and phlorizin). The chromatograms of the standards and samples were obtained at wavelengths of 254, 280, 340, and 350 nm. Spectral data for all peaks were accumulated in the range of 100–500 nm. Identification and quantification were carried out based on the retention time and UV spectra of each standard at its maximum wavelength. The quantitative results of each metabolite were subject to the corresponding family of phenolic compounds and flavonoids. They were expressed as the content of flavones, dihydroxychalcones, hydroxybenzoic acids, flavanols, and flavonols per gram of dry leaf.

Statistical Analysis

The dependent variables — total phenolic content, total flavonoids, antioxidant activity, and metabolite content — quantified by HPLC-DAD — were analyzed using one-way analysis of variance. The independent variables in this analysis were geographic region and species. To determine the differences between the means of each variable, Tukey's multiple range test was

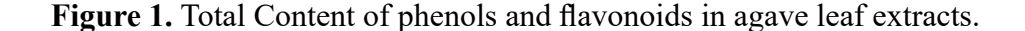
used with a significance level of 0.05 (95%). Additionally, the correlation between phenolic and flavonoid content and antioxidant activity was determined using the Pearson correlation coefficient (r²). Statistical analyses were performed in STATGRAPHICS Centurion XVI software.

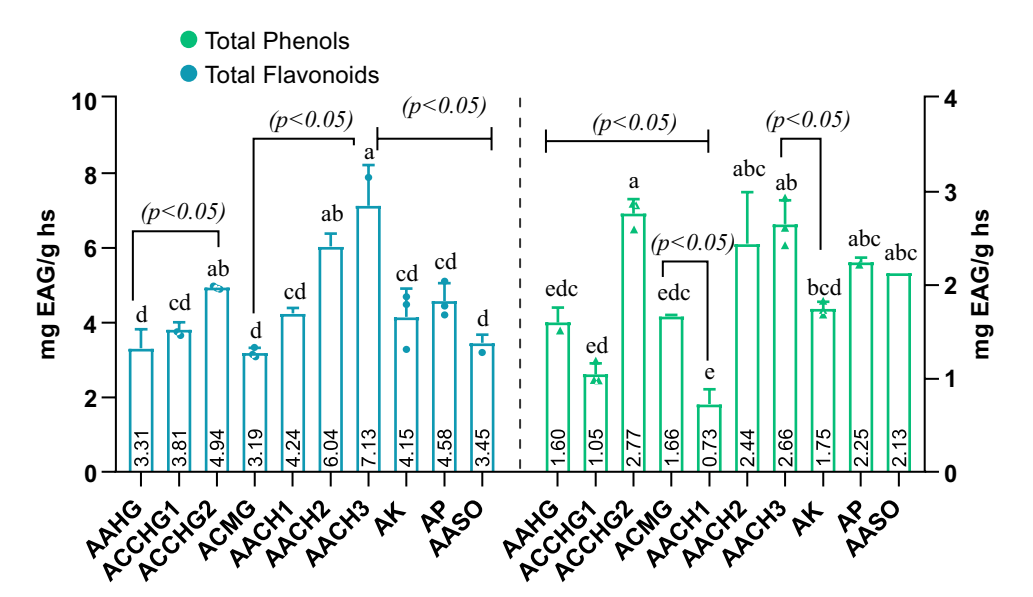
Results and Discussion

Total Flavonoid Phenol Content

According to Figure 1, the analysis of variance (ANOVA) for phenolic and total flavonoid content revealed a significant statistical difference by species (p < 0.05).

Tukey's multiple range test at α = 95% indicated that the extracts with the highest total phenolic content in decreasing order were AACH3; 7.13 \pm 1.09 > AACH2; 6.04 \pm 0.34 > ACCHG2; 4.94 \pm 0.05 mg EAG/g dry leaf, respectively. The extracts coded as AP, AACH1, AK, and ACCHG1 showed intermediate concentrations of phenols in a range of 4.58-3.81 mg EAG/g of dry leaf, while the extracts AASO, AAHG, and ACMG showed the lowest phenolic content in a range of 3.45





Different letters indicate significant statistical differences.

-3.19 mg EAG/g dry leaf.

In Figure 1, the extracts with the highest flavonoid content in decreasing order were ACCHG2 (2.77 ± 0.45) > AACH3 (2.66 ± 0.48) > AACH2 (2.44 ± 0.07) mg EQ/g dry leaf, respectively. The extracts with an intermediate content of these metabolites in decreasing order were AP>AASO>AK, while those with low flavonoid content corresponded to the extracts ACMG>AAHG>ACCHG1>AACH1.

The concentration of total phenolics was influenced by the geographic region (p<0.05); however, this did not occur for the content of total flavonoids. The phenolic and flavonoid content of the AP extract $(4.58 \pm 0.47 \text{ mg EAG/g hs}; 2.25 \text{ mg})$ \pm 0.05 EQ/g hs) was higher than that reported by Delia and colleagues [15], whose values were 1.73 \pm 9.36 mg EAG/g hs; 0.35 \pm 6.41 mg EQ/g hs, in the ethanolic extract of A. potatorum leaf. On the other hand, Lopez-Romero and colleagues [9] and Ahumada-Santos [16] reported a phenolic content of 21.7 ± 0.08 and 2.06 ± 0.25 mg EAG/g hs in methanolic and ethanolic extract of A. angustifolia leaves, respectively. The differences in the AAHG, AAOS, and AP extracts compared to those described by these authors can be attributed to the region of origin of the plant material, the type of solvent used, the extraction method employed, the age of the plant material, and the part of the leaves [15,17,18].

According to the ANOVA results, extracts from Comitán, Chiapas; Chilapa, Guerrero (Predio Los Amates), and San Juan del Río, Oaxaca regions showed an average total phenolic content of 5.80, 4.94, and 4.36 mg EAG/g dry leaf, respectively.

Extracts of A. americana from Comitán, Chiapas showed the highest content of total phenols compared to the other sampled regions. In [19], a total phenolic and flavonoid content of 14.70 ± 0.31 mg EAG/g fresh weight and 5.15 ± 0.18 mg rutin equivalents/g fresh weight is reported, which were higher than those found in AACH1, AACH2, and AACH3 of A. americana extracts. However, the results and standard quantification for total flavonoids described in Maazoun and colleagues

[19] differed from those in this study, which also contributes to the discrepancy in the results reported in the literature. Maazoun and colleagues [19] and Lopes-Romero and colleagues [20] reported quantifications with different standards and total flavonoids content, such as rutin and hesperidin, which implies the presence of these metabolites in *A. angustifolia* and *A. americana*.

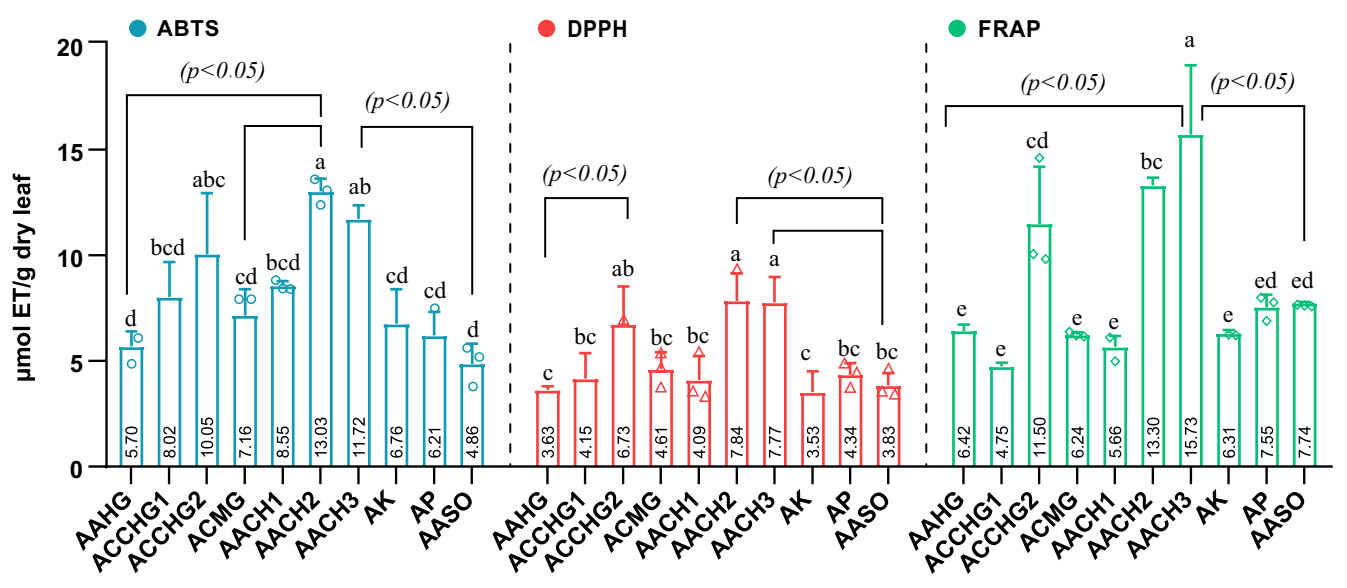
Evaluation of Antioxidant Activity

According to Figure 2 and Table 2, the species significantly influenced (p<0.05) the antioxidant activity (AA) determined in the ABTS, DPPH, and FRAP assays. The same thing happened with the geographic region factor. From the results illustrated in Figure 2, we observe that the species that resulted in the highest AA in the three analyses were the extracts AACH3 (11.72 \pm 0.64/ABTS; 7.77 \pm 1.20/ DPPH; 15.73±3.28/FRAP)>AACH2 (13.03±0.61/ ABTS; 7.84 ± 1.30 /DPPH; 15.30 ± 0.38 /FRAP) $(10.05\pm2.89/ABTS;$ >ACCHG2 6.73 1.80; 11.50±2.69/FRAP) umol trolox equivalents/g dry leaf, respectively.

With respect to the region, the ANOVA indicated that the extracts of sampled species from Comitán, Chiapas, and Chilapa, Guerrero (Los Amates), showed better antioxidant activity than those from other regions (data not shown).

It is worth noting that the species exhibiting the most significant antioxidant activity corresponded to those with the highest phenolic and total flavonoid content, suggesting a correlation between phenolic and flavonoid concentration and antioxidant activity. According to the results in Table 2, the total phenolic content exhibited a strong and significant correlation (p < 0.05) with the antioxidant activity evaluated by the ABTS, DPPH, and FRAP assays. A strong and significant correlation between phenolic content and antioxidant activity indicates that AA is mainly attributed to phenolic compounds [21], which was confirmed in this study. Furthermore, the reducing and free radical scavenging nature of the phenols present in the plant extracts was also observed in

Figure 2. Antioxidant activity in agave extracts from the southwestern area of Mexico by the ABTS, DPPH, and FRAP assays



Different letters indicate significant statistical differences.

Table 2. Correlation between total phenolic and flavonoid content and antioxidant activity.

| Variable | r ² | Variable | r ² |
|---------------|----------------|--------------|----------------|
| CFT vs. ABTS* | 0.732 | FT vs. ABTS | 0.342 |
| CFT vs. DPPH* | 0.757 | FT vs. DPPH | 0.591 |
| CFT vs. FRAP* | 0.836 | FT vs. FRAP* | 0.775 |

the three AA assays evaluated; these results are similar to those reported by Rover &Brown [22].

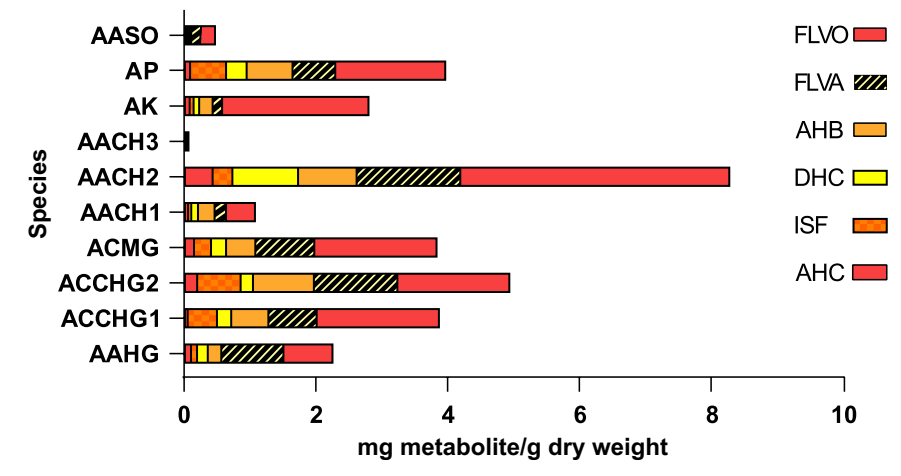
Determination of Phenolic Profile by HPLC-DAD-UV

The phenolic profiles of each plant extract from each agave species differed, as confirmed by the content of total phenolics and flavonoids (Figure 3). Likewise, it can be observed that, in nine plant extracts, the main compounds were flavonols (FLVO), where the concentrations of the routine standards, quercetin, myricetin, and kaempferol, are weighted. The following abundant compounds were flavonols (FLVA), where the concentrations of catechin and (+)-epicatechin are weighted. It is essential to note that the AACH3 extract exhibited a low richness in phenols and flavonoids, despite

its high antioxidant activity. This agrees with the low correlations between the content of flavonoids and antioxidant activity, indicating that even if these metabolites are not present in abundance, they will still have low antioxidant activity.

However, it is essential to note that the extracts with the highest antioxidant activity (AACH2 and ACCHG2) not only exhibited a high abundance of flavonols and flavanols but also contained other families of phenolic compounds. This indicates that, when more varieties of phenols and flavonoids are present in agave, the greater the antioxidant activity they have. Morreeuw and colleagues [23] reported that A. lechuguilla contains a rich variety of phenols and flavonoids, using methanol as a solvent. However, the highest abundance of the metabolites quantified by this author was hesperidin, isorhamnetin, and glycosylated forms of kaempferol, myricetin, and quercetin. However, the content of each quantified metabolite varied by region, which is consistent with the results of this research. El-Hawary and colleagues [6] reported a high abundance of flavonoids, phenolic flavonoids, homoisoflavonoids and saponins in A. angustifolia var. marginata and A. americana, and

Figure 3. Phenolic and flavonoid profile obtained by HPLC-DAD-UV from southwestern Mexico agave extracts.



FLVO: Flavonols; FLVA: Flavanols, AHB: Hydroxybenzoic acids; DHC: Dihydrochalcones; ISF: Isoflavones.

the anti-inflammatory and immunomodulatory activities attributed to these metabolites. Although the biological potential of the metabolites identified in the agave species was not evaluated in this work, the predominant metabolites, such as catechin, (-)-epicatechin, quercetin, myricetin, rutin, and kaempferol, are flavonoids related to these biological activities [24,25].

Conclusion

The agaves used in this study, the phenol content depends on the species and the geographical sampling area. The species with the highest phenolic and flavonoid content were *A. americana* (AACH3) from Comitán, Chiapas, and *A. cupreata* (ACCHG2) from Chilapa, Guerrero (Los Amates).

The species with the highest content of phenols and flavonoids exhibited high antioxidant activity, indicating a significant correlation with the antioxidant activity evaluated by the three chemical assays. This result confirmed that these metabolites are mainly responsible for this activity in all the species evaluated.

In the phenolic chemical profile, the samples that presented a variety and abundance of phenolic acids and flavonoids were the species *A. americana* (AACH3) from Comitán, Chiapas, and *A. cupreata*

(ACCHG2) from Chilapa, Guerrero (Los Amates). It confirmed that the greater the variety in phenols and flavonoids, the greater the antioxidant activity.

Acknowledgments

CONAHCYT funded this work within the framework of the FORDECYT 29247 project, "Multidisciplinary strategies to increase the added value of productive chains of coffee, beans, agave mezcalero and aquaculture products (tilapia) in the South Pacific region through science, technology and innovation."

References

- García Mendoza AJ, Cházaro Basañez MJ, Nieto Sotelo J. Agave: Sistemática, filogenia y taxonomía del género Agave. CONACYT, CIATEJ, AGARED; 2017.
- 2. COMERCAM. Informe Estadístico 2023. comercamdom.org.mx; 2023.
- 3. Bermúdez-Bazán M, Castillo-Herrera GA, Urias-Silvas JE, Escobedo-Reyes A, Estarrón-Espinosa M. Hunting Bioactive Molecules from the Agave Genus: An Update on Extraction and Biological Potential. Molecules. 2021;26(22). doi:10.3390/molecules26226789.
- 4. Hoz-Zavala MEE, Nava-Diguero P. Situación del Agave y sus residuos en Tamaulipas. Rev Energ Renovables. 2017;1(1):19–31.
- González-Jiménez FE, Barojas-Zavaleta JE, Vivar-Vera G, Peredo-Lovillo A, Morales-Tapia AA, Del Ángel-

- Zumaya JA, et al. Effect of Drying Temperature on the Physicochemical, Functional, and Microstructural Properties of Powders from *Agave angustifolia* Haw and Agave rhodacantha Trel. Horticulturae. 2022;8(11). doi:10.3390/horticulturae8111070.
- El-Hawary SS, El-Kammar HA, Farag MA, Saleh DO, El Dine RS. Metabolomic profiling of five Agave leaf taxa via UHPLC/PDA/ESI-MS in relation to their antiinflammatory, immunomodulatory and ulceroprotective activities. Steroids. 2020;160:108648. doi:10.1016/j. steroids.2020.108648.
- Esquivel-Gutiérrez ER, Manzo-Avalos S, Peña-Montes DJ, Saavedra-Molina A, Morreeuw ZP, Reyes AG. Hypolipidemic and Antioxidant Effects of Guishe Extract from *Agave lechuguilla*, a Mexican Plant with Biotechnological Potential, on Streptozotocin-Induced Diabetic Male Rats. Plants. 2021;10(11). doi:10.3390/ plants10112492.
- Gutiérrez Nava ZJ, Jiménez-Aparicio AR, Herrera-Ruiz ML, Jiménez-Ferrer E. Immunomodulatory effect of Agave tequilana evaluated on an autoimmunity like-SLE model induced in Balb/c mice with pristane. Molecules. 2017;22(6). doi:10.3390/ molecules22060848.
- López-Romero JC, Ayala-Zavala JF, Peña-Ramos EA, Hernández J, González-Ríos H. Antioxidant and antimicrobial activity of *Agave angustifolia* extract on overall quality and shelf life of pork patties stored under refrigeration. J Food Sci Technol. 2018;55(11):4413– 23. doi:10.1007/s13197-018-3351-3.
- Espinosa-Andrews H, Urías-Silvas JE, Morales-Hernández N. The role of agave fructans in health and food applications: A review. Trends Food Sci Technol. 2021;114:585–98. doi:10.1016/j.tifs.2021.06.022.
- Herrera-Ruiz M, Jiménez-Ferrer E, González-Cortazar M, Zamilpa A, Cardoso-Taketa A, Arenas-Ocampo ML, et al. Potential Use of Agave Genus in Neuroinflammation Management. Plants. 2022;11(17). doi:10.3390/plants11172208.
- 12. Rover MR, Brown RC. Quantification of total phenols in bio-oil using the Folin-Ciocalteu method. J Anal Appl Pyrolysis. 2013;104:366–71. doi:10.1016/j.jaap.2013.06.011.
- 13. Dewanto V, Wu X, Adom KK, Liu RH. Thermal Processing Enhances the Nutritional Value of Tomatoes by Increasing Total Antioxidant Activity. J Agric Food Chem. 2002;50(10):3010–4. doi:10.1021/jf0115589.
- Zhang XL, Zhang YD, Wang T, Guo HY, Liu QM, Su HX. Evaluation on Antioxidant Effect of Xanthohumol by Different Antioxidant Capacity Analytical Methods. J Chem. 2014;2014:249485. doi:10.1155/2014/249485.
- Delia S, Pérez-Herrera A, García-Sánchez E, Santiago Garcia P. Identification and Quantification of Bioactive Compounds in *Agave potatorum* Zucc. Leaves at

- Different Stages of Development and a Preliminary Biological Assay. Waste Biomass Valorization. 2021;12. doi:10.1007/s12649-020-01329-2.
- 16. Ahumada-Santos YP, Montes-Avila J, Uribe-Beltrán MJ, Díaz-Camacho SP, López-Angulo G, Vega-Aviña R, et al. Chemical characterization, antioxidant and antibacterial activities of six Agave species from Sinaloa, Mexico. Ind Crops Prod. 2013;49:143–9. doi:10.1016/j.indcrop.2013.04.050.
- 17. Rahmani H, Benali F, Koudach F, Dif MM, Mekhfi N, Nouredine N, et al. First determination of phenolic compound concentration and antioxidant activity of *Agave americana* leaves extracts from different regions of Algeria (NW). J Med Plant Res. 2015;3(3):1–6.
- 18. Rahmani H, Toumi Benali F. Phenolic quantification and antioxidant activity of *Agave americana* leaves depending on solvent and geoclimatic area. Adv Environ Biol. 2016;9(October):194–200.
- Maazoun AM, Hamdi SH, Belhadj F, Jemâa JM Ben, Messaoud C, Marzouki MN. Phytochemical profile and insecticidal activity of *Agave americana* leaf extract towards *Sitophilus oryzae* (L.)(Coleoptera: Curculionidae). Environ Sci Pollut Res. 2019;26(19):19468–80. doi:10.1007/s11356-019-05316-6.
- 20. Lopez Romero J, Ayala-Zavala JF, Aguilar G, Peña-Ramos E, Ríos H. Biological activities of Agave by-products and their possible applications in food and pharmaceuticals. J Sci Food Agric. 2017;98. doi:10.1002/jsfa.8738.
- 21. Aryal S, Baniya MK, Danekhu K, Kunwar P, Gurung R, Koirala N. Total Phenolic content, Flavonoid content and antioxidant potential of wild vegetables from western Nepal. Plants. 2019;8(4). doi:10.3390/plants8040096.
- Lebedev VG, Lebedeva TN, Vidyagina EO, Sorokopudov VN, Popova AA, Shestibratov KA. Relationship between Phenolic Compounds and Antioxidant Activity in Berries and Leaves of Raspberry Genotypes and Their Genotyping by SSR Markers. Antioxidants. 2022;11(10). doi:10.3390/ antiox11101961.
- 23. Morreeuw ZP, Castillo-Quiroz D, Ríos-González LJ, Martínez-Rincón R, Estrada N, Melchor-Martínez EM, et al. High Throughput Profiling of Flavonoid Abundance in *Agave lechuguilla* Residue-Valorizing under Explored Mexican Plant. Plants. 2021;10(4). doi:10.3390/plants10040695.
- 24. Fan FY, Sang LX, Jiang M, McPhee DJ. Catechins and their therapeutic benefits to inflammatory bowel disease. Molecules. 2017;22(3). doi:10.3390/molecules22030484.
- Isemura M. Catechin in Human Health and Disease. Molecules. 2019;24(3). doi:10.3390/ molecules24030528.

Study of Fuel Quality in the State of Maranhão Through Principal Component Analysis

Morgana Cristhya Silva dos Santos^{1*}, Luciana Pereira Barbosa¹, Allan Kardec Duailibe Barros Filho¹

Postgraduate Program in Electrical Engineering, Federal University of Maranhão; São Luis, Maranhão, Brazil

This study evaluated the quality of S10 and S500 diesel sold in the state of Maranhão, using data from the National Petroleum Agency (ANP) and the Principal Component Analysis (PCA) technique, to identify patterns in quality indicators. PCA simplified the data, highlighting the most relevant characteristics that influence diesel quality. The results revealed relationships between indicators and groups of samples with similar characteristics, which can be helpful for fuel monitoring. The research demonstrated that PCA is an effective tool to assist in the assessment and control of fuel quality, highlighting the importance of continuous monitoring and advanced statistical analysis in determining fuel quality.

Keywords: PCA. Quality. Fuels.

In Brazil, fuels are produced in several different regions and basins. The quality and properties of these hydrocarbons depend on their region of origin. However, these characteristics are also subject to change at the retail stations. Currently, there are approximately 43,266 petroleum product resale stations distributed throughout the country [1], which undergo regular monitoring and inspection processes throughout the year. To this end, the National Petroleum and Biofuels Agency (ANP) set up the Fuel Quality Monitoring Program (PMQC) in 1998, which is used to identify areas of fuel non-compliance. The analysis of these samples refers to various technical requirements established by the program. The fuels most consumed in Brazil are gasoline and diesel [2,3]. Diesel is the primary fuel used to transport passengers, cargo, and agricultural products in Brazil.

In February 2024, diesel production in Brazil increased by approximately 8.5% compared to the previous year and continues to exceed growth expectations for the current year [4]. Maranhão reflects this national diesel consumption, mainly due to intense agricultural activities and cargo

Received on 18 May 2025; revised 25 July 2025. Address for correspondence: Morgana Cristhya Silva dos Santos. Avenida Hiram Saboia, 777, Centro, Balsas. São Luis, Maranhão. Zipcode: 65800-000. E-mail: morgana.santos@discente.ufma.br.

J Bioeng. Tech. Health 2025;8(4):333-338 © 2025 by SENAI CIMATEC University. All rights reserved.

transportation. In terms of characteristics, diesel has chains composed of 8 to 16 carbons and has lower concentrations of nitrogen, sulfur, and oxygen [3]; however, these characteristics can be transformed with the addition of other substances. Fuel contamination can cause several problems in terms of burning and storage quality, the latter of which is directly related to the oxidative stability of fuels, referring to how well they resist degradation processes [5]. Additionally, interference in fuel composition is a concern, primarily due to engine operation and the release of atmospheric pollutants. In this regard, the monitoring and control of these fuels are critical, as indicated by the compliance indices (%IC) observed in the PMQC [6].

Identifying these parameters can ensure that the fuels that reach the consumer are increasingly better. Monitoring is now carried out in most of Brazil, in partnership with educational and research institutions. According to the ANP Statistical Yearbook [7], in 2020, Maranhão had 1,477 fuel retail outlets. The following year, it monitored 170 municipalities, with 192 samples of ethanol, 1,035 of gasoline, and 1,021 of diesel oil.

In Maranhão, fuel quality analysis is carried out by the Laboratory of Analysis and Research in Petroleum Analytical Chemistry at the Federal University of Maranhão (LAPQAP/UFMA). The laboratory's objectives are to automate the analysis and data processing processes as a decision support tool. A single sample offers a set of variables [8],

so the acquisition of fuel samples from Maranhão, collected together with all their physicochemical properties, constitutes a high-dimensional database, making it difficult to process them. In this sense, the main characteristics analyzed for diesel types are Distillation (10% and 50%), Specific Mass at 20°C, Biodiesel Content, Boiling Point, and Color.

Advances in computational techniques for data analysis are becoming increasingly important for classification. Thus, a common technique is Principal Component Analysis (PCA) [9]. PCA is a technique that has been applied to the treatment of multivariate data and has yielded satisfactory results [8]. As it is an exploratory technique, it enables the identification of correlations between quality indices, the analysis of irregular samples, and the examination of relationships between measured variables, as well as the identification of relationships or groupings within samples. This type of analysis can offer a more efficient arrangement of data distribution in a smaller set than the original, while preserving most of the information.

Therefore, this paper proposes the application of Principal Component Analysis for the exploratory analysis of fuel quality data, aiming to reduce data dimensionality and identify possible patterns and correlations between fuel quality indicators in the state of Maranhão.

Principal Component Analysis (PCA)

Principal Component Analysis applied to the analysis of data with a large number of variables can be described as presented by Correa [10] as a method that evaluates interrelationships with the "aim of recognizing patterns in the distribution of samples, evaluating the relationship between samples and variables, and also detecting the presence of samples that show a distinct behaviour (outliers)". PCA is a dimensionality reduction technique that transforms a data set with a large number of variables into a smaller set. Data reduction using PCA is achieved by linearly combining the correlations of the original variables. In this way, a smaller representation is obtained through the resulting principal components (PCs). The mathematical model behind PCA can be described as follows, where the matrix X is decomposed according to Equation 1 [10, 11].

$$X_{nxm} = U_{nxn} \Sigma_{nxm} V_{mxm}^T \tag{1}$$

Where n is the number of samples and m is the number of initial attributes that make up the data set of interest, X. The PCA assumption is that the first component should have the maximum variance explained and the second the variance not explained in the first component [10]. While Unxn e Vmxm are orthogonal and Σ is a diagonal matrix made up of the singular values [11]. Moreover, P is the weight matrix in which the elements in each column correspond to the coefficients of the linear combinations of the original variables, as shown in Equation 2 [10].

The results of applying PCA can be visualized using score plots, where the main relationships between the variables are clearly visible. With the different groupings of samples, similarities and differences, as well as trends and outliers, are identified.

Equation 2.

$$P = X \cdot V^{T} = X_{nxm} \cdot \begin{bmatrix} | & | & | & | \\ v_{1} & v_{2} & \cdots & v_{p} \\ | & | & | & | \end{bmatrix} = \begin{bmatrix} PC_{1,1} & PC_{1,2} & \cdots & PC_{1,q} \\ PC_{2,1} & PC_{2,2} & \cdots & PC_{2,q} \\ \vdots & \vdots & \ddots & \vdots \\ PC_{n,1} & PC_{n,2} & \cdots & PC_{n,q} \end{bmatrix}$$

Materials and Methods

To conduct this research, the state of the art on the subject was initially surveyed. After this, data on fuel quality in the state of Maranhão were acquired from the ANP's open database [12]. This data is obtained through the ANP's Fuel Quality Monitoring Program (PMQC).

The PMQC provides data on the analysis of the quality of diesel oil, hydrated ethanol, and gasoline. For this research, data were collected through the monitoring of the quality of ordinary diesel fuel (S10 and S500), with samples taken from various fuel stations in different municipalities in Maranhão throughout 2023.

After selecting the data, it was processed in accordance with the objectives of this work. Samples of ordinary S10 and S500 diesel oil and the tests corresponding to these samples were selected. These tests make up the group of variables used to apply the PCA technique. Figure 1 shows the characteristics analyzed by PCA in this study.

In Figure 1, the diagram shows the fuels analyzed and their respective tests. Samples with null data for the tests were excluded from the study. For the ordinary diesel oil samples selected, the following tests were considered as variables for the application of PCA: (1) distillation - 10%, (2) distillation - 50%, (3) specific mass at 20°C, (4) biodiesel content, (5) flash point, and (6) color. As the result of the color test is found in the data set as a word, rather than a number, for the PCA application, these results were replaced with numerical values (Table 1).

Table 1. Numerical correspondents assigned to the colors of the samples for the application of PCA in Matlab.

| Sample Color | Corresponding Number |
|--------------|-----------------------------|
| Yellow | 1 |
| Orange | 2 |
| Red | 3 |

After selecting the characteristics to be analyzed using PCA, a data matrix was assembled, with rows containing samples of standard diesel oil (S10 and S500) and columns containing the variables corresponding to these samples, forming a 775 × 7 matrix. With the matrix formed, an algorithm was implemented in MATLAB R2023b software (academic version) to apply PCA to the study dataset.

Results and Discussion

The application of the PCA technique to the data sets related to fuel quality in the state of Maranhão, as provided by the PMQC bulletins available on the ANP website, enabled the acquisition of results in the form of graphs and tables relating to the application of this technique to the data under study.

Table 2 presents the percentage of explained and accumulated variance values, as well as the number of principal components (PCs) obtained by applying the PCA method to the data for the S10 and S500 ordinary diesel fuel samples.

Figure 1. Diagram illustrating the characteristics analyzed by the PCA technique in this research.

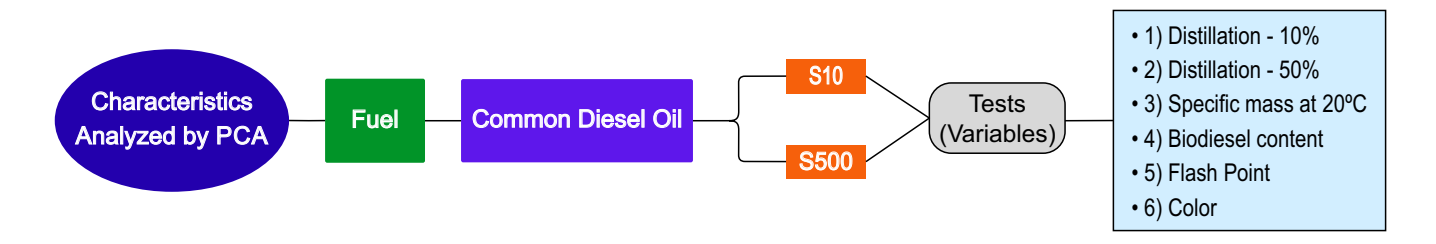


Table 2. Values, in percentages, of explained variance and accumulated variance obtained by applying PCA to the data referring to S10 regular diesel oils and S500 regular diesel oils.

| PC | Explained Variance (%) | Accumulated Variance (%) |
|----|---------------------------|-----------------------------|
| 1 | 36.68 | 36.68 |
| 2 | 18.25 | 55.63 |
| 3 | 14.53 | 70.16 |
| 4 | 13.18 | 83.34 |
| 5 | 11.26 | 94.61 |
| 6 | 5.39 | 100.00 |

According to Table 2, the 6 PCs obtained after applying PCA to the diesel oil samples are observed. Therefore, this number of PCs was modeled in the algorithm implemented in Matlab. One of the objectives of applying the PCA technique is to reduce the dataset's dimensionality without losing information. Therefore, when applying this technique, the result must show that the maximum number of PCs needed to represent the data set is lower than the number of original variables considered in the analysis [13]. Therefore, in this work, the application of PCA made it possible to reduce the number of variables analyzed, eliminating the PCs that presented lower explained variance. In this study, the explained and accumulated variances represent how the chemical information distributed in the original variables can be represented by a smaller number of variables, which are the PCs.

Thus, it was found that it is possible to eliminate PC6, which has the lowest explained variance (5.39%), and still have more than 94% of the data explained by the set of data analyzed with only the five remaining PCs, leading to a reduction in the dimensionality of these data. Furthermore, it is observed that the PC's that most contribute to the representation of the information contained in the common diesel oil data are the first four

PC's, which together represent more than 80% of the total variance of these data, with PC1 and PC2 being the ones that contribute most to this representation.

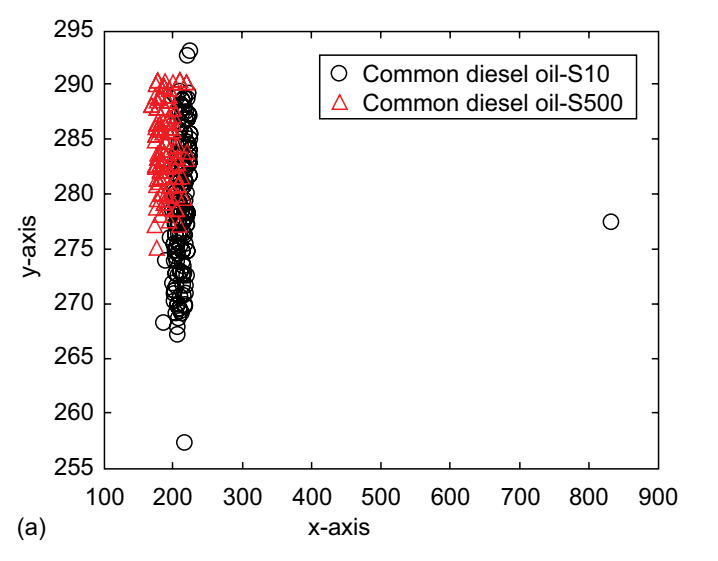
Figure 2 shows graphs with data from diesel oil samples before applying PCA (see Figure 2 (a)) and a biplot graph of scores and loadings of PC1 in relation to PC2 after applying PCA (see Figure 2 (B)).

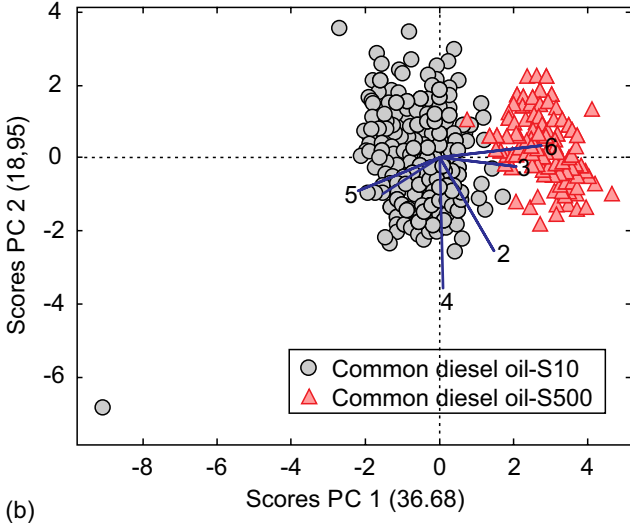
When comparing Figure 2(a) with Figure 2(b), it is observed that the application of PCA allows for a better visualization of the data related to the diesel oil samples. Furthermore, Figure 2(b) shows that after applying PCA, a grouping was obtained between data from samples of the same type and a separation between data referring to samples of standard diesel oil S10 and data referring to diesel oil samples standard S500.

The data for standard diesel oil S10, which is further removed from the vast majority of data (see Figures 2(a) and 2(b)), corresponds to the samples that, in the tests, exhibited an orange color, a distinct color from the others observed. Because, in the other samples, the S10 diesel oil presented a yellow color in the tests. S500 diesel oil was red in the tests.

Thus, it is observed that color was a determining variable for both the grouping and separation of data for standard diesel oil S10 and S500. Figure 2(b) presents data relating to diesel oil samples in the biplot graph of scores and loandings obtained after applying PCA, in which each symbol represents a sample of standard diesel oil S10 or S500 in relation to PC1 and PC2, which are the scores. The blue lines represent the weights of the analyzed variables (tests referring to these samples, which PMQC carried out) in relation to PC1 and PC2, which are the loandings. When analyzing the biplot graph, it is essential to consider that the relevance of the variables analyzed in this study can be measured by the size and direction of loadings (blue lines on the biplot graph). In this case, the biodiesel content variable has a greater weight in relation to the PC2 axis. On the other hand, the color variable, represented

Figure 2. Graphs with data from standard diesel oil samples S10 and S500: (a) graph with data before applying PCA; (b) biplot graph of scores and loandings with the data after applying PCA.





in Figure 2(b) by line 6, has a greater weight in relation to the PC1 axis.

The PCs are the new variables obtained through the application of PCA, and they are capable of explaining a certain amount of characteristics of the analyzed dataset, in this case, the samples of standard diesel oil S10 and S500. According to the explained and accumulated variances presented in Table 2, it is observed that PC1 and PC2 explain over 50% of the data set analyzed in this study. Thus, the variables biodiesel content and color contribute more to explaining the variations present in the data from the standard diesel oil samples S10 and S500.

Analyzing Figure 2(b), it is possible to observe correlations between the variables being analyzed. As the straight lines represent the original variables analyzed, it is observed that there is a correlation between the variables biodiesel content (4) and flash point (5) in relation to the color variable (6). This correlation can be observed, as the straight lines have an angle of almost 180° between them, indicating that the variables related to these straight lines are correlated and inversely proportional to each other [13].

According to the results obtained, it is noted that research carried out on the quality of S10 and

S500 diesel in the state of Maranhão is of great relevance both for the state, where the fuel sector plays a crucial role in energy supply, and for assessing fuel quality, which is essential to ensure engine efficiency, reduce atmospheric emissions, and protect public health. The application of Principal Component Analysis (PCA) enables you to monitor diesel quality more precisely, identifying patterns and trends that help classify and control the fuel, thereby guaranteeing that end consumers receive quality fuel.

Conclusion

The use of the Principal Component Analysis technique is relevant when we want to simplify the analysis of large datasets. In this study, the application of the PCA technique to data from samples of standard diesel oil (S10 and S500) allowed for an exploratory analysis of several variables that contribute to determining the quality of this fuel. We observed that applying PCA to data from diesel oil samples enabled a reduction in the dataset's dimensionality without loss of information by extracting the main components. Therefore, the first four PCs are capable of representing the variance of more than 80% of the studied dataset.

Furthermore, the color variable was highly relevant for analyzing these results, as it is a crucial factor in determining the groupings and separations between the analyzed diesel oil data, in addition to correlating with other variables studied, such as biodiesel content. Therefore, color can help in determining possible patterns existing between the characteristics of the data referring to samples of standard diesel oil S10 and S500.

Therefore, the application of PCA provided both data dimensionality reduction and the identification of groupings and correlations between the analyzed variables, thus allowing the objective of this work to be achieved. This demonstrates that this technique can contribute to the ongoing improvement of programs such as the ANP's PMQC, thereby enhancing the quality of fuels sold at stations not only in the state of Maranhão but also throughout Brazil.

For future work, it is proposed to apply the Principal Component Analysis technique to other fuels, such as gasoline and ethanol, to verify the accuracy of this technique in these additional fuels and in a larger dataset.

References

- Brasil. Anuário Estatístico Brasileiro do Petróleo, Gás Natural e Biocombustíveis: 2023. Rio de Janeiro: Agência Nacional do Petróleo, Gás Natural e Biocombustíveis; 2006.
- 2. Oliveira EP, et al. Investigação do teor de água no biodiesel utilizado na composição do diesel B comercializado por uma distribuidora de combustíveis em Manaus/AM. Braz J Dev. 2021;7(9):89663-80.
- Ribeiro CB, Schirmer WN. Panorama dos combustíveis e biocombustíveis no Brasil e as emissões gasosas decorrentes do uso da gasolina/etanol. BIOFIX Sci J. 2017;2(2).
- Instituto Brasileiro de Petróleo (IBP). Boletim do ciclo diesel 2024 [Internet]. Rio de Janeiro: IBP; 2024. Available from: https://www.ibp.org.br/personalizado/

- uploads/2024/03/boletim-ciclo-diesel-i-marco-de-2024-9.pdf
- 5. Moura HO, et al. Advances in chemometric control of commercial diesel adulteration by kerosene using IR spectroscopy. Anal Bioanal Chem. 2019;411:2301-15.
- 6. Agência Nacional do Petróleo, Gás Natural e Biocombustíveis (ANP). Boletim de biocombustíveis e qualidade de produtos 2022b [Internet]. ANP; 2022. Available from: https://www.gov.br/anp/pt-br/centraisde-conteudo/publicacoes/boletins-anp/arquivosboletim-de-biocombustiveis-e-qualidade-de-produtos/ boletimsbq2022.pdf
- Agência Nacional do Petróleo, Gás Natural e Biocombustíveis (ANP). Anuário Estatístico Brasileiro do Petróleo, Gás Natural e Biocombustíveis 2021a [Internet]. ANP; 2021. Available from: https://www.gov.br/anp/pt-br/centrais-de-conteudo/publicacoes/anuario-estatistico/arquivos-anuario-estatistico-2021/anuario-2021.pdf
- 8. Blanco ALP, Carauta ANM. Análise de componentes principais aplicada à espectroscopia no infravermelho de misturas de diesel e biodiesel: estudos de casos. Rev Souza Marques. 2018;18(37):9-44.
- 9. Alves WF, et al. Análise multivariada dos parâmetros físico-químicos da gasolina "tipo C" comercializada no Vale do Juruá-Acre. South Am J Basic Educ Tech Technol. 2019;6(1).
- Correa C. Metodologias analíticas para avaliar a biodegradabilidade do diesel, biodiesel e blendas B10 [tese]. Porto Alegre: Universidade Federal do Rio Grande do Sul; 2021.
- Parente LER. Análise exploratória de perfilagem acústica para avaliação da qualidade de cimento com simulações computacionais. Rio de Janeiro: Departamento de Engenharia Mecânica, Pontificia Universidade Católica; 2022.
- 12. Agência Nacional do Petróleo, Gás Natural e Biocombustíveis (ANP). PMQC – programa de monitoramento da qualidade dos combustíveis 2023c [Internet]. ANP; 2023. Available from: https://www. gov.br/anp/pt-br/centrais-de-conteudo/dados-abertos/ pmqc-programa-de-monitoramento-da-qualidade-doscombustiveis
- 13. Folli G, et al. Tutorial para aplicação didática de quimiometria em software gratuito Parte I: análise de componentes principais em dados de infravermelho médio e propriedades físico-químicas de amostras de petróleo. Rev Ifes Ciênc. 2023;9(1):1-14.

The Importance of Conducting Tests to Ensure the Proper Functioning of Chemical Injection and Lift Gas Valves

Carlos Eduardo Santos Cruz^{1*}

**ISENAI CIMATEC, Brazil

This work aims to highlight the importance of Chemical Injection Test Units and Check Valve Test Benches for offshore operations, which involve high costs. The objective is to ensure the efficient and safe operation of lift gas valves and chemical injection valves through leak-tightness, performance, and durability tests. This testing circuit follows a specific sequence to guarantee its effectiveness and safety, resulting in the delivery of a technical report presenting the obtained results.

Keywords: Pre-Salt. Valves. Test.

Most oil wells at the beginning of production have enough energy for the fluids from the deposits to reach the surface naturally. This occurs due to the high pressure in the well, which, after drilling, allows the oil to rise spontaneously. Over time, as the well continues to produce fluids from the reservoir, the bottom pressure tends to decrease, becoming insufficient for the natural elevation of the oil. It becomes necessary to implement artificial elevation methods in the production column [1].

LIFT gas is one of the widely used methods for lifting oil, especially in wells that lack sufficient pressure for natural flow or require increased production. This technology involves injecting pressurized gas into the lower part of the production pipeline to maintain or increase the well's potential. The injected gas mixes with the produced fluid, significantly reducing its density and consequently reducing the pressure necessary to lift the oil at the bottom of the well [2].

In cases of oil extraction in deep waters, such as the Brazilian pre-salt, paraffin waxes can form, which are the primary components of the solids encrusted by crude oil in production pipes. This occurrence reduces the diameter of the production pipe, causing significant losses in oil extraction.

Received on 12 May 2025; revised 21 July 2025. Address for correspondence: Carlos Eduardo Santos Cruz. Av. Orlando Gomes, 1845, Piatã, Salvador, Bahia, Brazil. Zipcode: 41650-010. E-mail: carlos.cruz@fieb.org.br.

J Bioeng. Tech. Health 2025;8(4):339-342 © 2025 by SENAI CIMATEC University. All rights reserved.

In more extreme cases, it can block the flow and interrupt production.

Paraffin can precipitate when there is a change in the oil's composition, a reduction in pressure, or mainly due to the temperature difference between the well and the platform in deep waters. The oil is at a temperature of approximately 60 °C, while the external environment is at around 5 °C, resulting in rapid cooling [3].

The difficulty of access aggravates the problem of paraffin crystallization in deepwater production pipes. When this occurs, it results in significant production losses, and the maintenance costs are high due to the required downtime for carrying out the necessary repairs. Given this scenario, this work aims to bring knowledge about the importance of chemical injection test units and check valve test benches for offshore operations. These operations are carried out in difficult-to-access locations, at high costs and under high pressures, making it crucial to ensure that the LIFT gas valves and Chemical Injection valves operate effectively and safely. This is achieved through leak-tightness, performance, and durability tests conducted on these units, thereby guaranteeing their proper functioning.

Materials and Methods

The method used in this work to highlight the importance of test units in ensuring the reliability of valve usage involved a comparative study based on several scientific works. This study addressed

the difficulty in extracting oil from offshore wells that have been in operation for a long time in deep waters, such as the Brazilian pre-salt, where the pressure is no longer sufficient for the natural rise of oil. It is necessary to use extraction methods, such as artificial lift, as in the case of gas lift valves. Paraffin wax encrustations inside the production pipes were also analyzed, which formed due to the temperature difference between the well and the platform. This is exacerbated by the difficulty of access in deep waters, necessitating the use of chemical injection valves to remove them.

Based on this information, the importance of the chemical injection valve test units and the check valve test bench was highlighted in terms of conducting tightness, durability, and performance tests to ensure their proper functioning, given the conditions encountered during activities in the Brazilian pre-salt.

The method used in the test units aims to highlight the importance of these installations and ensure the reliability of valve use. This process follows a test circuit that begins with a planning phase, followed by the receipt of the test demand to be carried out. Then, the requested operational scope is aligned with the units' capabilities, resulting in the preparation of the test matrix. Finally, detailed work instructions are prepared to carry out operational tests (Figure 1).

Results and Discussion

The Check Valves Test Bench is a unit designed to perform tightness tests on retention devices

Figure 1. Description of the test planning phase.

present in gas lift valves (GLV) and chemical injection valves (CIQ). To assess tightness, an inert gas is used, such as Nitrogen (N₂), Helium (He), or another compressive gas at room temperature, with a pressure of 100 psi ± 10 psi. This pressure is maintained for at least 10 minutes at room temperature. Tightness is assessed by measuring the leak rate, observing the pressure drop recorded on the pressure gauge or pressure transmitter.

The Chemical Injection Valve Test Unit is an industrial plant that utilizes demineralized water at room temperature to conduct a test circuit evaluating the performance of VIQ under various conditions.

To carry out operational tests on these units, a specific sequence is followed to ensure their effectiveness and safety, such as:

- 1. Initially, the tightness test of the retention devices is conducted on the check valve test bench to verify the functioning of the retention mechanism at the beginning of the test circuit [4].
- 2. Following this, a brief tightness test is performed. This involves checking the performance of the chemical injection valves during the opening and closing phases at the start of the test circuit. After subjecting the component to a liquid flow, counter pressure is applied to the valve discharge to ensure no leakage occurs. Variables such as flow rate, pressure, and time are controlled during these tests to assess the results [4].
- 3. Subsequently, the performance test is carried out to evaluate the valve's capacity under simulated operating conditions. The performance curve is used to assess whether the valve has satisfactory performance before the durability test begins [4].

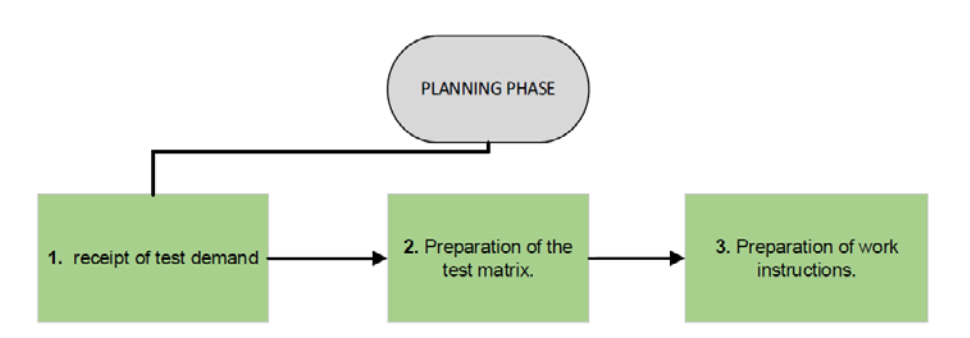
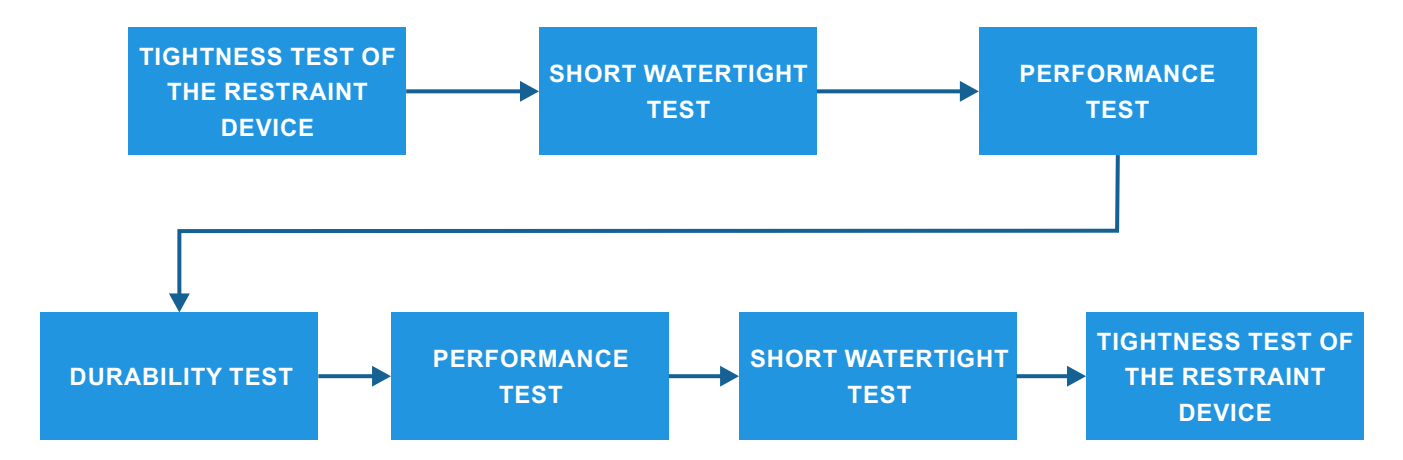


Figure 2. Operational test circuit.



- 4. Soon after, a durability test is carried out to verify the valve's durability after continuous use. This ensures that the valve can withstand prolonged operating conditions without failure, taking into account the variables of flow, pressure, and time to evaluate the results [4].
- 5. Then, the performance test is carried out again to evaluate the valve's capacity in simulated operating conditions, using the performance curve to assess whether the valve maintains its performance after the durability test, with flow and time as controlled variables [4].
- 6. Next, the tightness test is performed again to assess the valve's behavior during opening and closing at the conclusion of the test circuit. After subjecting the component to liquid flow, counter pressure is applied to the valve discharge to ensure there are no leaks following the durability and performance tests. Controlled variables, including flow rate, pressure, and time, are used during the tests to evaluate the results [4].
- 7. Finally, the tightness test of the retention device is repeated on the check valves test bench, to ensure that the retention mechanism is working correctly after the sequence of tests carried out there [4].

The test circuit is conducted according to the sequence in Figure 2.

At the end of the test circuit carried out in the units, a technical report is prepared to present

the results obtained. Furthermore, the entire acquired database is delivered to the test requester.

Conclusion

This study highlights the importance of testing chemical injection valves (CIVs) and gas lift valves (GLVs) used in offshore oil extraction operations. As time passes and oil wells lose their natural pressure, reliance on artificial lifting methods, such as gas lift, becomes increasingly indispensable. These methods, along with the injection of chemicals to manage issues such as paraffin crystallization, ensure continuous and efficient production.

The study highlights the tests necessary to ensure the adequate performance, tightness, and durability of these valves under high-pressure conditions, typical of deep-water environments, such as the Brazilian pre-salt fields. Test units, including the Check Valves Test Stand and Chemical Injection Valve Test Unit, play a key role in verifying the reliability and safety of valves through a structured test circuit.

This study reinforces that without these tests, the operational integrity of the valves cannot be guaranteed, which could lead to significant production losses and high maintenance costs. Ensuring valves operate effectively and safely is crucial to maintaining productivity and minimizing downtime in the demanding conditions of offshore oil extraction.

By implementing these testing methodologies, operators can significantly mitigate risks and improve the longevity and performance of their equipment, thus ensuring more stable and profitable operations.

References

- Thomas JE. Fundamentos de Engenharia de Petróleo. 2ª ed. Rio de Janeiro: Interciência; 2004. Disponível em: http://www.escolaelectra.com.br/alumni/biblioteca/ Fundamentos da Engenharia do Petroleo.pdf.
- Santos GS. Abordagem para o problema de gás lift com quantidade de petróleo pré-planejada utilizando metaheurísticas [Monografia de Graduação]. Natal (RN): Universidade Federal do Rio Grande do Norte – UFRN; 2022.
- 3. Santana EA. Avaliação da temperatura de cristalização da parafina em sistemas: parafina, solvente e tensoativo

- [Dissertação de Mestrado]. Natal (RN): Universidade Federal do Rio Grande do Norte UFRN, Programa de Pós-graduação em Engenharia Química; 2005.
- Petrobras. Especificação Técnica ET-3000.00-1244-220-P9D-001. Revisão B. Válvulas de Gás Lift. Available at: https://canalfornecedor.petrobras.com.br/documents/10591749/12053533/valvula_de_gas_lift.pdf?download=true.
- 5. Sabóia GO. Equipamentos submarinos para produção de petróleo e gás. Disponível em: https://www.seaerj.org.br/pdf/equipetro.pdf.
- 6. Petrobras. Pré-sal. Disponível em: http://www.petrobras.com.br/pt/nossas-atividades/areas-de-atuacao/exploracao-e-producao-de-petroleo-e-gas/pre-sal/.
- Silva DYC, Franciss R. A completação de poços de petróleo – uma revisão do planejamento das operações e equipamentos. Petrópolis (RJ): Centro de Engenharia e Computação, Universidade Católica de Petrópolis; 2019.

Hydrological Rainfall-Runoff Modeling Using the WRF-Hydro Model

Carolina Sacramento Vieira^{1*}, Diogo Nunes da Silva Ramos¹, Antônio José da Silva Neto², Davidson Martins Moreira¹

'SENAI CIMATEC University; Salvador, Bahia; State University of Rio de Janeiro; Rio de Janeiro, Rio de Janeiro

This study aims to analyze the hydrological behavior of the Negro River basin, part of the greater Amazon Basin, through the simulation of rainfall and streamflow using the mesoscale Weather Research and Forecasting (WRF-Hydro) model. The premise is that streamflow simulation is a crucial tool for predicting environmental impacts, enabling timely decision-making and contributing to the sustainable management of river basins. Simulations were conducted with a spatial resolution of 1 km and a 100 m channel network, covering the period from January 1st to January 31, 2024. It was possible to evaluate rainfall and streamflow distribution, exploring the behavior of variables in the region. Furthermore, the accuracy of streamflow simulation at each river gauging station is directly influenced by the temporal distribution of rainfall simulated within the drainage network. The simulations proved satisfactory, highlighting the model's potential to support studies and environmental analyses. Keywords: WRF-Hydro. Rainfall. Streamflow.

The Metropolitan Region of Manaus, also known as Greater Manaus, is one of the most populous and economically relevant areas in Brazil. The capital of Amazonas state, Manaus, is located on the left bank of the Negro River, covering a territorial area of 11,401 km². Situated in the Negro River Basin, in the heart of the Amazon, the municipality frequently experiences extreme rainfall events that result in floods and inundations, directly impacting urban infrastructure, mobility, and the quality of life for its population. These events, intensified by climate change and unplanned urban growth, reinforce the need for hydrometeorological monitoring and the implementation of mitigation strategies to reduce socioeconomic and environmental impacts.

One way to analyze the atmospheric events that cause severe and extreme weather conditions is to use numerical atmospheric modeling [1]. The numerical modeling proposed in this article, by coupling hydrological modeling with numerical weather prediction, aims to represent

Received on 17 May 2025; revised 27 July 2025. Address for correspondence: Carolina Sacramento Vieira. Av. Orlando Gomes, 1845, Piatã, Salvador, Bahia, Brazil. Zipcode: 41650-010. E-mail: carolinavieira265@gmail.com. Original extended abstract presented at SAPCT 2025.

J Bioeng. Tech. Health 2025;8(4):343-346 © 2025 by SENAI CIMATEC University. All rights reserved.

the hydrological processes of the land surface [2]. The main model of this type, the Weather Research and Forecasting Model (WRF-Hydro), which is the focus of this work, was initially designed as a coupled framework to facilitate the integration between the WRF model and terrestrial hydrological components [3].

The WRF-Hydro modeling system was developed to simulate hydrometeorological variables, floods, and the spatial distribution of water resources [4], to provide an enhanced numerical tool to address global needs in water resource planning, environmental impact assessment, risk prediction, and mitigation [5].

Within this context, the primary objective of this study is to assess the model's ability to accurately represent the hourly rainfall—runoff behavior in the Negro River basin in the Amazon, specifically in Manaus, during the period from January 1 to January 31, 2021. The simulations were conducted with a spatial resolution of 1 km and a 100 m channel network.

Materials and Methods

Simulations with the WRF model (version 3.6) were conducted to generate the initial conditions of soil moisture, soil temperature, soil water content, and atmospheric forcing, among other variables, for the WRF-Hydro model. The model

was configured with three nested grids with spatial resolutions of 9, 3, and 1 km (Figure 1). The first grid covers part of the Amazon Basin and the entire Negro River Basin (D01), while the second grid includes the Lower Negro River region (D02). Finally, the domain of interest (D03), with 1 km resolution and 50 vertical levels, encompasses the city of Manaus.

The simulations were initialized at 00 UTC on January 1, 2021, and extended until 18:00 UTC on January 31, 2021. The physics options adopted, which remained unchanged for all simulations, were: the WRF Single-Moment 6-class scheme for microphysics, the Grell-Freitas cumulus parameterization, the Mellor-Yamada Nakanishi and Niino Level 2.5 PBL scheme, the RRTMG shortwave and longwave radiation schemes, and the Noah land-surface model. The parameterization of aerosol-radiation interactions followed Ruiz-Arias and Thompson's water- and ice-friendly scheme.

Figure 1. Location of the domains.

Results and Discussion

Figure 2 presents the hyetograph and hydrograph for two stations located in the drainage network of each river, based on the arithmetic mean of accumulated daily rainfall at each WRF grid point and on the daily streamflows simulated by WRF-Hydro, considering the same analysis periods.

The two selected stations present distinct characteristics in terms of streamflow behavior [6,7]. For both stations, rainfall values fluctuate throughout the month, with notable peaks in specific periods. In the Rio Preto da Eva station graph, streamflow peaks are more pronounced and occur shortly after rainfall events. In contrast, the Novo Airão station exhibits a more gradual streamflow behavior, suggesting a dampened hydrological response to rainfall events.

At Rio Preto da Eva, streamflow peaks mostly ranged between 125 and 150 m³/s, reaching a maximum above 150 m³/s. In contrast, Novo Airão

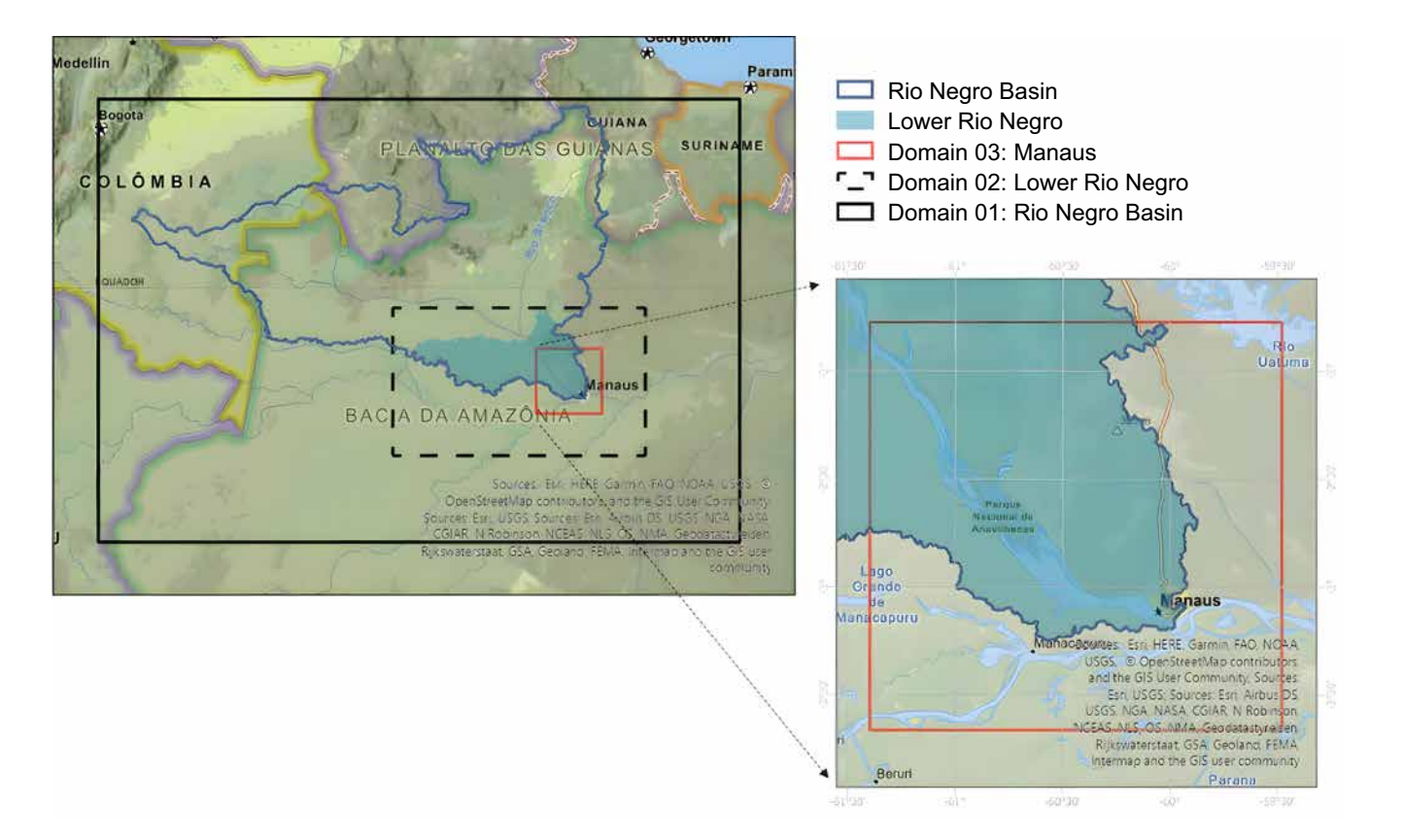
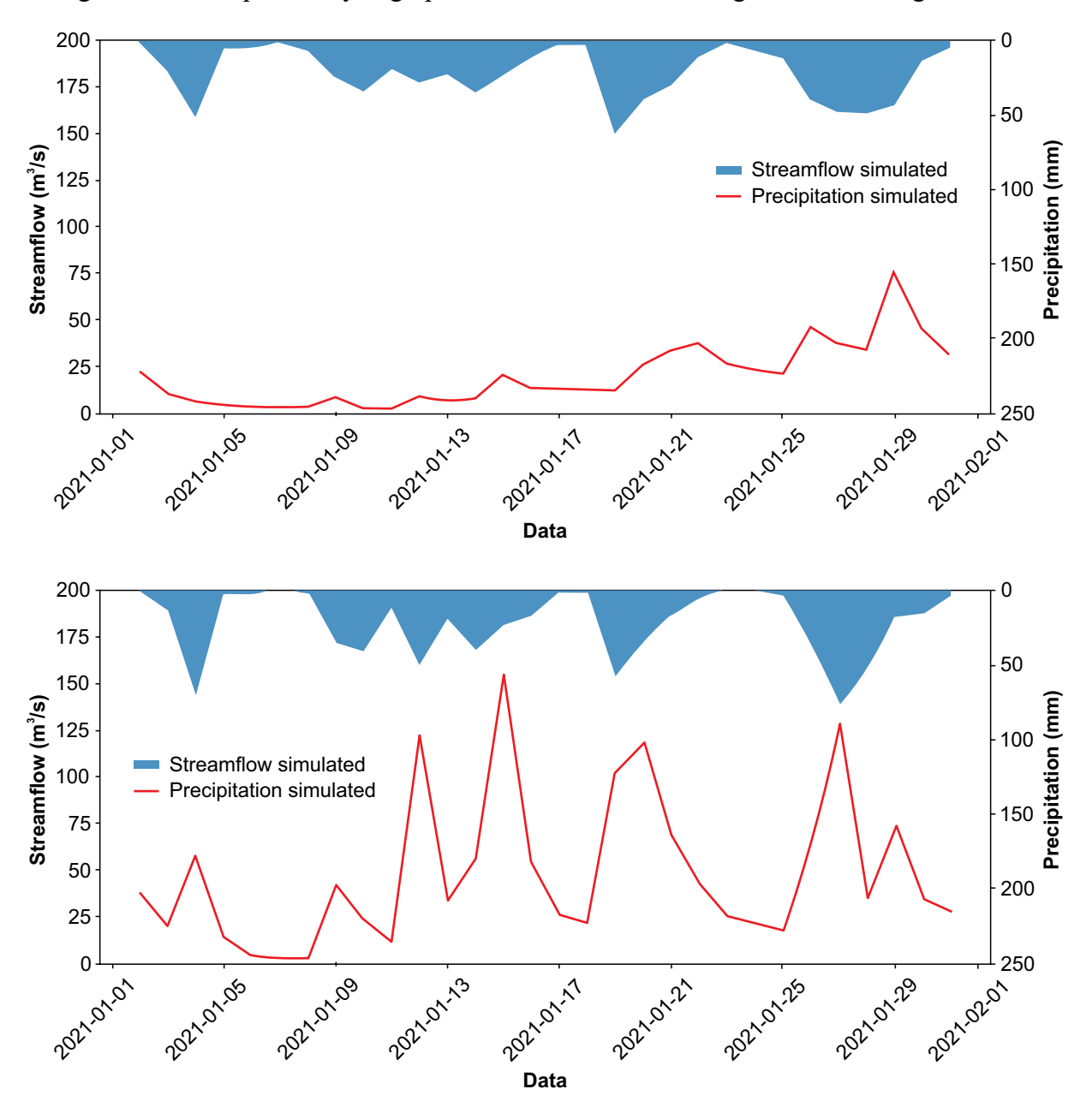


Figure 2. Hydrographs simulated by WRF-Hydro at the stations (a) Novo Airão and (b) Rio Preto da Eva, along with their respective hyetographs simulated within the Negro River drainage network.-



showed a more gradual pattern, with only one peak of 75 m³/s at the end of the period, despite similar rainfall volumes.

This behavior may indicate differences in infiltration and surface runoff modeling, suggesting that the terrain may have a lower water absorption capacity or that the basin has characteristics that favor rapid responses to intense rainfall.

Conclusion

This study aimed to analyze the temporal distribution of rainfall and streamflow in the Negro River basin, highlighting the model's potential to support environmental studies and analyses in the region. The results confirmed the correlation between rainfall and streamflow.

The comparison between hydrographs and their corresponding hyetographs illustrates rainfall as the most important factor for streamflow simulation. Furthermore, simulating streamflow behavior in a given region is a crucial tool for predicting environmental impacts, enabling timely decision-making and contributing to the sustainable management of river basins. Future research should encompass more extended periods of analysis and incorporate observational data to assess model accuracy.

Acknowledgments

The authors thank the SENAI CIMATEC Supercomputing Center for the computational infrastructure required to run the model and the Fundação de Amparo à Pesquisa do Estado da Bahia (FAPESB) for financial support.

References

 Da Cunha Luz Barcellos P, Cataldi M. Flash flood and extreme rainfall forecast through one-way coupling

- of WRF-SMAP models: natural hazards in Rio de Janeiro state. Atmosphere. 2020;11(8):834.
- Liu Y, Li H, Tian F, Zhang Q, Xu Y, Yang L, et al. Parameter sensitivity analysis of the WRF-Hydro modeling system for streamflow simulation: a case study in semi-humid and semi-arid catchments of northern China. Asia Pac J Atmos Sci. 2020;1–16.
- 3. Gochis DJ, Barlage M, Dugger A, FitzGerald K, Karsten L, McAllister M, et al. Coupled WRF/WRFHydro V5 test case user guide (version 5.0). NCAR Technical Note. 2018. 107 p.
- 4. Sun M, Liu Z, Guo Y, Wang C, Ma J, Chen X. Evaluation of flood prediction capability of the WRFHydro model based on multiple forcing scenarios. Water. 2020;12(3):874.
- 5. Maciel JSC, Faria S, Bentes C, de Souza EB, Ramos AM, Mota MAM, et al. Flood forecast in Manaus, Amazonas, Brazil. WIT Trans Built Environ. 2020:194:63–72.
- Dantas da Silva Júnior JR et al. Feasibility analysis on the construction of a web solution for hydrometeorological forecasting considering water body management and indicators for the SARS-COV-2 pandemic. AI Perspectives. 2021; v. 3, n. 1, p. 4.
- 7. Silva DG et al. WRF-Hydro for Streamflow Simulation in the MATOPIBA Region within the Tocantins/Araguaia River Basin—Brazil: Implications for Water Resource Management. Water. 2023; v. 15, n. 22, p. 3902.

Gamification in Electrical Energy Monitoring

Patrick Antonio Morelo^{1*}, Jorge Anderson de Jesus Santos², Pericles Vinicius Cerqueira Marques, Rebeca Oliveira dos Santos², Paulo Henrique de Jesus Santana², Marcus Vinicius Mendes²

¹Federal University of Santa Catarina; Florianópolis, Santa Catarina; ²SENAI CIMATEC University; Salvador, Bahia, Brazil

The project aimed to develop, in 8 months, a gamified digital platform for monitoring electrical parameters. A flexible user interface was designed to accommodate various usage requirements. The innovative factor lay in the application of gamified workflows, which facilitated the user experience and promoted greater engagement. In the current technological scenario, apps and digital platforms play a crucial role in many corporate sectors. Several service and industrial sectors have explored this trend to improve customer experience and optimize business management. In this project, the results culminated in the optimization of graphical visualizations on the platform, enabling detailed analyses at any time. The development also included gamification resources, such as a point system converted into currency (DeepCoin) and interactive screens with user-friendly navigation. Keywords: Gamification. Energy Consumption. Electric Power. Conscious Electricity Consumption.

Digital transformation has driven significant innovations across sectors, making gamification a promising strategy to enhance user experience and optimize system management. In the context of monitoring electrical parameters, the application of gamified elements can increase engagement, ease of use, and efficiency in data analysis [1,2].

This project aimed to develop, over an 8-month period, a gamified platform for monitoring electrical parameters, called Deep Monitor. The proposal focused on creating a flexible and customizable interface that incorporates interactive resources, encouraging active user participation through a point-and-reward system.

Additionally, the project encompassed conceptual research on gamification in the context of energy measurement and consumption, interface redesign implementation, solution architecture enhancements, and the development of additional functionalities. This expanded abstract presents the main challenges, methodologies, results, and

Received on 24 May 2025; revised 21 July 2025.

Address for correspondence: Patrick Antonio Morelo. Rua Eng. Agronômico Andrei Cristian Ferreira, s/n - Trindade, Florianópolis, Santa Catarina, Brazil. Zipcode: 88040-900. E-mail: patrick.a.morelo@gmail.com.

Original extended abstract presented at SAPCT 2025.

J Bioeng. Tech. Health 2025;8(4):347-348 © 2025 by SENAI CIMATEC University. All rights reserved.

conclusions obtained during the development of the platform.

Materials and Methods

The Deep Monitor platform was developed using lean inception (Paulo Caroli, 2017) and DIP&T, SENAI CIMATEC's product development and innovation methodology. The project followed five stages: (1) conceptual and informational research; (2) development; (3) implementation; (4) user testing; and (5) validation.

A literature review was conducted on gamification in energy monitoring, analyzing intrinsic and extrinsic approaches, and reviewing competitor platforms to identify trends and opportunities. Lean inception [3] was applied to understand technical requirements and user needs, using shared kanban boards segmented into critical functions and product features.

Conceptual design produced preliminary layouts and improved graphical interfaces, optimizing user navigation and developing a billing system for financial visualization of consumption. Due to the rigid software architecture, flexibility was limited; however, a future-scalable concept was proposed.

Gamification features were mapped using the Game Model Canvas (GMC) [4], defining points, leaderboards, achievements, virtual currency (DeepCoin), and rewards. During the implementation stage, gamified flows were integrated to provide tips, promote competition, track energy savings through rankings, and assist users in achieving their consumption goals. Usability tests were conducted [5] using the Task Success Rate (TSR) and System Usability Scale (SUS) metrics. Participants aged 20–40, from administrative, engineering, marketing, and design fields, performed tasks under controlled conditions.

Results and Discussion

The improvements led to a more intuitive and efficient platform, reducing cognitive load. Gamification research-informed redesigns of user flows, functionalities, and navigation. Code refactoring solved existing issues. Usability tests spanned three days:

Day 1: 2 users, TSR \approx 55.6%. Some obstacles with incomplete tasks.

Day 2: 3 users, TSR \approx 59.3%. Better performance overall.

Day 3: 3 users, TSR \approx 33.4%. Decline attributed to higher task complexity.

Post-test surveys praised the interface but noted technical terms that required clarification and steps that required external assistance. These insights were compiled into recommendations. The findings confirm that gamification and improved interface design enhanced user experience and platform efficiency.

Conclusion

The Deep Monitor development enhanced the interface structure and visualization of energy

monitoring data, making interpretation more transparent and intuitive. Gamified features such as point-to-currency conversion (DeepCoin) and interactive navigation provided a more immersive user experience.

The project demonstrated that gamification increases engagement and usability in electrical monitoring. The redesign, code refactoring, and testing improved usability and efficiency. The implementation of a documentation and billing system added value, making data analysis more accessible. The project achieved its goals and left a roadmap for future improvements.

Acknowledgements

The authors thank SENAI CIMATEC for the research scholarships.

References

- 1. Huseynli B. Gamification in energy consumption: a model for consumers energy saving. Int J Energy Econ Policy. 2024;14(1):312-20.
- Cravinho J, Lucas R, Brito M, Albuquerque DP, Mithoowani U, Mateus NM. Energy gamification: design and development of a user interface tool to upgrade social experience and energy literacy. Open Res Eur. 2023;2:130.
- 3. Caroli P. Lean inception. São Paulo: Caroli.org; 2017.
- 4. Keshmiri F. The effect of gamification in entrepreneurship and business education on pharmacy students' self-efficacy and learning outcomes. BMC Med Educ. 2025;25(1):491.
- 5. Albert B, Tullis T. Measuring the user experience: collecting, analyzing, and presenting usability metrics. Amsterdam: Newnes; 2013.
- 6. Cummins RA, Gullone E. Why we should not use 5-point Likert scales: the case for subjective quality of life measurement. In: International Conference on Quality of Life in Cities; 2000; Singapore. p. 74-93.

Roadmap for the Hydrogen Supply Network in Brazil

Lucca R. S. A. Bastos^{1*}, Leonardo O. S. Santana², Gerhard Ett²

**ISENAI CIMATEC University; Salvador, Bahia, Brazil

Brazil holds significant potential to become a leader in the global energy transition due to its predominantly renewable energy matrix. Hydrogen, particularly when produced from renewable sources, emerges as a crucial energy vector to decarbonize hard-to-electrify sectors, such as heavy transport, petrochemicals and refining, fertilizer production, and the steel industry. However, establishing a hydrogen supply network in Brazil faces substantial challenges. This project aims to create a roadmap for the hydrogen refueling network in Brazil, aligning economic and governmental interests. It is a strategic initiative to ensure that the country not only follows but leads the transition to a hydrogen economy, promoting sustainable economic growth and energy security. Keywords: Hydrogen. Roadmap. Energy Matrix.

The transportation sector in Brazil accounts for around 20% of global CO₂ emissions, one of the main greenhouse gases, without considering other harmful pollutants [1]. Due to high emissions, the Brazilian market has gradually introduced cleaner fuels, such as hydrogen, produced from renewable sources, playing an important role in reducing atmospheric pollution.

From this perspective, different methods of production were studied, such as natural gas steam reforming and electrolysis supported by solar energy (photovoltaic and photothermal processes), as well as water electrolysis [2]. For storage, the LOCHs technology was analyzed, which consists of storing H₂ in aromatic substances [3]. For distribution, coupling hydrogen with natural gas was considered to increase safety during transportation [4].

The roadmap design relies on this knowledge. A roadmap acts as a guide, a compass leading teams through sequential steps until the final goal. Using software such as ClickUp and Lucidchart [5], the study mapped optimal routes to achieve objectives, considering the integration of new technologies and hydrogen properties. The focus is on heavy

Received on 12 May 2025; revised 26 July 2025. Address for correspondence: Lucca R. S. A. Bastos. Av. Orlando Gomes, 1845, Piatã, Salvador, Bahia, Brazil. Zipcode: 41650-010. E-mail: lucca.bastos@aln.senaicimatec. edu.br.Original extended abstract presented at SAPCT 2025.

J Bioeng. Tech. Health 2025;8(4):349-351

transport, especially trucks, which emit significant amounts of CO₂, contributing to climate change.

Materials and Methods

To design a hydrogen roadmap, beyond the production, storage, and distribution stages, the study reviewed the autonomy of hydrogen, diesel, and electric vehicles, as well as the location and spacing of fueling stations.

A table (Table 1) was created to support a case study in the Northeast region, considering the main highways, refineries, and distribution points, with data provided by Google Maps.

Table 1. Comparison table.

| | Gas Station | Distance |
|---------------|-------------|----------|
| Fuel | 44054 | 150 km |
| Electric Fuel | 10622 | 445 km |

Case Study

A field study was conducted between Salvador and Barreiras, analyzing the following variables: price, distance traveled, fuel consumption, and CO₂ emissions. The case compared five trucks powered by hydrogen and diesel.

Due to the high cost of hydrogen, sold by kilogram, a conversion to liters was necessary. Results showed a consumption of 11.2 L/km.

^{© 2025} by SENAI CIMATEC University. All rights reserved.

Diesel trucks, in contrast, consume between 1.5 L/km and 4 L/km, with considerable CO₂ emissions. The study also considered the three sustainability pillars: economic, environmental, and social.

Using these data, the team simulated a fleet transition from diesel to hydrogen along the Salvador–Barreiras corridor. A second table (Table 2) was developed, based on the averages obtained.

The equation used to calculate fuel consumption was:

$$Consumption = \frac{Distance\ traveled}{Fuel\ consumed}$$
 [6]

Additional data sources included InsideEVS (hydrogen pricing), Petrobrás (diesel pricing), and SigaVerde (CO₂ emission calculations).

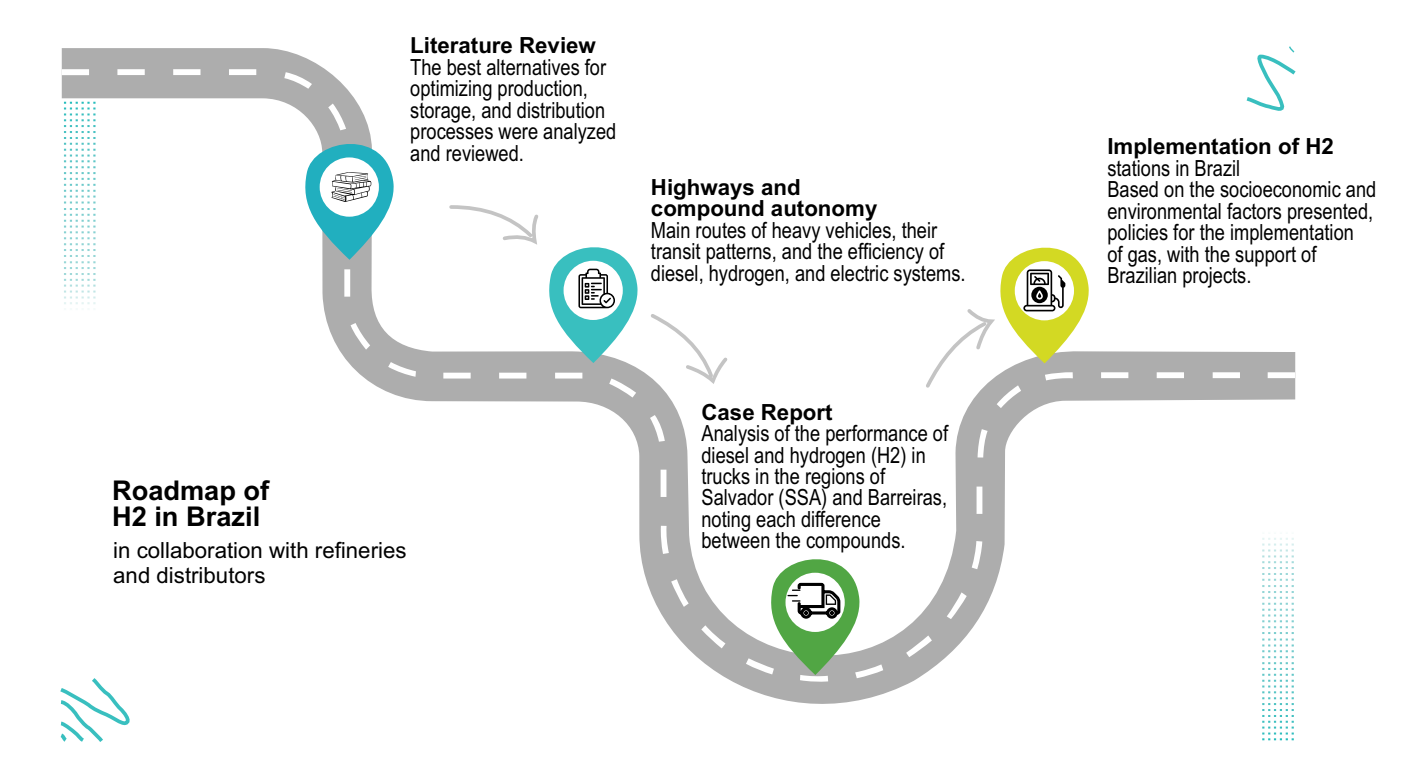
Results and Discussion

The final roadmap was built considering economic challenges (e.g., the high commercial value of hydrogen, making it scarce among heavy vehicles), environmental advantages (zero greenhouse gas emissions), and infrastructure (station placement between Salvador and Barreiras).

Table 2. Case study table.

| Gas Station | Price (R\$) | Distance | Consume | CO ₂ Emission (kg/L) |
|--------------------|-------------|----------|------------|---------------------------------|
| Fuel | 6.44 | 862 | 215.5 km/L | 3.2 |
| Hydrogen | 186.49 | 862 | 77.5 km/L | Non |

Figure 3. Roadmap for hydrogen in Brazil.



The study proposed a roadmap highlighting the main production, storage, and distribution methods for hydrogen and identifying priority areas for hydrogen fueling stations (Figure 3). The calculations assumed an autonomy of 500–700 km per tank.

Conclusion

The study concludes that Brazil faces major challenges for hydrogen adoption, including limited infrastructure and the urgent need for strategic planning to build a robust national supply network. However, investments in renewable energy, particularly in the Northeast, are advancing. Bahia is already focusing on hydrogen through the Corredor Verde project, funded by SENAI CIMATEC and Petrobrás, which aims at decarbonization and energy development.

Tools such as the Atlas platform, which maps hydrogen production areas and related value chains, strengthen the Brazilian industry and facilitate integration of the national hydrogen network with international markets. This study thus contributes to Brazil's path toward a low-carbon economy.

Acknowledgements

The author thanks CNPq for the scientific initiation scholarship and the Green Hydrogen Competence Center for technical support.

References

- 1. De Carvalho CH. Emissões relativas de poluentes de transporte. Brasília (DF); 2011.
- 2. Aravindan M. Hydrogen towards sustainable transition: A review of production, economic, environmental impact and scaling factors. Tamil Nadu (IN); 2023.
- 3. Chu KC, Luo QB, Zhang H. Hydrogen storage by liquid organic hydrogen carriers: Catalyst, renewable carrier, and technology A review. Nanjing (CN); 2023.
- 4. Tian X, Pei J. Study progress on the pipeline transportation safety of hydrogen-blended natural gas. Beijing (CN); 2023.
- FIA Business School. Roadmap: o que é, para que serve, modelos e como fazer o seu. Disponível em: https://fia.com.br/blog/roadmap/#:~:text=Roadmap%20 %C3%A9%20uma%20ferramenta.

Reproduction and Adaptation of Literature-Derived Modeling: Numerical Simulation of Methane/Hydrogen Non-Premixed Combustion

Paulo Roberto Santana dos Reis^{1*}, Felix Emile Martin¹, Turan Dias Oliveira¹, Luzia Aparecida Tofaneli¹, Alex Álisson Bandeira Santos¹

¹SENAI CIMATEC University; Salvador, Bahia, Brazil

It is crucial to reduce CO₂ (Carbon dioxide) emissions to mitigate climate impacts. A viable strategy for this reduction is to wholly or partially replace the use of natural gas with hydrogen, a carbon-free molecule, in the combustion processes of the industrial and residential sectors. In this context, the objective of this study is to investigate the combustion of methane/hydrogen binary mixtures using Computational Fluid Dynamics (CFD). Combustion will be simulated in the vertical non-premixed burner of the Senai CIMATEC Laboratory. To optimize computation time, a 2D axisymmetric model was developed. Fundamental aspects of combustion, including flow velocity, temperature, species formation, fuel consumption, and pollutant emissions, will be analyzed to evaluate the impact of partial methane substitution with hydrogen.

Keywords: Combustion. Hydrogen. Methane. Computational Fluid Dynamics.

By the early 2030s, an annual investment of USD 4.5 trillion will be needed to accelerate the deployment of clean energy technologies and infrastructure, up from USD 1.8 trillion in 2023 [1]. A strong dependence on natural gas characterizes the industry. Even in the paper, pulp, and printing industry, where renewables, biofuels, and electricity are more significant, natural gas still represents around one-quarter to one-third of final energy consumption in various sectors [2]. Blending hydrogen into natural gas is a cost-efficient alternative for transitioning to cleaner combustibles, enabling the use of existing pipelines and machinery for industrial and domestic purposes, such as burners and gas turbines.

This study provides a numerical approach to predict the effect of a hydrogen-enriched methane diffusion flame. Small additions of hydrogen were chosen to precisely understand and quantify the impact of incremental hydrogen concentrations on the combustion process. Previous works using flamelet models have achieved low error results

Received on 10 May 2025; revised 20 July 2025. Address for correspondence: Paulo Roberto Santana dos Reis. Av. Orlando Gomes, 1845, Piatã, Salvador, Bahia, Brazil. Zipcode: 41650-010.. E-mail: paulo.roberto@fieb.org.br.

J Bioeng. Tech. Health 2025;8(4):352-358 © 2025 by SENAI CIMATEC University. All rights reserved.

when simulating non-premixed combustion blends of methane and hydrogen, showing good agreement with experimental data [3]. Kubilay Bayramoğlu and colleagues (2023) [3], Lotfi Ziani and colleagues (2012) [4], and Ravikanti (2009) [5] used GRI 3.0 mechanism to predict NOX formulation in a turbulent flame of blended methane and hydrogen. Their studies demonstrated excellent agreement with experimental data for temperature and major species.

Lotfi Ziani and colleagues (2012) [4] conducted a numerical study comparing the influence of changing modeling parameters. They achieved good results using the turbulence k- model for methane and hydrogen mixtures, with the approximation of experimental data becoming more accurate as the coefficient C1s was increased. These numerical approaches reduce project budgets and process time while ensuring high accuracy in predicting combustion properties such as temperature, velocity, and species concentration.

Due to the differences in the properties of these two fuels, the flames exhibit distinct characteristics, necessitating technological adaptations in systems subjected to new conditions to minimize the impact on processes. Combustion behavior involves complex processes, including fluid flow, heat transfer, chemical reactions, and radiative heat transfer, all of which require detailed models for accurate numerical predictions. The complexity of fluids and combustion dynamics, coupled with varying fuel compositions, properties, and geometry, makes this a non-trivial task. By refining and applying these models, we aim to further enhance our understanding and control of hydrogen-enriched methane combustion systems for industrial applications.

Materials and Methods

A Computational Fluid Dynamics (CFD) approach, utilizing the Ansys Fluent software, has been chosen for this study of methane/hydrogen blend combustion. The 2D axisymmetric model presented here is a pressure-based steady model governed by two major equations [6]:

The continuity equation:

$$\nabla \cdot \rho \vec{v} = 0 \tag{1}$$

Whith ρ (in kg/m³), the density of the fluid and \vec{v} the velocity (in m/s).

And the momentum equation:

$$\nabla \cdot (\rho \vec{v} \vec{v}) = -\nabla p + \nabla \cdot \tau + \rho g \tag{2}$$

With ρ the static pressure, ρg the gravitational body force, and τ the stress tensor, which is defined as:

$$\overline{\overline{\tau}} = \mu \left[(\nabla \vec{v} + \nabla \vec{v}^T) - \frac{2}{3} \nabla \vec{v} I \right]$$
 (3)

Where μ is the molecular viscosity, and I is the unit tensor.

The turbulence treatment in this numerical study was performed using the RANS approach (Reynolds-Averaged Navier-Stokes equations) with the k-ε model. Various studies have shown that the precision of the k-ε model can be augmented by modifying the C1ε coefficient up to 1.6. [4,7]. For the simulations presented in this study, a C1ε of 1.5 has been chosen due to better accuracy in the results. The model has also been simplified to an adiabatic process, without considering radiation.

The different simulations have been conducted with a non-premixed model, a model particularly

suited for diffusion flames. In this model, the thermochemical state of the fluid is represented by a conserved scalar quantity, the mixture fraction, noted f. It varies between 0 (pure oxidizer) and 1 (pure fuel), and can be written as:

$$f = \frac{X_i - X_{i,ox}}{X_{i,fuel} - X_{i,ox}} \tag{4}$$

Where X_I represents the elemental mass fraction for element i. The subscript "ox" is used to define the value at the oxidizer stream inlet, and the subscript "fuel" is used to define the value at the fuel stream inlet.

In addition to the non-premixed model, a steady laminar flamelet approach is used to represent the detailed chemistry and thermodynamics of a flame in a simplified manner. It assumes that the flame is composed of a series of thin, locally one-dimensional flame structures, known as flamelets. These flamelets are calculated using a chemical mechanism. The mechanism used in this study is the GRI Mechanism 3.0, a widely recognized and detailed chemical model consisting of 53 species and 325 reactions. It has already demonstrated accurate results in methane-hydrogen combustions [8,9].

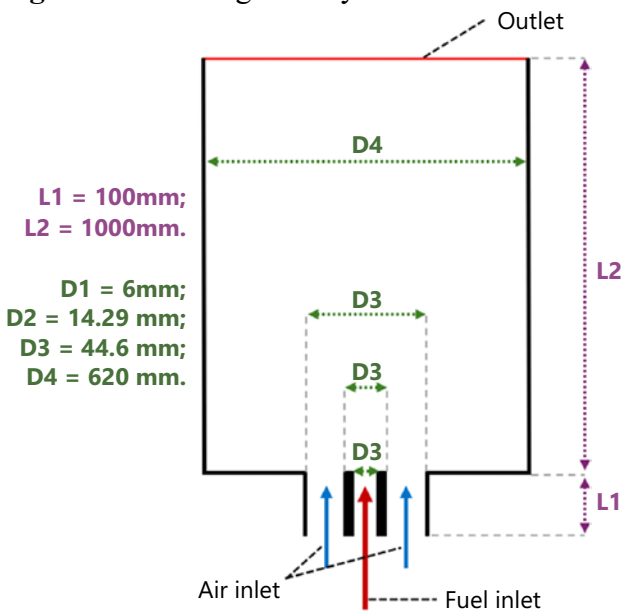
This adiabatic model, using the flamelet method, calculates energy based on pre-generated flamelet tables. These tables are generated by solving detailed chemistry for a range of mixture fractions and scalar dissipation rates, using the chemical mechanism thermodynamic data imported. Based on the local mixture fraction and dissipation rate, interpolations from these tables are then made to calculate temperature. This method captures the effects of detailed chemical kinetics and turbulencechemistry interactions, allowing efficient and accurate determination of thermal properties without directly solving energy equations. A laminar opposed-flow diffusion flamelet is then calculated and embedded in a turbulent flame using the statistical Probability Density Function (PDF) method. The pressure-velocity coupling is achieved using the Simple algorithm, with the

Green-Gauss Gradient Schemes. At the same time, the equations of momentum, pressure, turbulent kinetic energy, turbulent dissipation rate, and species are discretized using a secondorder scheme.

The model described earlier has been used to simulate the Sandia flame D [9-11]. Figure 1 illustrates that the numerical and experimental results are inclose agreement, validating the model. The average of the error between numerical and experimental data is about 10.6 %, with a slight overprediction of the temperature from x/d = 25 to the exit of the combustion chamber. Before x/d = 25, the numerical model provides a temperature lower than the experimental data due to the flame starting further away (with d = 7.2 mm, the fuel inlet diameter of the system used for the Sandia Flame D experimental data acquisition).

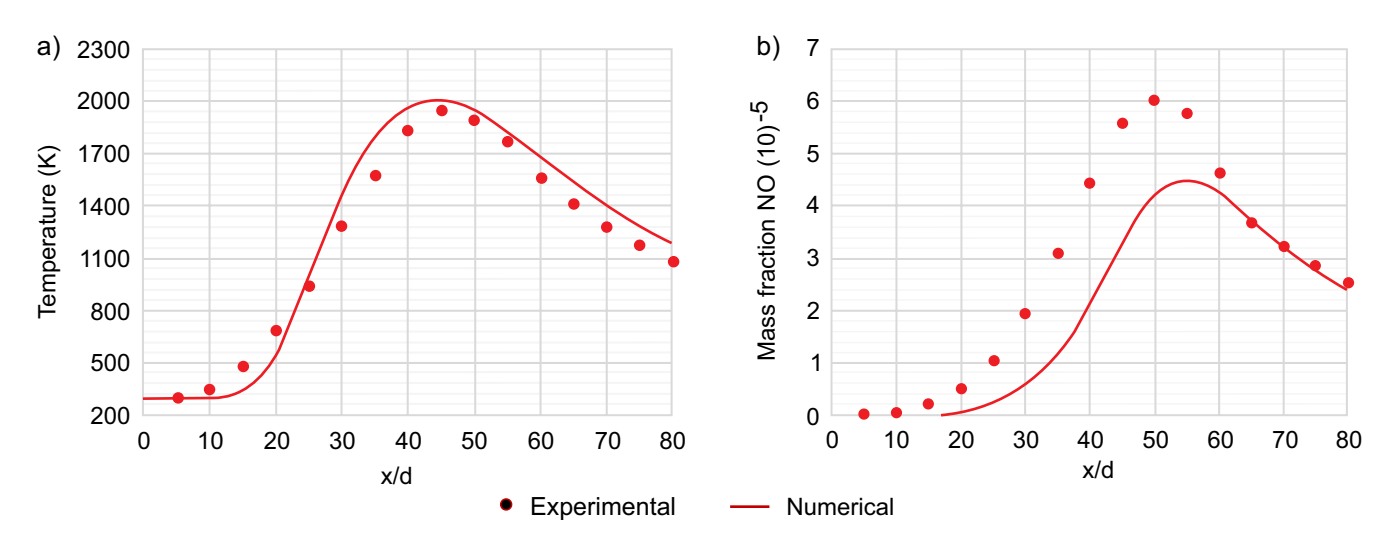
The circular shape of the vertical coaxial non-premixed burner used in this article for the simulations enables the creation of a numerical 2D axisymmetric model, as shown in Figure 2. A mesh of 65,700 cells was used for simulations. Significant refinement was applied along the axial direction and at the beginning of the combustion chamber to provide a more detailed mesh in the combustion zone, where the flame occurs. A total of 5 simulations were conducted in this study.

Figure 2. Burner geometry.



Each simulation was performed with a constant fuel inlet velocity of 12 m/s. The fuel mixtures used consisted of methane with varying concentrations of hydrogen, ranging from 0% to 20% (vol.). To maintain an equivalence ratio of 1 for each simulation, the air inlet velocity was adjusted accordingly, varying from 0.712 m/s for the 80% methane – 20% hydrogen fuel to 2.3 m/s for the 100% methane fuel. The walls are considered adiabatic, and the pressure outlet is fixed at 101,325 Pa.

Figure 1. Experimental and numerical data comparison of Sandi Flame D.



Results and Discussion

By adjusting the air velocity according to the hydrogen concentration in the fuel, five different simulations were conducted. The temperature contour of the five flames is presented in Figure 3.

It shows that increasing the hydrogen concentration in the fuel up to 20% reduces the length of the flame and increases the temperature slightly. Indeed, the maximum temperature calculated for the methane flame is 1,819 K. In contrast, the maximum temperature of the methane flame with 20 % hydrogen reaches 1,854 K. This increase in temperature can be attributed to the higher calorific value (PCI) of hydrogen compared to methane. Hydrogen has a higher energy content per unit mass, resulting in greater heat release during combustion. Additionally, hydrogen's higher flame speed enhances the combustion process, contributing to higher peak temperatures

The axial temperature profiles of the five flames, presented in Figure 4(a), allow us to

observe that the maximum temperatures in the axial direction are reached between a length of 426 mm (for the methane fuel with 20% hydrogen) and 467 mm (for the 100% methane flame) along the centerline of the combustion chamber. The addition of hydrogen to the fuel accelerates the temperature rise, resulting in a steeper initial increase in temperature. This indicates that hydrogen enhances the combustion process, leading to quicker and higher peak temperatures. After reaching the peak temperature, the fuel with higher hydrogen content shows a faster reduction in temperature. This indicates that while hydrogen accelerates the heating process, it also leads to a faster cooling post-combustion phase compared to pure methane. This faster reduction in temperature can be attributed to several factors. Enriching methane with hydrogen accelerates the combustion process, promoting rapid heat release and energy transfer within the combustion chamber. This efficient combustion results in a more complete utilization of fuel energy, reducing

Figure 3. Temperature contours.

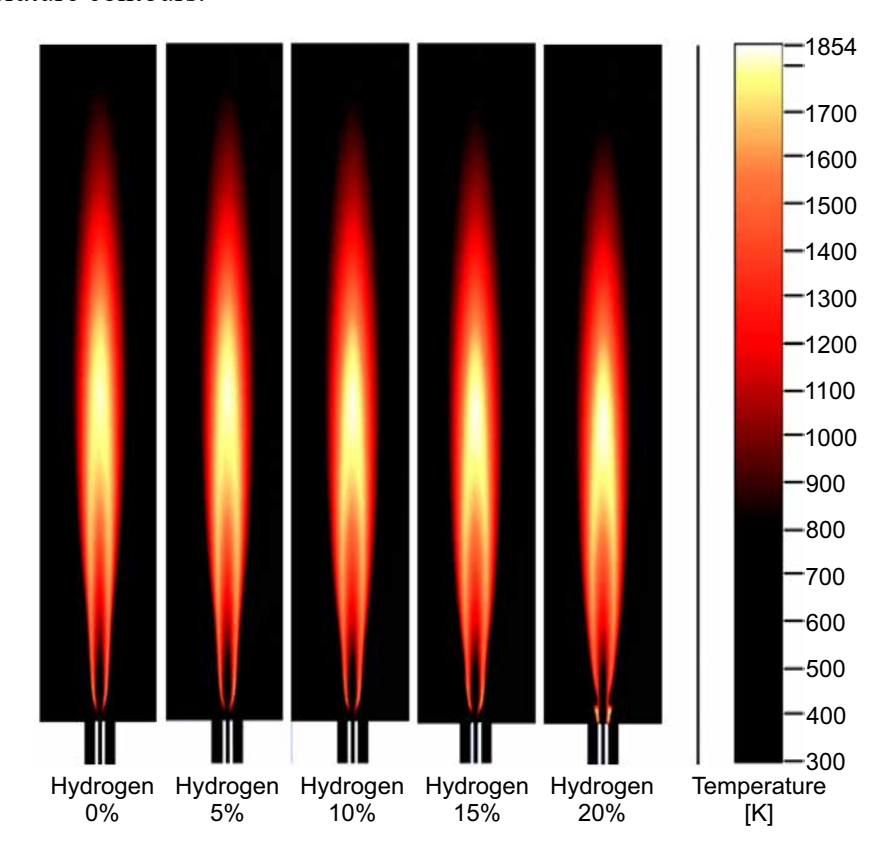
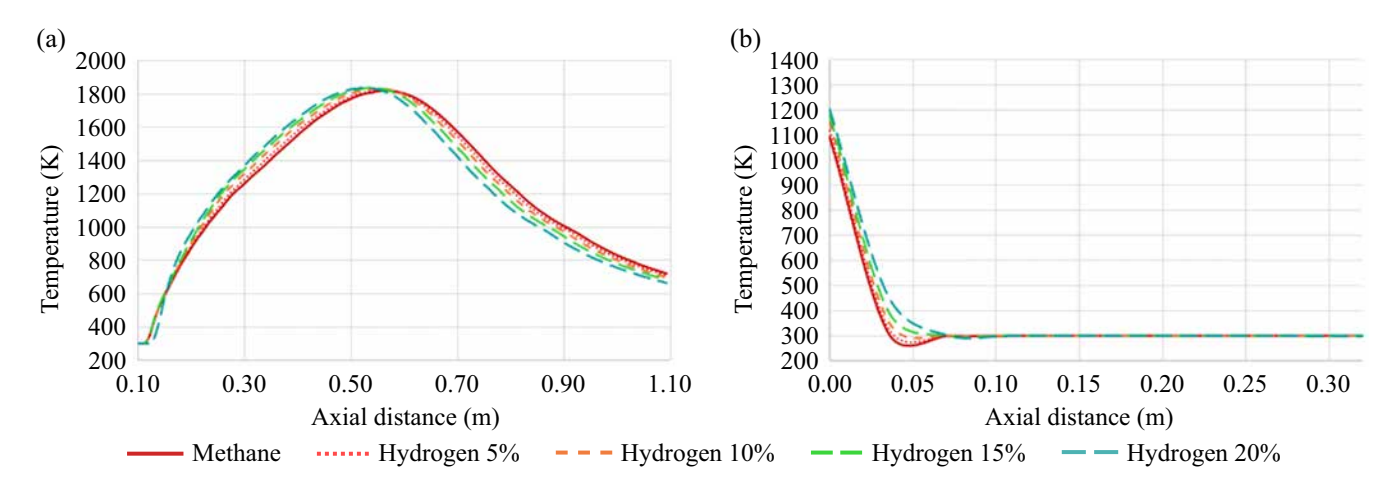


Figure 4. Temperatures along the central axial direction (a) and radial temperatures at x = 0.25 m (b).



the residual heat in the combustion zone after peak temperature is reached. Moreover, the specific heat capacity of hydrogen is lower compared to methane, which means that it requires less energy to raise the temperatures of hydrogenenriched flames, but also cools down faster once combustion is made. These dynamics show the hydrogen addition effect in combustion efficiency post-combustion thermal dynamics. Figure 4(b) also shows the radial temperature profiles of the five flames at x = 0.25 m. It is observable that increasing the hydrogen concentration in the fuel results in a broader flame, due to higher temperatures from y = 0 to y = 0.075m. For flames with lower hydrogen content, a slight temperature depression is observable around y = 0.4 m, indicating a less intense combustion process compared to hydrogen-enriched flames. This trend highlights that even small additions of hydrogen can significantly impact the flame structure and combustion characteristics.

Figure 5 shows the mol fraction of species along the combustion chamber. The addition of hydrogen to methane significantly alters flame behavior, accelerating the overall combustion process. The mole fraction of methane decreases rapidly along the flame axis, indicating efficient combustion of methane. Concurrently, the mole fractions of CO₂ and H₂O increase, reflecting the oxidation of methane. As hydrogen is introduced into methane, the mole fractions of the chemical

species along the flame axis undergo notable changes. For a mixture with 5% hydrogen, methane still decreases rapidly; however, the presence of H₂ influences the product distribution.

Formixtures containing 15% and 20% hydrogen, the H₂ mole fraction decreases rapidly, attributed to the faster formation of H₂O for these mixtures, indicating a higher combustion rate of hydrogen compared to methane. With hydrogen addition, the H₂O fraction increases due to the additional contribution of hydrogen to water formation. All H₂ mole fractions decrease at approximately 36% of the axial distance of the combustion chamber. At this point, the CO fraction begins to increase slightly, indicating changes in oxidation pathways. Similar results are reported by Lotfi Ziani and colleagues (2012) [4].

The CO appears as an intermediate product of incomplete oxidation. In all mixtures, CO shows a noticeable increase in mole fractions, suggesting that the presence of hydrogen favors the formation of intermediate combustion products. The CO_2 fraction reaches its maximum at approximately x=0.6 m of the combustion chamber, with a difference in mole fraction of 0.418% for the 20% hydrogen mixture compared to pure methane. The presence of hydrogen also tends to raise the flame temperature, which can explain the increase in CO mole fraction, a byproduct of incomplete combustion. It also increases the NO mole fraction. The variance of CO, CO_2 , and NO

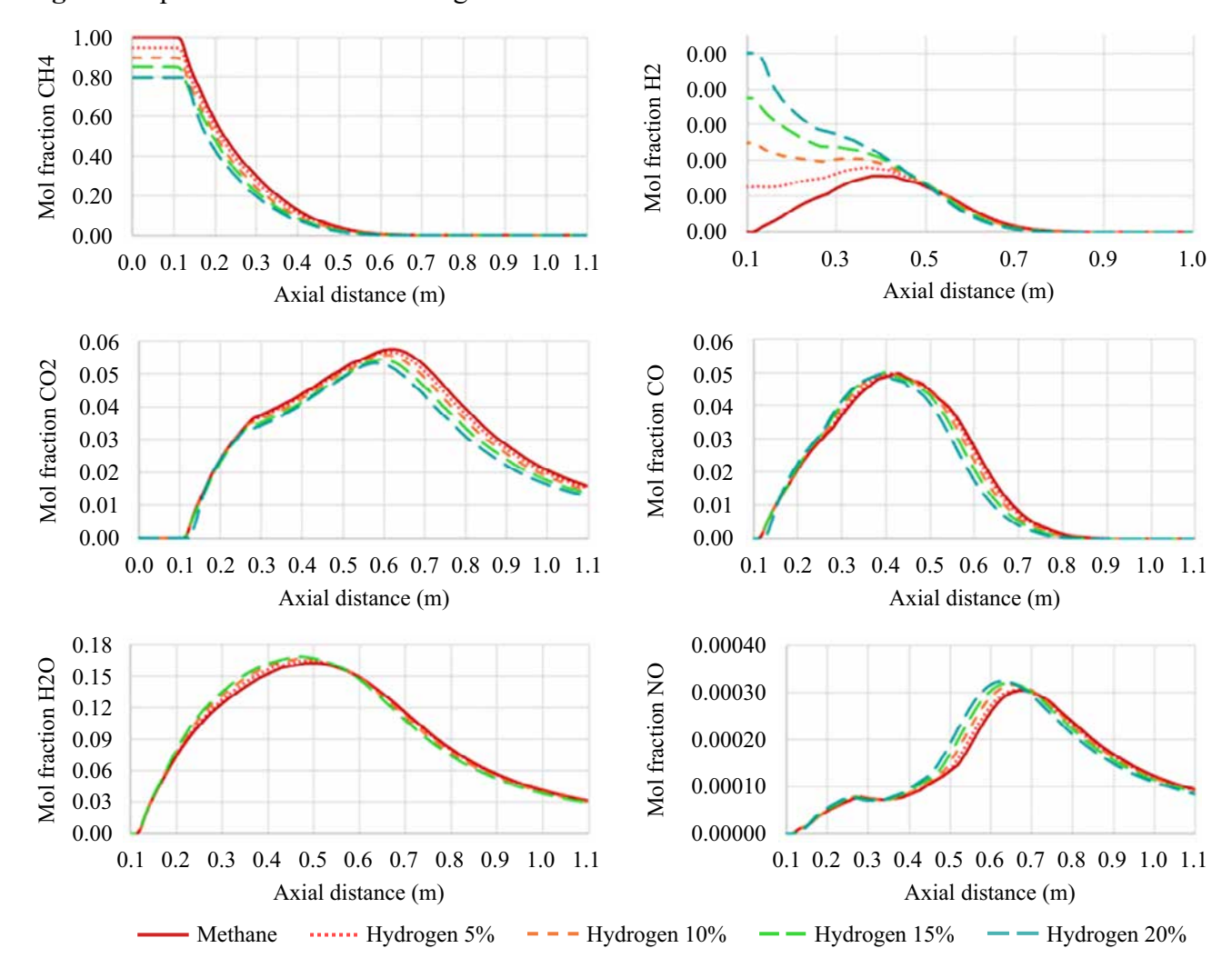


Figure 5. Species mole fraction along the central axial direction.

becomes significant by 27% of the axial distance of the combustion chamber. The rapid combustion rate of hydrogen also contributes to an increase in flame temperature. Hydrogen's higher diffusivity compared to methane allows it to spread more quickly and evenly in the fuel mixture, improving the air-fuel mixture and resulting in more efficient and complete combustion. As the hydrogen content in the mixture increases, the amount of carbon available for CO2 formation decreases, leading to a significant reduction in CO₂ emissions. While hydrogen oxidation mainly produces water, combining with methane can lead to greater formation of CO and other intermediate products due to changes in chemical reactions and temperature distribution.

Previous studies have shown a substantial reduction in CO2 emissions with increased hydrogen content in the mixture, attributed to hydrogen's carbon-free nature. Additionally, it has been observed that hydrogen addition enhances combustion efficiency due to the higher flame speed and superior diffusivity of hydrogen. This effect is consistent with observations in the combustion of hydrogen and ammonia mixtures, where increasing the hydrogen rate significantly enhances the maximum flame temperature and the surface area of the maximum temperature zone [4]. The results of this study also demonstrate that adding hydrogen leads to slightly higher temperature distributions in the central region of the flame. This increase in temperature can lead to higher NOx emissions.

Conclusion

The numerical model used in this study allowed for the investigation of the effect of hydrogen enrichment on methane fuel combustion within a coaxial non-premixed burner. The various simulations have demonstrated that adding a small hydrogen fraction (ranging from 0% to 20%) to methane fuel has a significant impact on global combustion.

Increasing the hydrogen amount in the fuel affects the flame structure, reducing its length and increasing its width. As light temperature depression on the side of the flame, observable for methane combustion, disappears when hydrogen is added to the fuel. Moreover, it has been demonstrated that the maximum temperature of hydrogenenriched fuels is higher. These two phenomena, observed at varying temperatures, affect the global flame behavior and have a significant impact on the species created during and after combustion.

Hence, the addition of hydrogen to methane also alters the distribution of chemical species. Higher hydrogen content results in a faster decrease in H₂, increased H₂O formation, and slightly higher CO due to changes in oxidation pathways. The flame temperature rises with the addition of hydrogen, which increases NOx emissions, as thermal NOx production is directly related to the flame temperature. The consistency of these results with previous studies reinforces the conclusion that adding hydrogen to fuel mixtures can improve combustion efficiency while reducing CO₂ emissions; however, it may also increase NOx emissions, presenting new challenges in emissions control.

Acknowledgment

The authors acknowledge the financial support provided by the National Department of SENAI- Brazil, SENAI CIMATEC, and the

National Council for Scientific and Technological Development (CNPq).

References

- International Energy Agency. Scaling up of innovative clean energy technologies needed to achieve net zero emissions targets globally [Internet]. Available from: https://www.iea.org/news/scaling-up-of-innovativeclean-energy-technologies-needed-to-achieve-netzero-emissions-targets-globally.
- 2. Eurostat. Industry relied mostly on natural gas & electricity [Internet]. Available from: https://ec.europa.eu/eurostat/web/products-eurostat-news/w/ddn-20230512-1.
- Bayramoğlu K, Bahlekeh A, Masera K. Numerical investigation of the hydrogen, ammonia and methane fuel blends on the combustion emissions and performance. Int J Hydrogen Energy. 2023;48(99):39586-98. doi:10.1016/j.ijhydene.2023.06.079.
- 4. Ziani L, Chaker A, Chetehouna K, Malek A, Mahmah B. Numerical simulations of non-premixed turbulent combustion of CH4–H2 mixtures using the PDF approach. Int J Hydrogen Energy. 2013;38(20):8597-603. doi:10.1016/j.ijhydene.2012.11.104.
- Ravikanti M, Hossain M, Malalasekera W. Laminar flamelet model prediction of NOx formation in a turbulent bluff-body combustor. J Power Energy. 2009.
- 6. Versteeg HK, Malalasekera W. Computational fluid dynamics: the finite volume method. 2nd ed. Harlow (UK): Pearson Education; 2007.
- Sayadzadeh ME, Samani MR, Toghraie D, Emami S, Eftekhari SA. Numerical study on pollutant emissions characteristics and chemical and physical exergy analysis in mild combustion. Energy. 2023;278(Pt B).
- 8. Xiao J, Liu Q, He S, Wang S, Zhang Z. Numerical simulation on combustion characteristics of methane/hydrogen blended fuel for non-premixed conical bluff body burner. Int J Hydrogen Energy. 2024;65:50-60. doi:10.1016/j.ijhydene.2024.03.377.9.
- Barlow RS, Frank JH. Proc Combust Inst. 1998;27:1087-05
- 10. Barlow RS, Frank JH, Karpetis AN, Chen JY. Piloted methane/air jet flames: scalar structure and transport effects. Combust Flame. 2005;143:433-49.
- 11. Schneider C, Dreizler A, Janicka J. Flow field measurements of stable and locally extinguishing hydrocarbon-fuelled jet flames. Combust Flame. 2003;135:185-90.

Development of Coating to Mitigate Chromium Contamination from Bipolar Plates in a Metal-Supported Solide Oxide Fuel (MS-SOFC)

Ricardo Lima Travassos^{1*}, Marcos Makoto Toyama¹, Fernando Pellegrini Pessoa¹, Gerhard Ett¹

'SENAI CIMATEC University; Salvador, Bahia, Brazil

Metal-Supported Solid Oxide Fuel Cells (MS-SOFCs) are electrochemical devices applicable to sustainable power generation. The main reason for efficiency loss in these cells is chromium contamination, leading to degradation and reduced lifetime. In order to improve cell durability and minimize the need for frequent replacement of its components, an extensive literature review was carried out to select the most suitable materials for the fabrication of bipolar plates and their coatings. Selection criteria included cost, ease of manufacturing, thermal expansion coefficient (TEC), and electrical conductivity, ensuring compatibility with the cell stack materials. Ferritic stainless steels were selected for the plates, and oxides and spinels of specific metals for coatings. These choices will directly impact the commercial and environmental viability of this technology.

Keywords: MS-SOFC. Coating. Chromium Contamination. Chromium Evaporation.

The growing global demand for energy, together with the urgency to reduce greenhouse gas emissions harmful to the environment, has driven the search for alternative sources of clean energy to replace fossil fuels. Hydrogen and biofuels such as ethanol are positioned to play a key role in the energy transition, particularly in electricity generation as well as in mobility, using devices that employ them; in this case, fuel cells such as PEM and MS-SOFC. These technologies are alternatives to enable electrification and possibly overcome dependence on fossil fuels.

However, these devices present limitations regarding efficiency and durability, strongly depending on the materials of the bipolar plates, electrodes, electrolytes, and coatings, among other components. Therefore, the objective of this research is to develop suitable coatings for MS-SOFC bipolar plates at operating temperatures of 600 to 800 °C, improving cell performance by mitigating chromium contamination and plate oxidation. The coatings will be formed using the Physical Vapour Deposition (PVD) process on test coupons simulating bipolar plates.

Received on 26 May 2025; revised 29 July 2025. Address for correspondence: Ricardo Lima Travassos. Av. Orlando Gomes, 1845 - Piatã, Salvador – BA – Brazil, Zip Code: 41650-010. E-mail: ricardo.travassos@fieb.org.br.

J Bioeng. Tech. Health 2025;8(4):359-362 © 2025 by SENAI CIMATEC University. All rights reserved.

Structural and chemical composition analyses of the coatings will be carried out, aiming to minimize the volatilization and deposition of chromium on the internal components, under MS-SOFC operating conditions, thus improving the efficiency, durability, and sustainability of this electrochemical system.

Materials and Methods

Searches were conducted through websites such as the CAPES journals platform, ScienceDirect, Web of Science, Google Scholar, articles, reviews, and online books, using the keywords SOFC, MSSOFC, coatings, chromium poisoning, bipolar plates, fuel cell.

Representative references of the existing problems in the fuel cell involving the bipolar plates and the internal components of the stack (cell pile), such as cathode, anode, and solid electrolyte, were found and selected. Various materials were verified and selected for each of the components mentioned, always considering the correspondence between the required properties for the proper functioning of the set, such as oxidation resistance, thermal expansion coefficient (TEC), and electrical conductivity. In addition, the electrochemical process that occurs inside the cell was studied to understand the complete functioning of the MS-SOFC fuel cell for electricity generation.

Results and Discussion

Among the existing fuel cells, the MS-SOFC (Metal Supported Solid Oxide Fuel Cell) stands out, operating at temperatures between 600 and 800 °C, with continuous high efficiency. The differential of this cell is the possibility of using several fuels such as hydrogen (H₂), whose byproduct is water (H₂O), with zero carbon emission, or when using other fuels such as hydrocarbons (HC), generating very low levels of greenhouse gas (GHG) emissions, releasing carbon dioxide (CO₂), carbon monoxide (CO), and water (H₂O) [3].

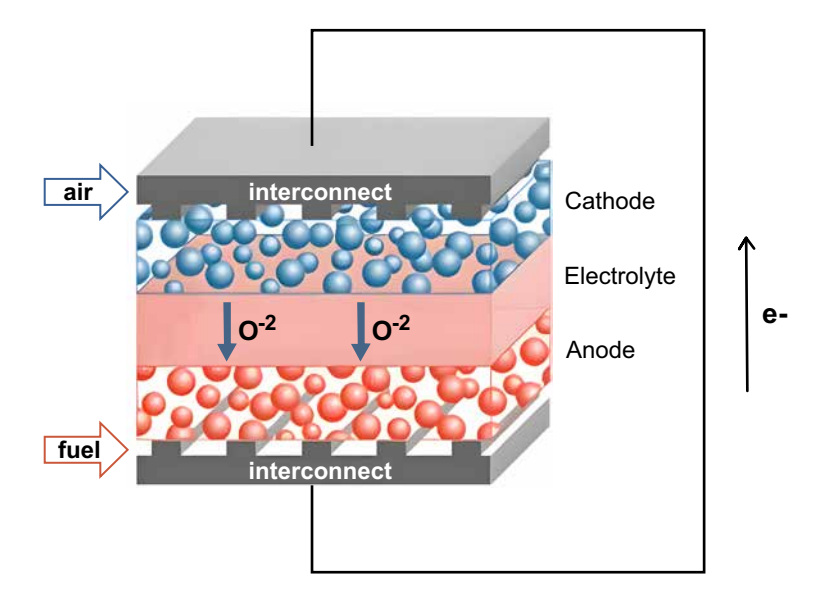
However, there are challenges to be overcome, such as the most appropriate choice of metallic support material, the coating to be used, the deposition process, and the thermal and chemical behavior with each component, to ensure the best SOFC efficiency. The metallic support or interconnectors shown in Figure 1 provide electrical connection between the cells, act as a physical barrier separating the fuel (anode) from the oxidizing gases (cathode), and allow more innovative designs with the formation of coatings with thin layers of electrochemically active material (electrodes and electrolyte). The cell can be used in several applications, from power

generation to mobility, such as in the automotive sector.

The material used for metallic supports must be low-cost, have excellent oxidation resistance, high electrical conductivity, good thermal conductivity, and a TEC close to that of other functional components, in order to prevent mechanical damage to the cell during thermal cycling inherent to MS-SOFC operation. It must also be resistant to oxidizing atmospheres and chemically stable at the operating temperature [1]. Stainless steels (Table 1), based on chromium, nickel, and iron, are widely used as interconnection materials due to their adequate TECs as well as their ability to form protective films and their relatively low cost.

Some metallic alloys are applied, such as Crofer 22 APU, Sandvik Sanergy HT, AISI 441, and AISI 430, which are ferritic stainless steels [4]. The major challenge for these chromium-containing steels, which will be exposed for prolonged periods to typical MS-SOFC operating temperatures (up to 1000 °C), is the potential for chromium migration to the cathode-electrolyte-air triple phase boundary, resulting in the formation of compounds such as Cr₂O₃. This fills pores with chromium, restricts O₂⁻ diffusion, and reduces the number of active sites in the electrode. The degradation is shown in the second graph of

Figure 1. Conceptual diagram of MS-SOFC based on oxygen ions [6].

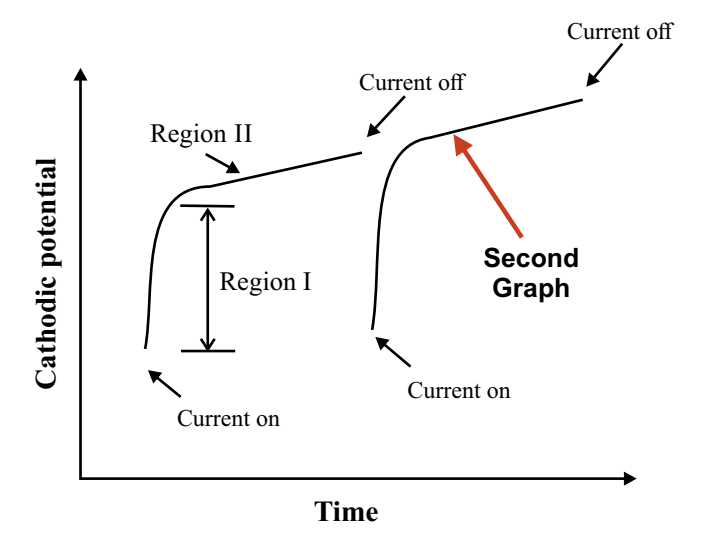


| Candidate Material | Matrix Structure | TEC x 10 ⁻⁶ K ⁻¹ (RT–800 °C) | Oxidation Resistance | Electrical Conductivity | Mechanical Strength | Manufactur- ability | Cost |
|-----------------------|---------------------|--|-------------------------|----------------------------|------------------------|------------------------|-------------------|
| Cr-based alloy | CCO | 11.0 – 12.5 | Good | Good | High | Hard | Very Expensive |
| Fe-stainless steel | CCO | 11.5 – 14.0 | Good | Good | Low | Easy | Cheap |
| Ni-superalloy | FCC | 14.0 - 19.0 | Good | Good | High | Easy | Expensive |

Table 1. Comparison of potential candidates for metallic interconnections [1].

Figure 2, due to the rapid increase in polarization potential in region I, followed by a much slower increase in polarization potential in region II, when a current is applied to the cell [5], decreasing its electrochemical oxygen reduction properties, affecting cell efficiency and lifetime [5].

Figure 2. Cathodic potential for O₂ reduction reaction [5].



To improve the durability of MS-SOFCs, protective coatings with low electrical resistance are used, capable of acting as effective barriers against chromium migration to the interconnection surface. Among the materials, spinels and perovskites stand out, compounds based on elements such as Mn, Co, Cu, Ni, defined below [1].

Perovskites, with the general formula ABO₃, contain trivalent rare-earth cations (La, Y, or Sr) at the A site and transition metal cations (Cr, Ni, Fe, Co, Cu, or Mn) at the B site. This material has high

electronic conductivity in oxidizing atmospheres and good stability under low oxygen partial pressure conditions. However, despite advances, perovskites have limitations as barriers against volatile Cr species and oxygen diffusion [1].

Spinel oxides, with the general formula AB₂O₄, have a crystalline structure characterized by the distribution of divalent, trivalent, or quadrivalent cations in octahedral and tetrahedral sites, while oxygen anions are arranged in a face-centered cubic lattice. These materials have been widely used due to their effectiveness in mitigating the migration of volatile Cr species and the formation of Cr₂O₃ layers on the interface surface. In addition, they have high electrical conductivity and a TEC compatible with the other components of the cell. The properties of spinels can be optimized by adjusting the selection and proportion of cations A and B, allowing improvements in the structural stability and functionality of the material [1].

According to Mah and colleagues [1] (Table 2), spinel oxide is the best option among the coatings cited.

Several techniques are employed in the deposition of spinel-based coatings, including the sol-gel method, Physical Vapor Deposition (PVD – specifically Magnetron Sputtering), electroplating, and electrophoretic deposition (EPD) [1]. The PVD process was selected for its efficiency in producing dense and uniform coatings and reducing residual stresses on the substrate, since deposition occurs at low or moderate temperatures [7]. This thermophysical method consists of vaporizing the target material into atomic particles, which are directed as a gaseous plasma toward the substrates, promoting the controlled deposition of atoms on the surface.

| Coating Material | Electronic Conductivity, | Inhibition of Cr Reduction of Migration Oxidation Rat | | Deposition Simplicity |
|---------------------------|--------------------------|---|------|--------------------------|
| Reactive Element Oxide | Fair | Poor | Good | Good |
| Rare-Earth Perovskites | Good | Fair | Poor | Fair |
| Spinel Oxide | Good | Good | Fair | Good |

Table 2. Comparison of various coating materials [1].

This process involves the use of two electrodes connected to a high-voltage source inside a vacuum chamber, allowing the deposition of one or multiple materials. In addition, the deposited materials replicate the stoichiometry of the target, ensuring homogeneous and reproducible coating adhesion [7].

Conclusion

Based on the study carried out so far, it is verified that the metal-supported solid oxide fuel cell (MS-SOFC) stands out as one of the most promising within fuel cell technology, due to its high energy efficiency and greater flexibility in the use of different fuels. Chromium deposition contamination on cell components, however, remains a problem resulting from operating conditions characterized by high temperatures and oxidizing environment.

In this context, spinels emerge as a highly promising alternative as coatings, as they present high chemical stability, excellent ability to suppress volatile Cr compounds, good electrical conductivity, and a thermal expansion coefficient (TEC) compatible with the other components of the cell. Thus, spinel-based coatings will be applied to ferritic stainless steel coupons, which will be subjected to the operating conditions of

an MS-SOFC. Analytical and performance tests will then be carried out, with the objective of identifying the characteristics and improvements that may contribute to increasing the efficiency and lifetime of the fuel cells in question.

References

- 1. Mah JCW, et al. Metallic interconnects for solid oxide fuel cell: A review on protective coating and deposition techniques. Int J Hydrogen Energy. 2017;42(14):9219–29.
- Cheng F, et al. Performance of CoMnO Spinel Coating onto 441 SS for SOEC Interconnect Application. Coatings. 2022 Nov 11;12(11):1723.
- 3. Mohd Affandi NS, Osman N. Short review on global trends in SOFC scenario and future perspective. Mater Today Proc. 2022 Jan 1;66:3981–4.
- 4. Reddy MJ, et al. 11–23% Cr steels for solid oxide fuel cell interconnect applications at 800 °C How the coating determines oxidation kinetics. Int J Hydrogen Energy. 2023 Apr 22;48(34):12893–904.
- Jiang SP, Chen X. Chromium deposition and poisoning of cathodes of solid oxide fuel cells – A review. Int J Hydrogen Energy. 2014 Jan 1;39(1):505–31.
- 6. Zhou L, et al. Comprehensive review of chromium deposition and poisoning of solid oxide fuel cells (SOFCs) cathode materials. Renew Sustain Energy Rev. 2020 Dec;134:110320.
- 7. Baptista A, et al. Sputtering Physical Vapour Deposition (PVD) Coatings: A Critical Review on Process Improvement and Market Trend Demands. Coatings. 2018 Nov 14;8(11):402.

Computational Model to Optimize the Prediction of Fouling in the Deposition Process During Oil Pre-Processing in Heat Exchanger Networks Based on Machine Learning

Adroaldo Soares^{1*}, Marcelo Albano Moret¹, Oberdan Pinheiro¹, Fernando Luiz Pellegrini Pessoa¹

'SENAI CIMATEC University; Salvador, Bahia, Brazil

The accumulation of deposits in heat exchangers during oil pre-processing, known as fouling, is a reality in the oil and gas industry. This deposition, caused by the presence of suspended solids, organic, and mineral compounds, compromises the thermal and hydraulic efficiency of heat exchangers, resulting in less efficient operations and increased maintenance and energy costs. The implementation of predictive computational models aims to ensure the functioning of heat exchangers and is essential for maintaining refinery operations. The objective of this work was to analyze models for managing deposition in heat exchangers during oil pre-processing, in order to maximize operational efficiency and minimize costs associated with maintenance and energy, using Artificial Intelligence with machine learning models capable of processing sequential data, which is particularly useful in deposition processes that evolve, as in the network of heat exchangers used in oil pre-processing. The computational models were developed using historical measurement data from a network of 25 heat exchangers at a refinery in southeastern Brazil, spanning from September 1, 2014, to July 25, 2021, and comprising a total of 57,225 records stored in a CSV (Comma-Separated Values) file. For prediction, the independent variables were the operating parameters of the exchangers, and as dependent variables, the fouling factor (Rfs), which quantifies the resistance to thermal exchange due to deposition. The prediction models were evaluated based on error metrics, and the DNN (Deep Neural Network) model presented MSE (Mean Squared Error) of 0.01835, RMSE (Root Mean Squared Error) of 0.13549, MAE (Mean Absolute Error) of 0.10743, and R² (Coefficient of Determination) of 0.3049. The LSTM (Long Short-Term Memory) model presented MSE of 0.01863, RMSE of 0.13649, MAE of 0.10895, and R2 of 0.29458. The Hybrid Model presented an MSE of 0.01856, an RMSE of 0.13624, an MAE of 0.10663, and an R² of 0.29720. We concluded that predicting the deposition coefficient is critical for operational planning. Computational fouling prediction models can be utilized to minimize costs and risks in the heat exchanger network during oil preprocessing, offering an efficient approach to process optimization.

Keywords: Modeling. Fouling. Heat Exchangers. Machine Learning. Optimization.

Oil pre-processing faces a series of complex challenges, reflecting the complexity and sensitivity of the process, as well as increasingly strict regulatory compliance requirements and environmental pressures. Among the main challenges is the considerable variation in the quality of crude oil from different sources and reservoirs [1]. This variability encompasses a wide range of physical and chemical characteristics, including sulfur content, density, viscosity, heavy metal content, and hydrocarbon composition, necessitating the development of flexible pre-

Received on 28 May 2025; revised 31 July 2025. Address for correspondence: Adroaldo Soares. Av. Orlando Gomes, 1845 - Piatã, Salvador — BA — Brazil, Zip Code: 41650-010. E-mail: adroaldo.soares@ba.estudante.senai.br. Original extended abstract presented at SAPCT 2025.

J Bioeng. Tech. Health 2025;8(4):363-369 © 2025 by SENAI CIMATEC University. All rights reserved.

processing strategies that can accommodate these variations [2].

The oil and gas industry extensively utilizes shell-and-tube heat exchangers, primarily due to their ability to operate under high pressures and temperatures. These heat exchangers are employed to exchange heat between fluids at different temperatures without direct contact. In oil preprocessing, shell-and-tube heat exchangers are used before crude oil refining, as crude oil undergoes desalination and dehydration processes to remove water and dissolved salts that can cause corrosion or deposit formation in processing units. Heat exchangers are used to heat the crude oil before these processes, facilitating the separation of water and salts.

Fouling in heat exchangers is an undesirable phenomenon that can reduce heat transfer efficiency and lead to corrosion and premature equipment failure [3], contributing to the loss of primary energy, particularly in refineries, which accounts for up to 2% of total energy consumption [4]. To improve the performance and efficiency of heat exchangers, it is crucial to control and mitigate fouling through strategies such as periodic cleaning, chemical treatments, and the selection of appropriate materials and designs [5]. Modeling fouling in heat exchangers is crucial for understanding and predicting the deposition phenomenon, which can significantly impact equipment performance and efficiency [6].

An efficient way to determine when cleaning shutdowns are necessary is through the use of Artificial Neural Networks (ANNs), which are computational techniques for mathematical modeling based on the human brain, capable of solving both simple and complex problems. For this, it is necessary to monitor fouling in a heat exchanger by training Artificial Neural Networks and testing the types of strategies and structures that best perform the simulation for this system [7].

Materials and Methods

The elaboration of this work was organized according to the flowchart illustrated in Figure 1. The selection of these variables is based on case studies in refineries, where historical data indicate strong statistical correlations between heat transfer coefficients, flow rates, and inlet/outlet temperatures and the actual fouling levels measured in the field [8]. In general, it is recommended to continuously monitor such variables to allow machine learning algorithms to update their deposition predictions, incorporating possible regime changes and unexpected oscillations. The output variable Rf (Fouling Factor) is a leading indicator of deposit accumulation over time in shell-and-tube heat exchangers. The dataset creation process involved information from an oil refinery in southeastern Brazil, where a network of heat exchangers consists of seven branches (A, B, C, D, E, F, and G), comprising a total of 25 shelland-tube exchangers. The data, obtained under

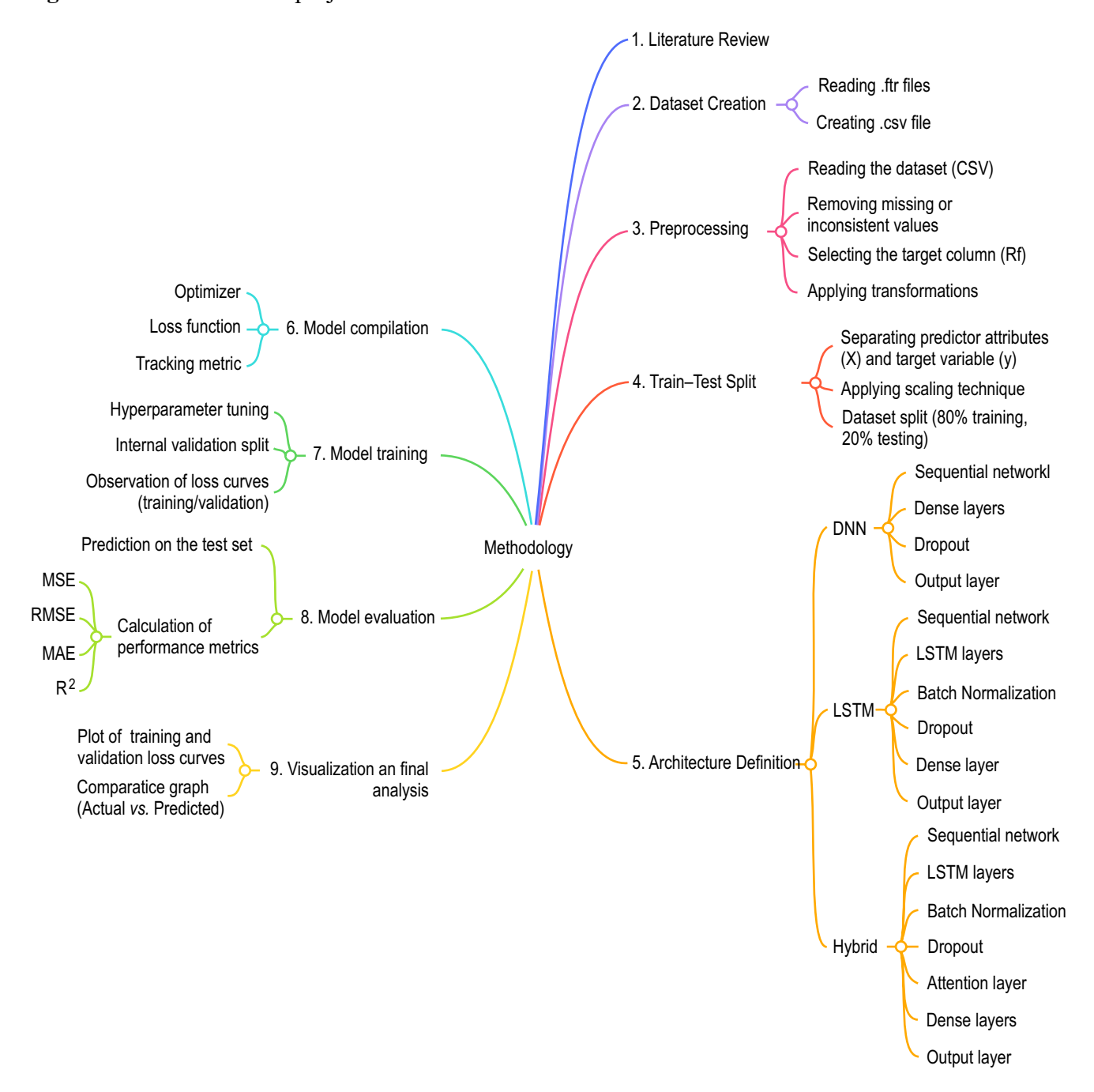
confidentiality, included operational measurements collected between September 1, 2014, and July 25, 2021, totaling 57,225 records. These measurements include variables such as inlet and outlet temperatures, flow rates of hot and cold fluids, global heat transfer coefficients of the hot and cold fluids in operation, and, as the dependent variable, the deposition coefficient (Rf), which quantifies the resistance to deposition.

The pre-processing stage was designed to ensure the consistency and adequacy of the data before being provided to the prediction model. Initially, the .csv file containing the dataset was read, gathering the variables relevant to the performance of the heat exchangers, such as temperatures and flow rates, among other operational information, in a DataFrame. This type of data structure, commonly used in analysis applications, stores information in a tabular format with clearly identified rows and columns, which facilitates the manipulation, querying, and processing of recorded values. After reading, inconsistent values were removed. First, rows whose Rf attribute showed values less than or equal to zero were excluded, as they were interpreted as measurements outside the operational range or registration errors.

The training and testing split aimed to create two datasets: one for model training and another for evaluation, ensuring that performance would be measured reliably. Before this split, it was essential to define which variables would compose the inputs (X) and which would be the target variable (y). In this study, the Rf attribute was set as the reference column for y. In contrast, the other columns formed X. This distinction oriented the learning process exclusively toward the parameter of most significant interest (the target variable), while keeping all other parameters as predictors.

With this structure defined, data scaling was performed. Initially, the MinMaxScaler was applied, converting attribute values to the 0–1 interval. This transformation reduced adverse effects caused by drastic differences in magnitude between variables while preserving proportionality. Thus, both the predictor variables

Figure 1. Flowchart of the project method.



and the target variable were rescaled, promoting a more uniform distribution of inputs and the predicted value. Next, the StandardScaler was applied to center the data around a mean of zero with a variance of one. This dual scaling approach stabilized the neural network optimization process, improving performance and convergence during training. After scaling, the dataset was split

into training (80% of the observations) and testing (20%) for final evaluation.

Definition of the Architeture

This section describes the three neural network architectures proposed for the prediction problem under study. The choice of multiple models allowed comparisons between different configurations of layers and neuron counts, seeking to understand the impact of these variations on final performance. DNN Model.

The first model followed the architecture of a Deep Neural Network (DNN), comprising two hidden dense layers and a linear output layer. At the input layer, the number of neurons corresponded to the input variables defined during pre-processing.

The first hidden layer consisted of 64 neurons, utilizing the ReLU activation function. This quantity strikes a balance between representation capacity and the risk of overfitting, offering sufficient complexity for regression problems with a moderate number of input dimensions. A Dropout layer was then added, randomly zeroing a

fraction of connections during training to promote regularization.

The second hidden layer, with 32 neurons (utilizing ReLU activation), gradually reduced dimensionality, contributing to the extraction of hierarchical patterns and preventing learning overload. Another Dropout layer is used to further mitigate overfitting. Finally, the output layer had a single neuron with linear activation, reflecting the continuous nature of the target variable (Rf).

LSTM Model

The second model (Figure 3) adopted an LSTM (Long Short-Term Memory) architecture to handle temporal or sequential aspects of

Figure 2. DNN summary.

| Layer (type) | Output | Shape | Param # |
|---|--------|-------|---------|
| dense (Dense) | (None, | 64) | 832 |
| dropout (Dropout) | (None, | 64) | 0 |
| dense_1 (Dense) | (None, | 32) | 2080 |
| dropout_1 (Dropout) | (None, | 32) | 0 |
| dense_2 (Dense) | (None, | 1) | 33 |
| Total params: 2,945 Trainable params: 2,945 Non-trainable params: 0 | | | |

Figure 3. LSTM summary.

| Layer (type) | Output | Shape | Param # |
|---|--------|--------|---------|
| lstm (LSTM) | (None, | 1, 64) | 19712 |
| batch_normalization (BatchNo | (None, | 1, 64) | 256 |
| dropout_2 (Dropout) | (None, | 1, 64) | 0 |
| lstm_1 (LSTM) | (None, | 32) | 12416 |
| batch_normalization_1 (Batch | (None, | 32) | 128 |
| dropout_3 (Dropout) | (None, | 32) | 0 |
| dense_3 (Dense) | (None, | 16) | 528 |
| dense_4 (Dense) | (None, | 1) | 17 |
| Total params: 33,057 Trainable params: 32,865 Non-trainable params: 192 | | | |

the data. It also included Batch Normalization layers and additional Dropout layers, increasing depth and the ability to extract complex patterns. The first layer was an LSTM with 64 units, responsible for capturing initial temporal dependencies. A Batch Normalization layer was then applied to stabilize activations and gradients, followed by Dropout to reduce overfitting. The second LSTM layer, with 32 units, extracted deeper temporal features at a more condensed representation level. Again, Batch Normalization and Dropout followed. After these two recurrent layers, a dense layer with 16 neurons refined the aggregated information and prepared the regression model. The output layer consisted of a single neuron, providing the predicted continuous value. This architecture totaled 33,057 parameters (32,865 trainable and 192 non-trainable, mainly normalization parameters), highlighting increased complexity compared to the DNN.

Hybrid Model

third model incorporated multiple The normalization mechanisms, LSTM layers, and an Attention module to capture subtler interactions between input variables. Unlike previous models, this architecture employs two sequential LSTM layers (with 64 and 32 units, respectively), each followed by Batch Normalization and Dropout. Then, an Attention block emphasized relevant temporal patterns. The attention output was concatenated with the output of the previous layer, forming a richer contextual vector. A dense layer with 16 neurons refined this representation, followed by Dropout, and another dense layer with eight neurons. The final linear output layer predicted Rf. This model had 33,697 parameters (33,505 of which were trainable), demonstrating greater depth and complexity than the previous models.

Figure 4. Hybrid model summary.

| Layer (type) | Output Sha | pe | Param # | Connected to |
|--|------------|------|---------|--------------------------------------|
| input_2 (InputLayer) | [(None, 1, | 12)] | ø | |
| lstm_4 (LSTM) | (None, 1, | 64) | 19712 | input_2[0][0] |
| batch_normalization_4 (BatchNor | (None, 1, | 64) | 256 | lstm_4[0][0] |
| dropout_7 (Dropout) | (None, 1, | 64) | 0 | batch_normalization_4[0][0] |
| lstm_5 (LSTM) | (None, 1, | 32) | 12416 | dropout_7[0][0] |
| batch_normalization_5 (BatchNor | (None, 1, | 32) | 128 | 1stm_5[0][0] |
| dropout_8 (Dropout) | (None, 1, | 32) | 0 | batch_normalization_5[0][0] |
| attention_1 (Attention) | (None, 1, | 32) | 0 | dropout_8[0][0] dropout_8[0][0] |
| concatenate_1 (Concatenate) | (None, 1, | 64) | 0 | dropout_8[0][0] attention_1[0][0] |
| dense_8 (Dense) | (None, 1, | 16) | 1040 | concatenate_1[0][0] |
| dropout_9 (Dropout) | (None, 1, | 16) | 0 | dense_8[0][0] |
| dense_9 (Dense) | (None, 1, | 8) | 136 | dropout_9[0][0] |
| dense_10 (Dense) | (None, 1, | 1) | 9 | dense_9[0][0] |
| ====================================== | | | | |

Results and Discussion

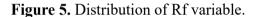
Before prediction modeling, an exploratory analysis of the fouling coefficient (Rf) was performed. The histogram (Figure 5) showed that most Rf values ranged from 60 to 80, indicating moderate to high levels of fouling. Lower concentrations (10–20) were less frequent, while extreme values near 90 suggested occasional severe fouling episodes.

The sequential plot (Figure 6) displayed oscillations, with Rf occasionally exceeding 80 or dropping below 30. Sharp declines (e.g., around observation 2000) may indicate cleaning or maintenance events, or abrupt operational changes.

These analyses confirmed Rf's dynamic behavior, characterized by oscillations and a concentration range of moderate to high levels. Models thus needed to handle frequent variations and sudden peaks.

The results of the models were: DNN Model: MSE = 0.01835; RMSE = 0.13549; MAE = 0.10743; R² = 0.3049. LSTM Model: MSE = 0.01863; RMSE = 0.13649; MAE = 0.10895; R² = 0.29458. Hybrid Model: MSE = 0.01856; RMSE = 0.13624; MAE = 0.10663; R² = 0.29720.

The DNN showed the best performance, with lower error metrics and greater training stability, while the LSTM exhibited instability. The Hybrid model performed better than the other two.



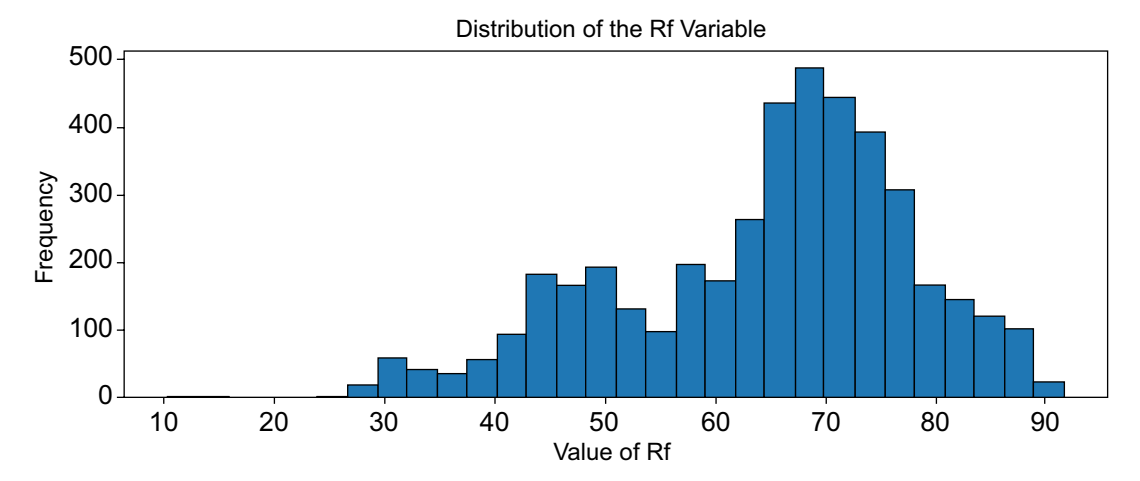
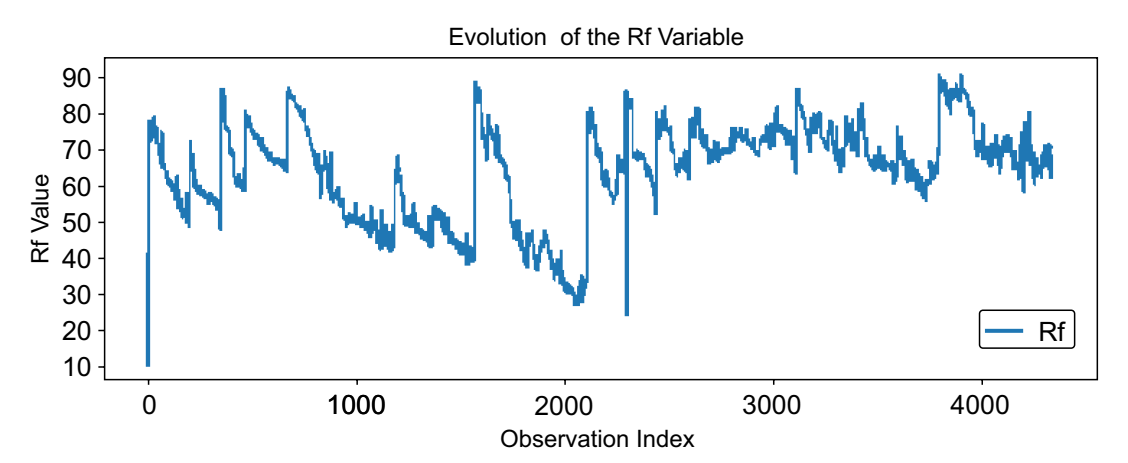


Figure 6. Evolution of Rf variable.



Conclusion

The reasonable agreement between actual and predicted values confirmed the feasibility of these models for practical applications. Predictive modeling can significantly enhance operational efficiency and lower maintenance and energy costs in refineries.

The comparison revealed that the DNN was more robust, with a lower MSE and more stable training, whereas the LSTM encountered generalization challenges. The Hybrid model improved representation, but with slightly higher complexity. These findings highlight the importance of carefully selecting deep learning models and tuning their hyperparameters for accurate industrial fouling prediction. Personalized AI solutions tailored to specific contexts and data characteristics are essential for reliability.

Acknowledgements

The authors acknowledge the financial support of the Human Resources Program of the National Agency of Petroleum, Natural Gas, and Biofuels (PRH/ANP–PRH27.1/SENAI CIMATEC), funded by investments from oil companies under the R&D Clause of ANP Resolution No. 50/2015, and the

São Paulo Research Foundation (FAPESP), process No. 2024/10433-6.

References

- França Netto L. Introdução ao controle de processos químicos. 2018. Available from: https://www.academia. edu/.
- Silva Filho AM. Autocorrelação e correlação cruzada: teorias e aplicações. 2014. Available from: https:// www.lareferencia.info/.
- Bott TR. Heat Exchanger Design Handbook (Mechanical Engineering). Amsterdam: Elsevier Science; 1995. ISBN: 978-0-444-82186-7.
- Madhu PKR, Subbaiah J, Krithivasan K. RF-LSTM-based method for prediction and diagnosis of deposition in heat exchanger. Asia Pac J Chem Eng. 2021;16(5):e2684. Available from: https://onlinelibrary.wiley.com/.
- Coletti F, Hewitt G, editors. Crude oil deposition: deposit characterization, measurements, and modeling. Oxford: Gulf Professional Publishing; 2014.
- Barbosa NS, Almeida IS, Gomes DS, Machado IL. Projeto de um protótipo de trocador de calor. Rev Bras Cienc Tecnol Inov. 2017;2(2):109-24. Available from: https://seer.uftm.edu.br/.
- Miguel Júnior AR. Análise comparativa de desempenho de modelos semi-empíricos na predição de deposição em baterias de trocadores de calor de refinarias de petróleo [dissertation]. Salvador: Centro Universitário SENAI CIMATEC; 2020.
- 8. Zhang S, Li Y. Hybrid deep learning for heat exchanger fouling: CNN meets particle swarm optimization. Appl Therm Eng. 2023;223:119903.

Thermal Analysis Algorithm for Oil and Gas Wells

João Victor Carvalho de Mattos^{1*}, Márcio de Melo Araújo¹, José Fábio Abreu de Andrade¹

SENAI CIMATEC University; Salvador, Bahia, Brazil

Thermal failures are common in oil and gas well structures, since they operate under extreme temperatures. Therefore, it is essential to investigate the thermal factors that can lead to failures in order to prevent accidents. This article presents an innovative thermal analysis method, based on steady-state heat exchanges, simulated using a Microsoft Excel algorithm to calculate the heat exchange processes among well components. The results proved to be adequate, illustrating numerically and graphically two operation scenarios proposed for the well. Therefore, it serves as an alternative to meet the growing demand for studies on thermal failures in the oil and gas industry.

Keywords: Oil and Gas. Wells. Structure Failures. Heat Exchange.

Oil and gas wells typically operate at high temperatures, either due to the heated fluids used or the geothermal properties of the geological formation in which the well is located [1,2]. These circumstances directly affect the components of a sound system, leading to mechanical and structural failures [3]. Those failures are, in part, due to thermal factors, as temperature or thermal gradients at the well's components generate stresses and deformations, increasing the likelihood of accidents [4-6]. Well casings are commonly affected by these thermal factors, being critical for oil and gas production; therefore, an operational well must have a casing project with a thorough thermal analysis [7].

Therefore, it is helpful to develop studies and methods that focus on analyzing the factors involved in these thermal failure processes, thereby minimizing the effects and accidents related to thermal reactions in oil and gas well operations [8-10]. This study presents a method, developed as a Microsoft Excel algorithm, for analyzing the effects of temperature on the components of an onshore laboratory well project, designed for testing in the oil and gas industry. This algorithm

Received on 18 May 2025; revised 21 July 2025. Address for correspondence: João Victor Carvalho de Mattos. Av. Orlando Gomes, 1845 - Piatã, Salvador – BA – Brazil, Zip Code: 41650-010. E-mail: joao.mattos@aln.senaicimatec. edu.br.

J Bioeng. Tech. Health 2025;8(4):370-375 © 2025 by SENAI CIMATEC University. All rights reserved.

aims to simulate the heat exchanges in a test well, facilitating thermal analysis of the structure and verifying the factors involved in the process. It calculates the temperature of the components applied to optimize a well project. In this case, the method was primarily applied to the analysis of well casing design.

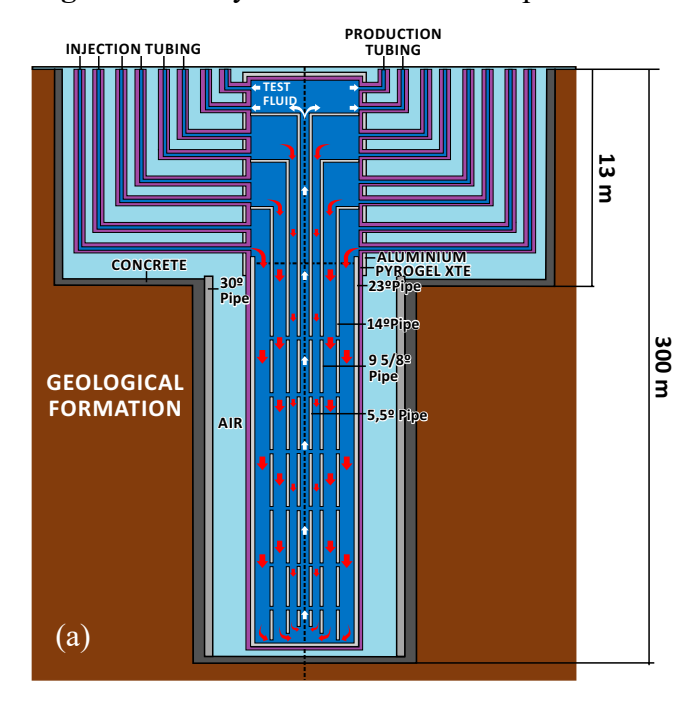
Materials and Methods

Well Description

In this work, the project of a 300 m well with a 13 m wellhead subsurface chamber was analyzed. Figure 1a presents a simplified model of the system considered for the calculations, consisting of: casing and pipes (in gray), two layers of insulation (in light gray and purple), a layer of cementation concrete (In black), the geological formation (In brown), the layers of air between in the well (In light blue) and a water-based test fluid (In dark blue).

Figure 1b illustrates the layout used for the cells in Microsoft Excel software, and their position, as an example for calculating the equilibrium temperature in the well. Each line represents 0.1 m of the well length, and each column one of its components. In this figure, the orange cells represent the masses whose equilibrium temperatures are being calculated. In contrast, the blue cells illustrate the masses whose temperatures influence the calculation of the equilibrium temperature at the determined orange cell.

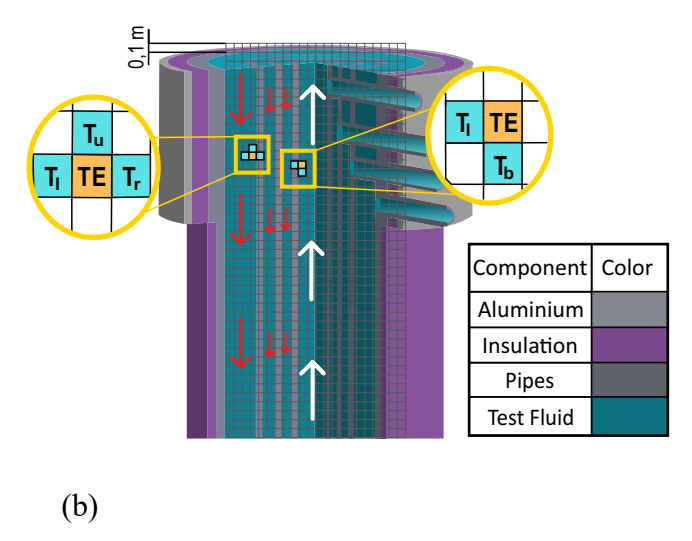
Figure 1. 2D layout of main well components and cell arrangements for calculations.



Thus, this well is a system composed of injection pipes connected laterally to different fluid spools, which are arranged above a 23-inch-diameter and 2-inch-thick steel tube that extends to the bottom of the well. Figure 1a shows fluid flow directions at healthy injection (red arrows) and production (white arrows) operations. The fluid is injected laterally, and the production consists of the passage of the fluid to the central tube and its return to the surface. To simplify the calculations without compromising the accuracy of the results, it was assumed that the fluid operates in a permanent flow regime and that the process experiences no thermal variation due to the mixing of fluids at different temperatures, only through heat exchanges. In this analysis, two scenarios were considered for the injection of heated and cooled test fluid, with different initial temperatures for each case: 150 °C for the first scenario and 4 °C for the second.

Calculation Model

The basis of the model calculation is the fluid's thermal energy, which is transferred or received, depending on the fluid temperature, to all other components through heat exchange processes.



These are categorized as conduction for both the processes between the formation, concrete, and 30" pipe, as well as for the insulation and the 23" pipe. Additionally, they are categorized as convection for those that occur between the air and the insulation, as well as for the fluid and the pipes. It was assumed that the heat flow in the well follows the same direction as the fluid flow, while spreading horizontally throughout the system.

To adapt these concepts to the calculations and the algorithm created in Microsoft Excel, the well length was segmented into a grid of cells, as shown. The temperature of each cell was calculated using the equations (1) and (2), according to its respective scenario, where T1 is the component initial temperature, "c" its specific heat, "m" its mass and the subscripts "u", "r", "l" and "b" to refer the terms respectively to the cells in the upper, right, left and bottom layer of the one whose equilibrium temperature (TE) is calculated [11].

$$T_E = \frac{m_u \cdot c_u \cdot T_u + m_r \cdot c_r \cdot T_r + m_l \cdot c_l \cdot T_l}{m_u \cdot c_u + m_r \cdot c_r + m_l \cdot c_l} (Injection) (1)$$

$$T_E = \frac{m_b \cdot c_b \cdot T_b + m_l \cdot c_l \cdot T_l}{m_b \cdot c_b + m_l \cdot c_l} (Production)$$
 (2)

Boundary Conditions

Considering the system as isolated, the maximum and minimum input temperatures were used as boundary conditions for the analysis, which was then used to calculate the temperature for the components that undergo heat exchange processes with others during operation.

The temperature of the geological formation at the end of the system was calculated as a function of the geothermal gradient, which is the rate of variation of soil temperature with depth (h), as shown in Eq. 3. In this study, an ambient temperature was considered a temperature of 25 $^{\circ}$ C [12] and a geothermal gradient (GT) of 0.025 $^{\circ}$ C/m [13].

$$TF = 25^{\circ}C + GT \cdot h \tag{3}$$

The air temperature inside the well also does not present significant changes, as this layer of air is not trapped inside the structure. Therefore, it continuously undergoes a convection process with the external air, continually renewing itself and dissipating the accumulated heat, maintaining an ambient temperature of 25 °C.

Calculation Algorithm

The algorithm follows the logic presented in Figure 2 to reproduce the cited calculations.

To obtain accurate results using Excel, the "Iterative Calculation" and "Circular Reference" functions were applied. From this data, graphs were

created that illustrate the temperature distribution of the well components according to depth, representing the actual geometric arrangement of the elements present in the system. This was achieved by inserting the calculated temperature data into the cells of a separate spreadsheet, organized to illustrate the well's component arrangement, and applying the Microsoft Excel "Conditional Formatting" function to them, which correlates cell values to a color pattern defined by the user.

Results Validation

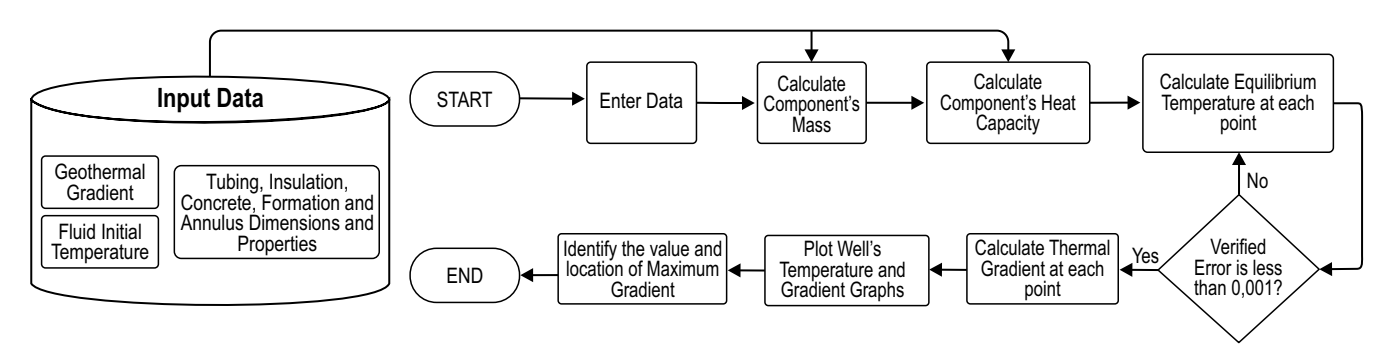
To minimize possible numerical errors or due to assumptions considered in relation to the algorithm, the temperatures of the 23" tube surfaces were analytically calculated. We calculated the total heat capacity of the system based on the thermal resistances of each component. Equation 6 was used to calculate the total heat capacity, with T_{max} and T_{amb} representing the maximum and minimum temperatures present, respectively. Equation 7 was used to define the temperature of the external surface of the tube [14]. Comparing the results of the equations with the temperature values obtained through the algorithm, it was possible to verify the accuracy of the developed method.

$$Q_{t=\frac{T_{max}-T_{amb}}{R_t}} \tag{3}$$

$$T_{ext} = T_{max} - Q_t \cdot R_{tube} \tag{4}$$

To verify the accuracy of the elaborated algorithm once more, a mesh convergence study

Figure 2. Flowchart of the developed calculation algorithm.



was conducted, in which other discretization parameters were applied in relation to the software grid line, with the lines representing 0.2 m and 0.5 m of the well length, unlike the 0.1 m used as the standard originally. After all, the results of each model were verified and compared.

Results and Discussion

In Scenario 1, as depicted in Figure 3, a liquid solution is injected at 150 °C into the well. At the operation's initial instant (Figure 3a), it is already possible to identify, in yellow, a slight heating in the produced fluid, due to its contact with the annular sections already filled with test fluid. Similarly, at the medium and final instant (Figure 3b and 3c,

respectively), the produced fluid tends to heat until it reaches a temperature closer to that of the injected fluid. Thus, there is a tendency for the temperature of the well elements to increase after the passage of the fluid, as continuous injection causes the system components to heat up. The thermal gradients acting in the casing were calculated by subtracting the external surface temperature from the internal surface temperature at each point along the pipe.

In Scenario 2, shown in Figure 4, a fluid is injected at 4 °C, exhibiting a behavior similar to that observed in Scenario 1, with the thermal gradient calculated in the same manner. However, in this case, the fluid inlet temperature is lower than the ambient temperature, and the other components tend to cool through their passage, reaching a final temperature of 4 °C.

Figure 3. Well temperature profile in Scenario 1.

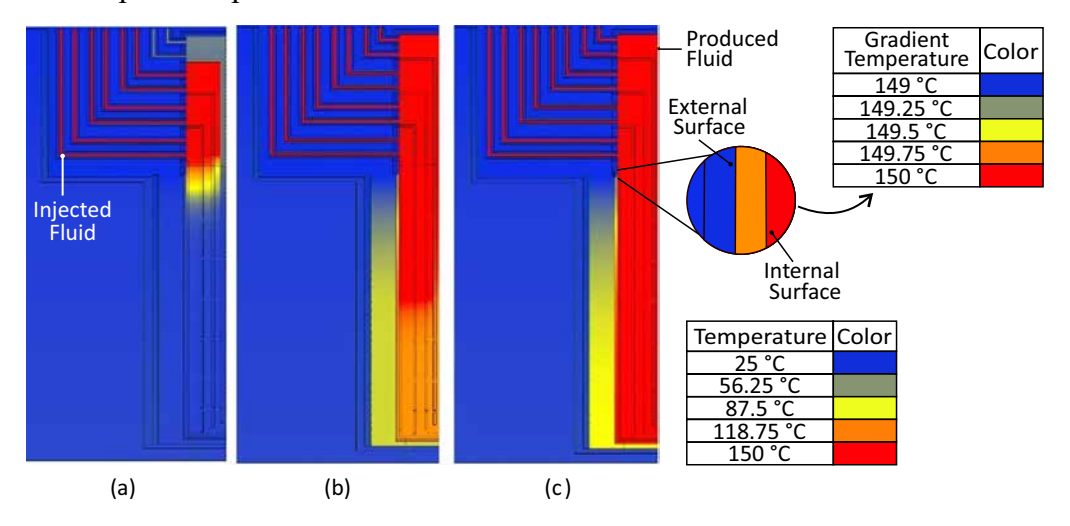
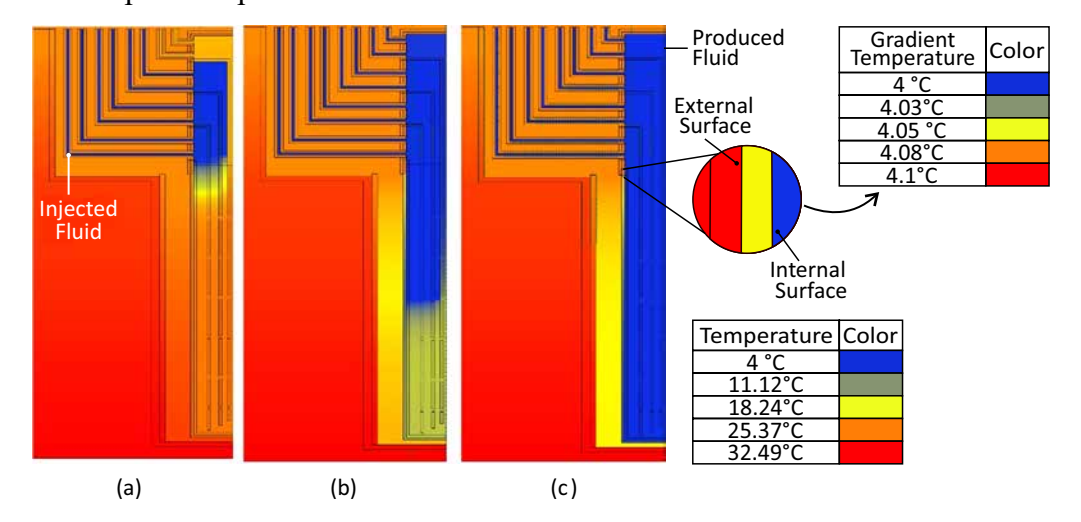


Figure 4. Well temperature profile in Scenario 2



Thus, it was possible to verify the temperature of each point of the structure, as well as the thermal gradient acting on them. The behavior of the thermal gradients acting on the casing was calculated for the final instants of both scenarios and shown in Figure 5, according to their respective inlet temperatures. Those instants are considered critical because all the annular spaces are filled with and at the temperature of the injected fluid, which brings the internal temperature of the casing near the boundary conditions for each situation.

The maximum gradients were identified at the top of the casing, primarily because this region is in contact simultaneously with the air at ambient temperature and with the injected fluid on its external and internal surfaces, respectively. This increases the temperature difference between those surfaces and maximizes the gradient. Scenario 1

presents a greater gradient because the fluid injected at 150 °C differs more from the air at 25 °C than the fluid at 4 °C, as in Scenario 2. This indicates that the maximum stresses are acting on this location, since thermal stress is directly proportional to the temperature gradient, classifying it as the critical region of the structure [15].

The validation test consisted of comparing the percentage divergence between the casing external surface temperature at the critical region calculated analytically using the mesh divergence models and by the algorithm, both of which were informed by Table 1.

Thus, the maximum difference calculated, considering both operation scenarios, did not exceed 1,88%, which is considered a divergence that did not significantly affect the results obtained, certifying the accuracy and viability of the developed method.

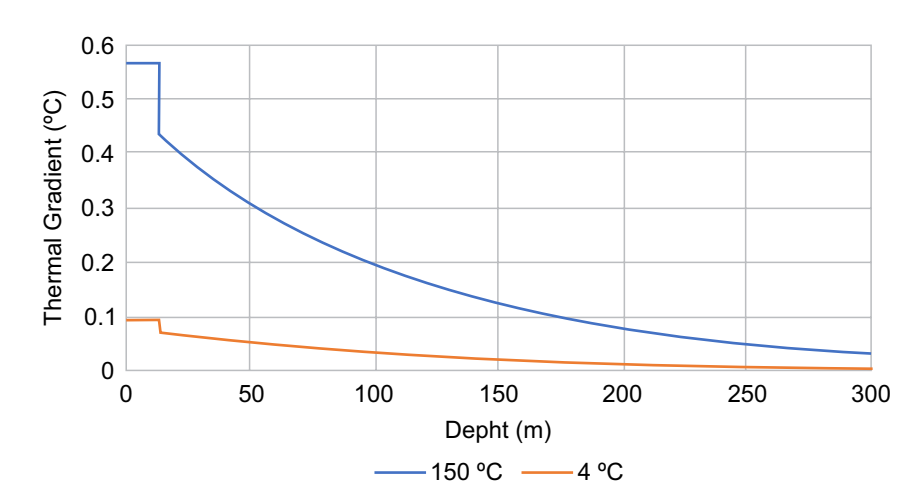


Figure 5. Thermal gradients acting on the well's casing at operation.

Table 1. Percentage divergence for each analyzed test model.

| Test Model | Calculated Temperature | | Standar Tempe | d Model rature | Percentage Divergence | | |
|------------|------------------------|------------|-----------------------|-------------------|-----------------------|------------|-------|
| | Scenario 1 | Scenario 2 | Scenario 1 Scenario 2 | | Scenario 1 | Scenario 2 | |
| Analytical | 149.4421 °C | 4.0937 °C | 149.4269 °C | | | 0.01% | 0.06% |
| 0.2 m Mesh | 149.7128 ℃ | 4.0482 °C | | 4.0962 °C | 0.19% | 1.17% | |
| 0.5 m Mesh | 149.8850 °C | 4.0193 °C | | | 0.31% | 1.88% | |

Conclusion

This study verified the behavior and influence of thermal factors on the structure of a laboratory well, identifying that the test fluid and the geological formation are the components that govern heat exchanges during operation. This means that the elements adjacent to them tend to reach thermal equilibrium at a temperature similar to their own.

A layer of non-trapped air is identified inside the well, acting as a heat sink that constantly transports air from the bottom of the well to the surface. Using the algorithm presented, it was possible to illustrate the thermal behavior of the well's components and accurately calculate the temperatures of each component in the system, as well as the thermal gradient in the well's casing. This allowed verification of the critical region and facilitated the analysis of the system's safety during operation. Thus, this proves that the developed method is a suitable technique for thermal analyses of wells, serving as an alternative to optimize analyses for projects and utilize robust software, providing a simple and innovative solution to mitigate failures and accidents. More studies have been conducted on the method presented in this article, including an analysis of the stresses acting on the well components, particularly on the casing, to determine possible failure modes for the structure and assess whether the project meets the required standards. It is intended to complement this work in the future, making it an applicable method for well projects in the oil and gas industry.

Acknowledgments

We thank to the Brazilian National Agency of Petroleum, Natural Gas and Biofuels (ANP), the ANP Human Resources Program (PRH 27.1), and to the SENAI CIMATEC.

References

- 1. Zhi Z, Wang H. Effect of thermal expansion annulus pressure on cement sheath mechanical integrity in HPHT gas wells. Appl Therm Eng. 2017;118:600–11.
- 2. Thorbjörnsson I, Kaldal GS, Ragnarsson Á. Testing flexible couplings for geothermal wells. Palm Springs: GRC; 2019.
- Thorbjornsson I, Kaldal GS, Gunnarsson BS, Ragnarsson Á. A new approach to mitigate casing failures in hightemperature geothermal wells. ISOR, Iceland. GRC Trans. 2017;41.
- 4. Maharaj G. Thermal well casing failure analysis. In: SPE Latin America/Caribbean Petroleum Engineering Conference; Apr 1996; Port-of-Spain, Trinidad.
- 5. Zhi Z, Wang H. Effect of thermal expansion annulus pressure on cement sheath mechanical integrity in HPHT gas wells. Appl Therm Eng. 2017;118:600–11.
- 6. Chen L, Yu W, Lu Y, Wu P, Han F. Characteristics of heat fluxes of an oil pipeline armed with thermosyphons in permafrost regions. Appl Therm Eng. 2021;190:116694.
- 7. Chilingarian GV, Rahman SS. Casing design theory and practice. Amsterdam: Elsevier; 1995.
- 8. Zhang B, Guan Z, Hasan AR, Lu N, Wang Q, Xu Y, et al. Development and design of new casing to mitigate trapped annular pressure caused by thermal expansion in oil and gas wells. Appl Therm Eng. 2017;118:292–8.
- Cao X, Deng Z, Nian Y. Evaluation of annual performances of crude oil pipeline transportation by solar heating. Appl Therm Eng. 2024;245.
- Fei Z, Li Y, Liu Z, Tang Y. Flow and heat transfer characteristics of oil-based drilling cuttings in a screwdriving spiral heat exchanger. Appl Therm Eng. 2020;181.
- 11. Incropera FP, DeWitt DP. Fundamentos de transferência de calor e de massa. 5th ed. Rio de Janeiro: LTC; 2003.
- 12. Lillo M, Suárez F, Hausner MB, Yáñez G, Veloso EA. Extension of duplexed single-ended distributed temperature sensing calibration algorithms and their application in geothermal systems. Sensors. 2022;22(9):3319.
- 13. Toledo MCM. Estrutura interna da Terra. São Paulo: USP/UNIVESP/EDUSP; 2014.
- 14. Çengel YA, Ghajar AJ. Transferência de calor e massa: uma abordagem prática. 4th ed. 2012.
- 15. Young WC, Budynas RG. Roark's formulas for stress and strain. 7th ed. New York: McGraw Hill; 2001.

Evaluation of the Degradation Process of Polyamide 12 Manufactured via Multi Jet Fusion: An FTIR Analysis

Beatriz Almeida Santos Castro^{1*}, Pollyana da Silva Melo², Rodrigo Santiago Coelho²

¹SENAI CIMATEC University, Postgraduate Program MPDS; ²SENAI Institute of Innovation in Conformation and Joining of Materials (ISI&FJ), SENAI CIMATEC University; Salvador, Bahia, Brazil

This study investigated the effects of accelerated weathering on Polyamide 12 (PA12) manufactured by Multi Jet Fusion (MJF) technology, focusing on the chemical and structural changes of the material. The samples were exposed to UV-A radiation in an accelerated weathering chamber for 360, 720, and 1080 hours. To evaluate the degradation effect, characterization was performed by Fourier Transform Infrared Spectroscopy (FTIR), which revealed minor changes in the functional bands between 1500 cm⁻¹ and 1300 cm⁻¹, indicative of photo-oxidation. Visual analysis, in turn, revealed no cracks or surface deformations. This study contributes to the understanding of the structural modifications of PA12 and its durability in extreme environments, which is essential for critical applications in the oil and gas sector, where resistance to aging is fundamental. Future research will continue to evaluate the impacts of prolonged exposures on the material's properties. Keywords: Polyamide 12. MJF, Accelerated Weathering, FTIR.

Additive manufacturing, particularly through Multi Jet Fusion (MJF) technology, has become crucial for producing high-precision components in industries such as oil and gas [1]. PA12 is a widely used polymer in this process, distinguished by its properties of mechanical strength, thermal stability, and chemical resistance, which are crucial to ensuring the functionality and reliability of components manufactured in demanding environments [2]. MJF enables the efficient production of complex geometry parts, which are vital for manufacturing components such as valves and connectors that require high precision and must withstand extreme conditions [3].

Exposure to environmental factors, such as UV radiation, humidity, and thermal cycling, can lead to degradation in PA12, which affects its properties over time. These effects include photodegradation, hydrolysis, and thermal aging, which can compromise the structural integrity of components. Studies indicate that encapsulation can mitigate these effects, but improvements in

Received on 15 May 2025; revised 23 July 2025. Address for correspondence: Beatriz Almeida Santos Castro. Av. Orlando Gomes, 1845 - Piatã, Salvador – BA – Brazil, Zipcode: 41650-010. E-mail: beatriz.castro@fbter.org.br. Original extended abstract presented at SAPCT 2025.

J Bioeng. Tech. Health 2025;8(4):376-378 © 2025 by SENAI CIMATEC University. All rights reserved.

the material itself are necessary to ensure greater durability and reliability [4]. Accelerated aging tests, which simulate extreme environmental conditions, are essential for better understanding the rate and nature of this degradation, providing crucial data for optimizing design and material properties [5].

This study aims to contribute to the oil and gas industry, where the durability and reliability of components are essential. Understanding how accelerated aging affects PA12 components manufactured by MJF may lead to the development of new materials and manufacturing processes that enhance resistance to environmental stressors. The results may also inspire the implementation of protective measures, promoting greater longevity and operational safety under extreme conditions [6].

Materials and Methods

The samples used in the study were printed in the Z orientation, with a 20° orientation and 7 mm spacing between each piece within the printing bed. Samples were produced with HP 3D High Reusability PA12, with a ratio of 80% reused powder and 20% virgin powder. Printing was performed on an HP Multi Jet Fusion 5210, following the manufacturer's recommendations.

The printer had a build volume of $380 \times 284 \times 380$ mm, a print speed of up to 5058 cm³/h, a resolution of 1200 dpi, and a layer thickness of 0.08 mm.

The accelerated weathering test was conducted in a BASS UUV/2009 chamber, utilizing UV-A lamps with a 340 nm emission. The exposure cycle was continuous for 24 hours a day, totaling 1,080 hours of exposure. Samples were removed for analysis after 360, 720, and 1080 h. To minimize interference from external factors, the samples were stored in aluminum foil until they were tested. This conditioning aimed to prevent exposure to humidity, oxygen, and especially electromagnetic radiation, particularly visible and UV light, whose protection is fundamental after the accelerated weathering cycles with UV exposure, ensuring the preservation of sample properties for subsequent tests.

FTIR analyses were performed on a Thermo ScientificTM Nicolet iS10 FTIR, using an Attenuated Total Reflectance (ATR) accessory. The equipment, with a KBr beam splitter, covered the spectral range from 7800 cm⁻¹ to 350 cm⁻¹, and analyses were carried out using OMNIC software.

Results and Discussion

For analyzing the behavior of Polyamide 12 samples subjected to accelerated weathering, FTIR characterization was employed. This technique plays a crucial role in identifying potential changes in the functional groups and chemical bonds of the polymer, thereby enabling a more detailed understanding of degradation, photo-oxidation, and material aging processes. The FTIR spectrum graph presented in Figure 1 shows the evolution of the characteristic bands of Polyamide 12 (PA12) after exposure to different periods of accelerated weathering. This behavior indicates changes in the chemical structure of the polymer, which are associated with degradation processes induced by aging conditions.

It is observed that the leading characteristic bands of PA12 remain throughout aging; however, small changes are noticeable, especially in the region between 1500 cm⁻¹ and 1300 cm⁻¹. These

changes suggest modifications in the chemical bonds of the polymer chain, possibly related to photo-oxidative degradation caused by UV radiation and thermal action [7].

Detailed studies on the effects of weathering in PA12 and other polymers demonstrate that prolonged exposure to UV radiation can lead to chemical changes in the material's structure, primarily due to the breaking of amide bonds and the formation of new functional groups, such as carbonyls. Furthermore, the intensification of specific bands in the region of 1650 cm⁻¹ is often attributed to degradation of the material [7].

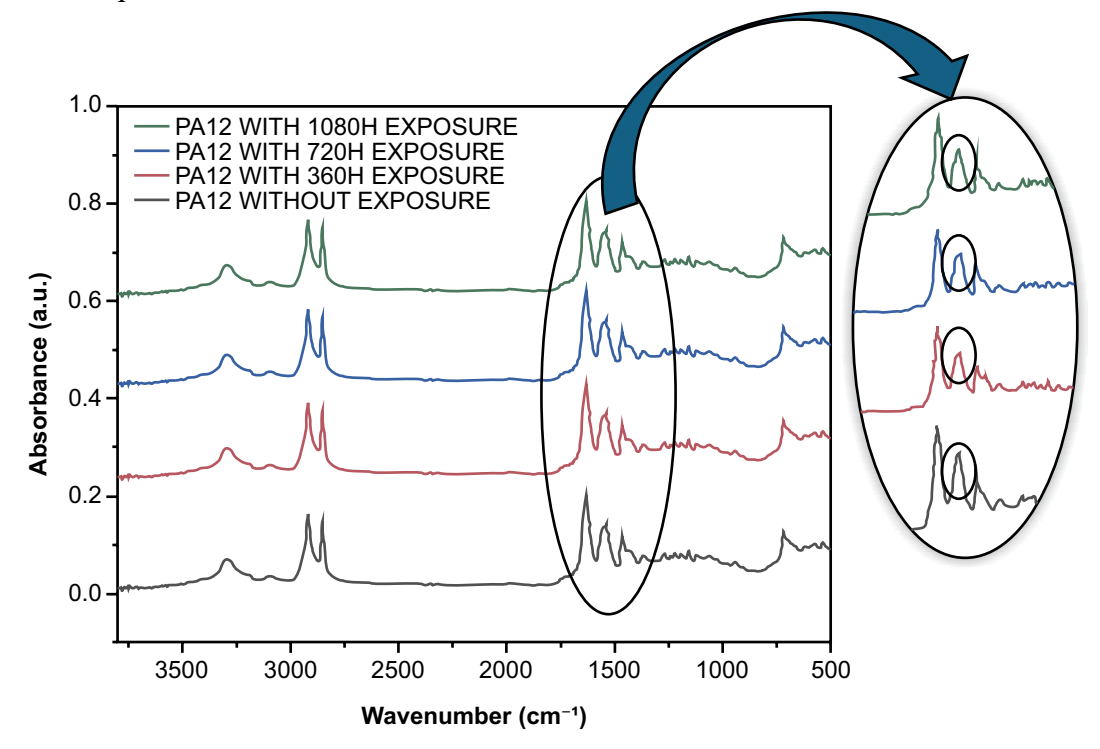
These results indicate that although PA12 maintains its overall chemical structure during aging, there is progressive degradation that can compromise its mechanical properties and long-term stability, a crucial factor for applications in the oil and gas sector. The use of stabilizing additives may be an interesting strategy to mitigate these effects and ensure greater durability of the material under severe operating conditions.

In visual analysis, no significant surface changes were observed in PA12 after accelerated weathering exposure. The absence of cracks, fissures, or apparent deformations suggests that although the material underwent aging processes, its surface morphology remained stable over the exposure period. This behavior may be related to PA12's intrinsic resistance to adverse environmental conditions such as UV radiation and humidity [8].

Conclusion

The results obtained so far indicate that PA12 exhibits structural and surface stability under the evaluated conditions, with minor changes in functional bands detected by FTIR and no visible cracks or deformations on the material's surface. However, due to the complexity of polymer degradation processes, such as photo-oxidation, and adverse environmental conditions, it is necessary to extend the exposure time in accelerated weathering to evaluate more deeply the degradation mechanisms involved. This research line aims to gain a deeper understanding





of the potential chemical and physical changes in the material over time, particularly regarding the behavior of polymer chains and the formation of specific groups related to photo-oxidation. This deeper analysis will provide more robust data on the durability of the material and possible strategies to enhance its resistance in critical applications, such as the oil and gas sector.

Acknowledgments

The authors acknowledge the financial support of the Human Resources Program of the National Agency of Petroleum, Natural Gas and Biofuels (PRH/ANP-PRH27.1/SENAICIMATEC), supported with resources from the investment of qualified oil companies under the R&D Clause of ANP Resolution No. 50/2015, and the São Paulo Research Foundation (FAPESP), process No. 2024/10433-6.

References

1. Yu S, et al. Additive manufacturing of flame retardant polyamide 12 with high mechanical properties

- from regenerated powder. Rapid Prototyping J. 2023;29(7):1409–19.
- 2. O'Connor HJ, Dowling DP. Comparison between the properties of polyamide 12 and glass bead filled polyamide 12 using the multi jet fusion printing process. Addit Manuf. 2020;31:100961.
- 3. O'Connor HJ, et al. Evaluation of the mechanical performance of polymer parts fabricated using a production scale multi jet fusion printing process. Addit Manuf. 2018;22:381–7.
- 4. Badji C, et al. Influence of weathering on visual and surface aspect of wood plastic composites: Correlation approach with mechanical properties and microstructure. Polym Degrad Stab. 2017;137:162–72.
- Başaran S, et al. Comparative study on the thermal and tribological properties of PA12 and PA11 for coating applications. J Appl Polym Sci. 2024 Aug 30.
- 6. Chee SS, et al. Accelerated weathering and soil burial effects on colour, biodegradability and thermal properties of bamboo/kenaf/epoxy hybrid composites. Polym Test. 2019;79:106054.
- 7. Ainali NM, et al. Physicochemical alterations on UV aged polymers leading to microplastics formation: A multi-tiered study of polyester, polycarbonate and polyamide. Polym Degrad Stab. 2024;222:110692.
- 8. Puttonen T, et al. Mechanical properties and fracture characterization of additive manufacturing polyamide 12 after accelerated weathering. Zenodo [Internet]. 2021 Jul 8. Available from: https://zenodo.org/.

Pipeline Leak Detection Using Infrared Cameras: A Convolutional Neural Network Approach

João Vitor S. Mendes^{1*}, João Pedro Almeida¹, Rodrigo Dias Paolillo², Alexandre Adonai Silva¹, Rodrigo F. Bastos¹, Herman A. Lepikson¹

¹Robotics Deptartment, SENAI CIMATEC University; ²Optics and Photonics Department, SENAI CIMATEC University; Salvador, Bahia, Brazil

Pipeline leak detection is crucial for maintaining pipeline safety, particularly in complex environments. This study proposes a novel approach that integrates infrared cameras with a convolutional neural network model, specifically VGG16, utilizing infrared cameras that do not inherently measure temperature. Our results indicate that this approach is highly effective, with the model achieving 100% accuracy on both the training and validation datasets, and a near-zero validation loss in a laboratory environment. The confusion matrix confirmed that there were no misclassifications, and the Receiver Operating Characteristic (ROC) curve demonstrated an Area Under the Curve (AUC) of 1.0. These findings underscore the model's potential for real-world pipeline monitoring applications.

Keywords: Infrared Cameras. Leak Detection. Computer Vision.

Pipeline leak detection is a critical concern in industries such as oil and gas, as well as water management, due to its significant economic and environmental implications. Effective detection of leaks is essential to minimize losses and prevent environmental damage [1,2].

Various methods have been developed for detecting pipeline leaks, including the use of ultrasonic sensors, thermal cameras, and infrared cameras. Ultrasonic sensors detect changes in acoustic signals within the pipeline but face limitations due to physical access constraints and environmental noise interference [3]. Thermal cameras identify variations in surface temperature, although their effectiveness can be compromised by environmental conditions and variations in ambient temperature [4]. Infrared cameras are particularly notable for their ability to detect temperature differences with high sensitivity without direct contact. These cameras capture emitted infrared radiation and convert it into visible images, enabling the detection of thermal anomalies that may indicate leaks [5].

Received on 24 May 2025; revised 15 July 2025. Address for correspondence: João Vitor S. Mendes. Av. Orlando Gomes, 1845 - Piatã, Salvador - BA - Brazil, Zipcode: 41650-010 E-mail: vitor.mendes@ieee.org.

J Bioeng. Tech. Health 2025;8(4):379-384 © 2025 by SENAI CIMATEC University. All rights reserved.

Infrared cameras operate by detecting thermal radiation emitted by all objects above absolute zero. This radiation is captured by sensors within the camera and converted into a visible image that represents the thermal distribution of the observed objects. The main advantage of infrared cameras is their ability to perform inspections without physical contact and in low-visibility conditions. However, these cameras can be expensive and require precise calibration to ensure measurement accuracy [1,2].

To analyze and classify images captured by infrared cameras, advanced image processing techniques and machine learning algorithms are employed. Traditional image processing techniques may include filtering to enhance specific features and segmentation to isolate areas of interest. Machine learning algorithms, particularly Convolutional Neural Networks (CNNs), are widely used to recognize patterns and detect anomalies in thermal images [4]. Recent advancements in deep learning have shown significant improvements in the automatic and accurate detection of leaks. These methods involve training models with extensive datasets of infrared images, enabling efficient differentiation between leaks and other thermal characteristics [3,5].

The work presented by Xie and colleagues [6] introduces an innovative automated leakage detection method that combines infrared thermography (IRT) with the Faster R-CNN object

detection technique. This methodology utilizes a modified VGG16 network for feature extraction, allowing for the detection of finer leakage features and details in the original infrared images. The study reports high performance metrics, with mean Average Precisions (mAPs) of 1.00, 0.98, and 0.99 for detecting leaks at pipes, valves, and flanges, respectively, under various leakage scenarios. The results demonstrate that the proposed system is both practical and robust, maintaining high detection accuracy even in complex backgrounds and diverse operational conditions, such as varying ambient light, changes in camera angles, and pedestrian interference.

In this study, we propose a similar pipeline leak detection system of Xie and colleagues [6]. However, we use an infrared camera that does not natively measure temperature. Our objective is to assess whether this non-temperature-measuring infrared camera can achieve comparable performance to the system described by Xie and colleagues [6]. By evaluating this alternative approach, we aim to determine its effectiveness in real-world leak detection scenarios and contribute to the broader application of infrared imaging technologies in pipeline monitoring. This investigation will provide insights into the feasibility and performance of using non-temperature-sensitive infrared cameras for detecting pipeline leaks, further advancing the field of automated pipeline monitoring and safety.

Materials and Methods

This study presents the development and validation of a convolutional neural network (CNN) for detecting leaks in images. The method covers the experimental setup description and model training details, divided into data preparation, model architecture, training procedures, and performance evaluation in detail.

Model Training

The dataset consists of images organized into 'leak' and 'noleak' categories. Each image is

resized to 224x224 pixels and normalized to a [0, 1] range to standardize input features. Labels are encoded as binary values, with '0' for 'noleak' and '1' for 'leak'. To ensure balanced representation, the data is split into training and validation sets using stratified sampling, which preserves the proportion of each class.

The model utilizes the VGG16 architecture, a well-known CNN pre-trained on the ImageNet dataset. The base model, which includes multiple convolutional layers followed by max-pooling layers, is used as a feature extractor by excluding its top classification layer. The extracted feature maps are processed by a custom classification head designed as follows:

- Flattening Layer: Converts the 2D feature maps into a 1D vector.
- Dense Layer: A fully connected layer with 512 units and ReLU activation, described by

$$ReLU(x) = ma x(0, x)$$
 (1)

where *x* is the input to the layer.

- Dropout Layer: Applied with a rate of 0.5 to reduce overfitting by randomly setting half of the neurons to zero during training.
- Output Dense Layer: A single unit with sigmoid activation, which outputs a probability *p* for the binary classification:

where x is the input to the sigmoid function.

$$\sigma(x) = \frac{1}{1 + e^{-x}} \tag{2}$$

The model is compiled using the Adam optimizer, which adjusts the learning rate adaptively based on estimates of first and second moments of the gradients. The learning rate is set to (1×10^{-4}) . Adam is defined by the under rule:

$$\theta_{t+1} = \theta_t - \frac{\alpha}{\sqrt{v_t + \epsilon}} m_t \tag{3}$$

where (θt) is the parameter, (α) is the learning rate, (mt) and (vt) are estimates of the first and second moments of the gradients, respectively, and (ϵ) is a small constant for numerical stability. Binary cross-entropy is used as the loss function,

which measures the difference between the accurate labels y and the predicted probabilities p:

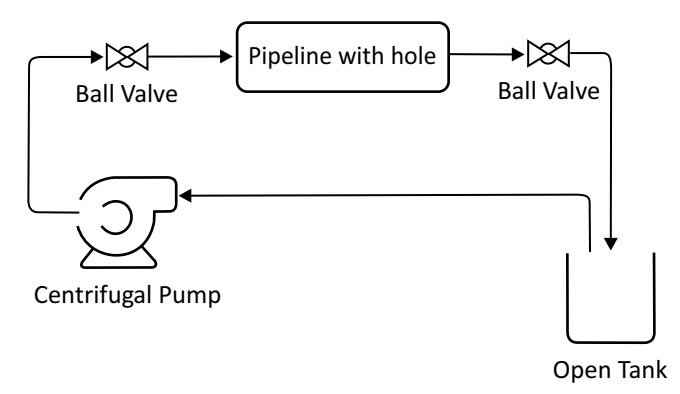
Loss =
$$-(y \log(p) + (1 - y) \log(1 - p))$$
 (2)

The model is trained for ten epochs with a batch size of 32. During training, the model's performance is monitored using accuracy and loss metrics, and training progress is recorded with a CSV logger. The average inference time per image is calculated to assess computational efficiency.

Experiment Setup (Figure 1)

To experiment, it was essential to establish a system capable of simulating a fluid leak in a pipe. The experimental setup comprised a cyclical water system utilizing an aquarium pump connected to a PVC pipe. The water transported by the pump traverses the pipe and is subsequently returned to the same receptacle as the pump, thereby completing the cycle. The water was heated using a portable electric heater/blower, thus enabling the camera to identify thermal variations in the fluid in relation to the pipe. Two distinct PVC pipes were used: one with an aperture to simulate the leak and one without, serving as a control. Data was collected using an FLIR ADK camera, which was connected to a computer running a Python script. This script was programmed to take pictures at 100-millisecond intervals, capturing thermal images of the pipe and allowing for a detailed analysis of the fluid conditions and identification of the simulated leak.

Figure 1. Technical setup drawing.



Results and Discussion

The model's performance was comprehensively evaluated using several metrics, including accuracy, loss, confusion matrix, and the Receiver Operating Characteristic (ROC) curve. The following analysis provides a detailed examination of each metric, offering insights into the model's performance.

Figure 2 presents the training and validation accuracy over the course of the epochs. The training accuracy increased from 52.5% in the first epoch to 100% by the final epoch, indicating that the model effectively learned from the training data. Similarly, the validation accuracy also reached 100% towards the end of the training, suggesting that the model generalized well to the unseen validation data. This high accuracy is indicative of the model's strong performance; however, achieving 100% accuracy may also raise concerns about potential overfitting. It is crucial to ensure that the training and validation datasets are sufficiently diverse to mitigate this risk.

The model's performance was comprehensively evaluated using several metrics, including accuracy, loss, confusion matrix, and the Receiver Operating Characteristic (ROC) curve. The following analysis provides a detailed examination of each metric and offers insights into the model's performance.

Figure 2 presents the training and validation accuracy over the course of the epochs. The training accuracy increased from 52.5% in the first epoch to 100% by the final epoch, indicating that the model effectively learned from the training data. Similarly, the validation accuracy also reached 100% towards the end of the training, suggesting that the model generalized well to the unseen validation data. This high accuracy is indicative of the model's strong performance; however, achieving 100% accuracy may also raise concerns about potential overfitting. It is crucial to ensure that the training and validation datasets are sufficiently diverse to mitigate this risk.

Figure 3 illustrates the training and validation loss over the epochs. The training loss decreased

Figure 2. Training and validation accuracy.

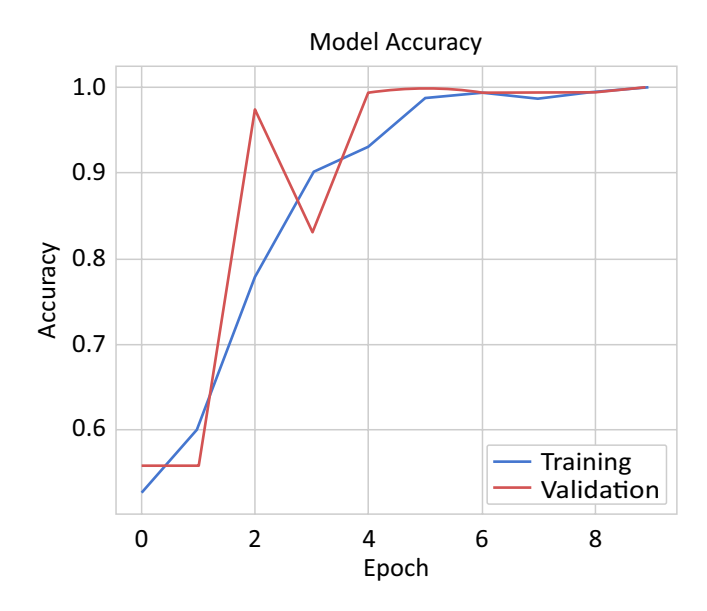
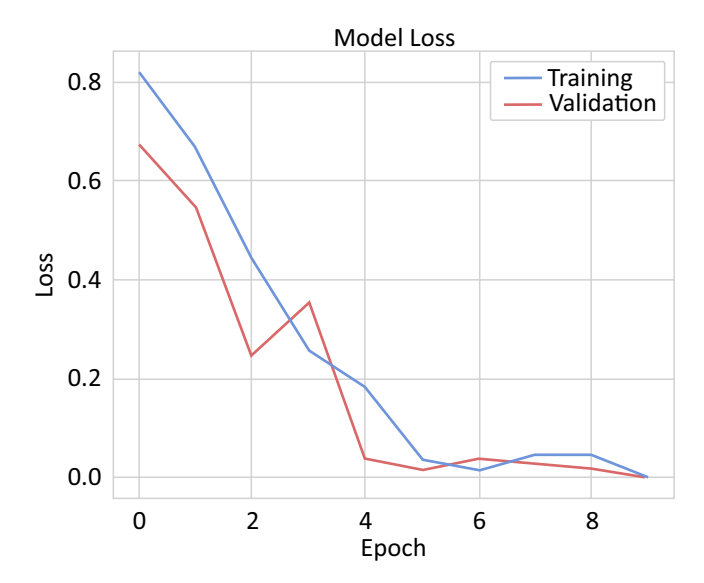


Figure 3. Training and validation loss.



significantly from 0.82 to 0.00188, while the validation loss dropped from 0.6775 to 0.0001258. This steady reduction in loss values indicates that the model improved consistently throughout the training process and maintained its performance on the validation set. The near-zero loss values for both training and validation phases underscore the model's effectiveness in minimizing error, although it is important to remain cautious about potential overfitting.

The confusion matrix shown in Figure 4 reveals a perfect classification result, with no false positives or false negatives. This matrix indicates that the model accurately identified all positive and negative cases, highlighting its reliability in distinguishing between classes. The absence of misclassifications reflects the model's high precision and effectiveness in the classification task.

Figure 4 shows the matrix with no misclassifications, reflecting the model's high accuracy in predicting the correct class for each sample.

Figure 5 presents the Receiver Operating Characteristic (ROC) curve, which demonstrates an Area Under the Curve (AUC) of 1.0. This perfect AUC indicates that the model has an exceptional ability to discriminate between positive and negative cases. The ROC curve reinforces the findings from the confusion showcasing matrix. the model's excellent performance in detecting the target class with an actual positive rate of 1.0 and no false positives. The results from the accuracy, loss, confusion matrix, and ROC curve collectively suggest that the model performs exceptionally well in detecting pipeline leaks. The high accuracy and low loss values indicate practical training and strong generalization capabilities. The perfect confusion matrix and ROC AUC further validate the model's robustness and reliability in classification tasks.

The results from the accuracy, loss, confusion matrix, and ROC curve collectively suggest that the model performs exceptionally well in detecting pipeline leaks. The high accuracy and low loss values indicate practical training and strong generalization capabilities. The perfect confusion matrix and ROC AUC further validate the model's robustness and reliability in classification tasks. Despite these positive results, it is important to consider the potential for overfitting, as indicated by the perfect performance across all metrics. Future work should involve evaluating the model on more diverse and realistic datasets to ensure its generalizability and effectiveness in real-world scenarios.

Figure 4. Confusion matrix.

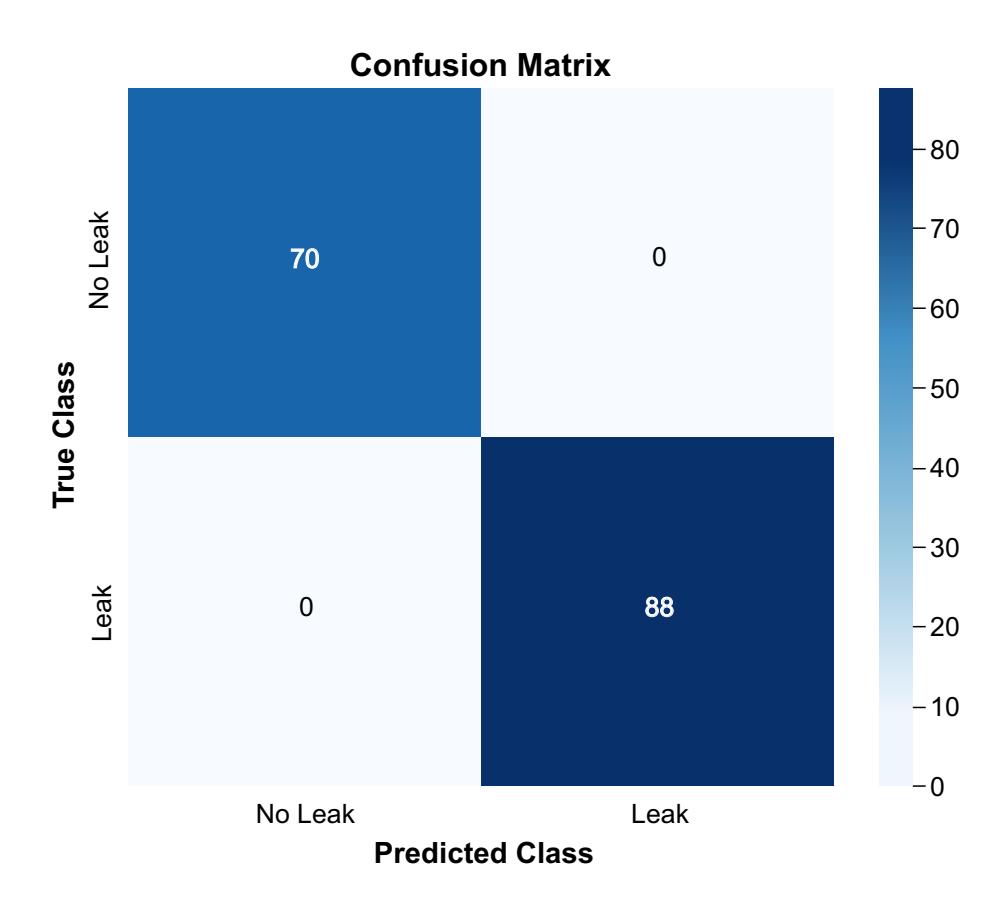
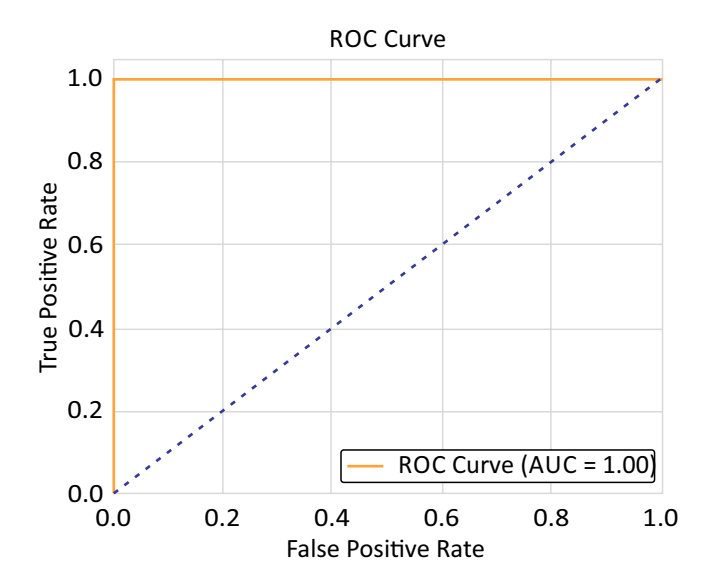


Figure 5. ROC curve.



Conclusion

This study evaluated a pipeline leak detection system that utilizes infrared thermography in conjunction with advanced machine learning techniques. Adapting a method based on a VGG16based Faster R-CNN approach, we tested an infrared camera that does not natively measure temperature to see if it could achieve comparable performance. The model performed exceptionally well, reaching 100% accuracy and showing no misclassifications, as confirmed by the ROC curve's AUC of 1.0. However, perfect accuracy suggests potential overfitting, indicating a need for further validation on more diverse datasets. The performance of this model has achieved better results than those shown in Xie and colleagues [6]. However, it is necessary to consider that this work has been tested only in a laboratory in one single pipeline; the work

developed in Xie and colleagues [6] was tested in an environment more similar to an operational system and has more complex structures.

While our findings are promising, future research should focus on testing the model in more complex environments, improving model robustness against overfitting, and exploring alternative infrared cameras that might enhance detection accuracy. Additionally, implementing the model in real-time systems and conducting comparative analyses with other leak detection methods will help to assess its real-world applicability and identify areas for improvement.

References

- Dogan E, Koc S, Koc M. Pipeline leak detection using infrared thermography: a review. J Pet Sci Eng. 2021;196:107741. Available from: https:// www.sciencedirect.com/science/article/pii/ S0920410521000544.
- Liu Y, Xu W, Li Y. Advanced techniques for pipeline leak detection: a review and future directions. Sensors

- (Basel). 2022;22(15):5604. Available from: https://www.mdpi.com/1424-8220/22/15/5604.
- 3. Yao H, Huang J, Zhang C. A comprehensive survey on pipeline leak detection methods and technologies. IEEE Trans Instrum Meas. 2023;72:3000107. Available from: https://ieeexplore.ieee.org/document/9428223.
- 4. Kumar A, Sharma S, Gupta R. Enhanced pipeline leak detection using thermal imaging and machine learning techniques. Sensors (Basel). 2023;23(4):2123. Available from: https://www.mdpi.com/1424-8220/23/4/2123.
- Cheng X, Li S, Wang C. Integration of infrared camera systems and AI for pipeline leak detection and monitoring. Comput Environ Urban Syst. 2023;90:101803. Available from: https://www.sciencedirect.com/ science/article/pii/S0197397523000834.
- Xie J, Zhang Y, He Z, Liu P, Qin Y, Wang Z, et al. Automated leakage detection method of pipeline networks under complicated backgrounds by combining infrared thermography and Faster R-CNN technique. Process Saf Environ Prot. 2023;174:39-52. Available from: https://www.sciencedirect.com/science/article/ pii/S0957582023002938.
- 7. BSI Engineering. Fluid thermal expansion. BSI Engineering. 2020. Available from: https://bsiengr.com/wp-content/uploads/2020/12/Fluid-Thermal-Expansion.pdf. White Paper Vol. 11.

3D Printing of PCL/HA Composite Scaffolds for Bone Tissue Regeneration: A Brief Review

Melissa de Souza Gomes dos Santos^{1*}, Henrique Cesar Santos de Jesus², Joanne Graziela Andrade Mendes², Imarally Vitor de Souza Ribeiro Nascimento², Josiane Dantas Viana¹

'SENAI CIMATEC University; Salvador, Bahia; 'Federal University of Recôncavo da Bahia, UFRB – CETENS; Feira de Santana, Bahia, Brazil

Tissue engineering aims to develop devices that assist in cell growth and tissue formation, making the use of biocompatible, biodegradable, and non-toxic scaffolds fundamental to promoting, for example, tissue regeneration. This review aimed to investigate the production of composites of poly(ϵ -caprolactone) (PCL) and hydroxyapatite (HA) applied to bone regeneration using 3D printing with the fused deposition modeling (FDM) technique. It is known that composites obtained from PCL, which is biocompatible and resorbable, combined with HA, which is also biocompatible and bioactive, exhibit osteoconductive properties and cell adhesion, making them effective for manufacturing scaffolds aimed at bone regeneration. The research shows that PCL/HA composite scaffolds obtained through 3D printing have promising results, which could serve as an alternative for use in bone regeneration. Keywords: Tissue Engineering. Bone Regeneration. Composites. Scaffolds.

Intending to create biological materials that promote the restoration, maintenance, or enhancement of tissue regeneration, tissue engineering has been the subject of numerous studies over the past few decades. This has intensified especially after technological advances related to bone fractures and bone tissue regeneration, which enabled improvements in patient treatments and, consequently, in outcomes [1].

Thus, scaffolds for bone tissue engineering require the use of bioactive materials, in addition to needing specific organization at both macroscopic and microscopic levels [3]. To meet these needs, one of the technological innovations that has shown positive results in this field was 3D printing, with fused deposition modeling (FDM) being the most popular technique. This process uses a heated nozzle that, when fed with a polymeric material, deposits material layer by layer onto a heated platform to create a three-dimensional object previously modeled by computer-aided design (CAD) software [2].

Received on 17 May 2025; revised 20 July 2025. Address for correspondence: Melissa de Souza Gomes dos Santos. Federal University of Recôncavo da Bahia - CETENS. Avenida Centenário, N. 697. Zipcode: 44042-280. Feira de Santana, Bahia, Brazil. E-mail: melissasouza194@gmail. com. Original extended abstract presented at SAPCT 2025.

J Bioeng. Tech. Health 2025;8(4):385-388 © 2025 by SENAI CIMATEC University. All rights reserved.

For scaffolds, they must provide support to the defective tissue, requiring specific mechanical strength. It is also essential that they present an adequate porous structure, allowing a favorable external environment for the proliferation and differentiation of the compromised tissue cells, thereby facilitating tissue repair. Therefore, this technology enables the creation of polymeric scaffolds with improved control over pore morphology, pore size, and porosity, aspects that are challenging to achieve with conventional methods [1,3].

Traditional techniques for obtaining scaffolds present several limitations, primarily because they are inadequate for producing pores with precise sizes, specific shapes, high levels of interconnectivity, and significant mechanical strength. In contrast, 3D printing has emerged as an innovative technology to overcome the limitations of traditional methods, thereby enhancing the efficiency and cost-effectiveness of final products, such as scaffolds with complex geometric designs [4,5].

Tissue engineering typically begins with a scaffold, which must be biocompatible, as well as its degradation products. This implies that the materials used in the scaffold must be non-toxic to cells, easily removable from the body, and elicit a minimal immune response due to their presence [6]. Thus, in tissue engineering, it is

crucial to comprehend the biological processes underlying cell proliferation and differentiation [4]. In general, the ideal scaffold should be made of a material that is both biocompatible and biodegradable, exhibiting mechanical characteristics similar to those of the tissue in which it will be inserted [6]. However, there is currently no biomaterial, whether inorganic or organic, that can meet all the requirements of an appropriate scaffold for bone tissue engineering. Therefore, composites emerge as a promising class of biomaterials aimed at regenerating this type of tissue [6].

Poly(ε-caprolactone) (PCL) is frequently used in scaffold manufacturing, standing out as an important polymeric matrix due to its notable characteristics, including biocompatibility, gradual resorption after implantation, and good shape retention properties [3,5]. Due to its melting point below 100 °C, PCL becomes an excellent choice for scaffold applications. This occurs because most polymeric biomaterials do not degrade at the temperature at which PCL melts, which is an advantage in polymeric operations that use thermal fusion [5,7].

This characteristic enables the combination of PCL with new types of composites, thereby enhancing the matrix properties. However, when used in bone tissue engineering, the new bone tissue does not adhere effectively to the polymer surface due to its low bioactivity. Hydroxyapatite (HA), which exhibits high bioactivity, has been utilized as a bone substitute since it constitutes approximately 70% of the composition of natural bone. Thus, it is believed that PCL/HA composites, combined with the biocompatibility of both materials, are viable for scaffold applications in bone tissue engineering [3,8].

Therefore, this research will present, clearly and concisely, a review of a composite biomaterial formed by PCL, a thermoplastic, and hydroxyapatite (HA), a bioceramic, for the production of scaffolds in bone regeneration applications.

Materials and Methods

The method approach adopted for this work was qualitative, combining an analysis of a set of

keywords in a database with the reading of works generated as a result of this search, to increase understanding of the topic and comprehend the various methodologies and material applications.

For the search, Scopus was used, a widely known and disseminated database in academia for its reliability in selecting published works. Applied to the titles, abstracts, and keywords of the articles, the searched strings were: ("FDM") OR ("Fused Deposition Modeling") AND ("PCL") OR ("Polycaprolactone") AND ("Hydroxyapatite") AND ("scaffolds"), limited to English-language articles only. All resulting works were considered, covering the period from 2015 to 2025.

As a result of the search, 58 articles were generated, and the titles were screened to identify those containing the words "PCL" or "Polycaprolactone," "Hydroxyapatite," and "Scaffolds." After that, the abstracts were read to identify the works that best fit the purpose of this review, resulting in 6 articles.

Theoretical Background

Fused Filament Fabrication (FFF), known as Fused Deposition Modeling (FDM), is an additive manufacturing (AM) technique that enables the creation of customized objects using a three-dimensional (3D) model developed through computer-aided design (CAD) software [2].

This process works by extruding a polymer through a heated nozzle and depositing it onto a platform (base). Upon contact with the base, which is also heated but at a lower temperature than the nozzle, the material solidifies. After the deposition of one layer, the cycle restarts until the structure designed in CAD is completed [4].

FDM stands out as one of the most popular and accessible methods within AM, also including techniques that provide a promising perspective for the production of 3D implants with variations in pore size and spatial distribution, enabling the adaptation of device geometry to patient needs [9].

This type of technology offers several advantages over conventional manufacturing, including the ability to create more complex parts and reduce production time and costs for unique items. With this, it becomes feasible to develop new products and significantly accelerate market launch, demonstrating that the applications of additive manufacturing technologies are broad, ranging from pre-production models and temporary parts to final components for aircraft, medical implants, and in tissue engineering, such as bone reconstruction [2].

Among the polymers most commonly used in 3D printing for bone reconstruction, PCL stands out as a semicrystalline polymeric material that is hydrophobic and soluble in organic solvents at room temperature. Its reduced melting temperature and ease of blending favor its processing. Combined with its biocompatibility and high permeability, this makes it ideal for several biomedical applications, such as scaffolds for bone regeneration and long-term implantable drug delivery systems [8,10].

However, its application in bone tissue engineering highlights its qualities in a particularly favorable way, enabling load support. In contrast, the original tissue gradually transforms into bone, due to its high mechanical strength and slow degradation rate [6].

Scaffolds made from a PCL matrix do not naturally exhibit osteoinductive properties; however, research indicates that they have high solubility and integrate well with other biomaterials, such as hydroxyapatite and tricalcium phosphates, which possess high bioactivity. This characteristic paved the way for an effective strategy to overcome these limitations, enabling the development of composites with various materials, including ceramics. There are studies aimed at promoting cell proliferation, migration, and nutrient transport by creating PCL/HA scaffolds [3,11].

HA, being an inorganic element of natural bone, stands out as a biomimetic material that presents excellent biocompatibility and bioactivity in bone tissue engineering applications [12]. For this reason, HA is frequently used in bone implant and bone cement applications, thanks to its similarities in both composition and biological characteristics with natural tissues [13].

HA is a crucial component in scaffold formation, as it constitutes approximately 70% of the natural bone composition. However, its fragility restricts its application; therefore, PCL is often combined with HA to provide the mechanical strength a scaffold requires [8,14].

In tissue engineering, a bone scaffold can be created by combining PCL and HA. This structure promotes bone cell migration, an essential process for vascularization and bone development. Additionally, it provides temporary mechanical support in fractured or injured areas [8].

Scaffolds are not designed to be permanent implants; their goal is to promote the deposition of extracellular matrix by host cells, thus replacing the scaffold structure over time. For this reason, an ideal scaffold must be made of a material that is biocompatible and biodegradable. Furthermore, its mechanical properties must be similar to those of the tissue in which it will be inserted, where the three-dimensional structure must be highly porous and interconnected, allowing for cell migration and nutrient passage [6].

Conclusion

This work provides an overview of the application of PCL and HA in the production of composite biomaterials for tissue engineering, with a focus on bone regeneration. The qualitative research is based on the review of scientific articles and academic works, highlighting the relevance of continuous advancement in this area for improving practices and methodologies that aid in building bone structures to accelerate and ensure good regeneration of fractured bone tissue, emphasizing patient individuality and the particularity of each clinical case.

In the selected studies, it is evident that FDM makes a significant contribution to tissue engineering. This technology enables the manufacture of scaffolds with complex porous geometries, making it particularly useful in bone tissue engineering. It provides superior control and optimization of pore structure at the microscale, favoring bone healing and vascular infiltration.

Furthermore, it enables exact customization of scaffold geometry at the macroscale to meet the specific needs of each patient.

Acknowledgments

The authors thank UFRB-CETENS and SENAI CIMATEC University Center.

References

- Kao CT, Lin CC, Chen YW, Yeh CH, Fang HY, Shie MY. Poly(dopamine) coating of 3D printed poly(lactic acid) scaffolds for bone tissue engineering. Mater Sci Eng C. 2015;56:165-173.
- Zander NE, Gillan M, Lambeth RH. Recycled polyethylene terephthalate as a new FFF feedstock material. Addit Manuf. 2018;21:174-182.
- Jiao Z, Luo B, Xiang S, Ma H, Yu Y, Xie L, et al. 3D printing of HA/PCL composite scaffolds for tissue engineering. Adv Ind Eng Polym Res. 2019;2(4):196-202.
- Do AV, Khorsand B, Geary SM, Salem AK. 3D printing of scaffolds for tissue regeneration applications. Adv Healthc Mater. 2015;4(12):1742-1762.
- 5. Karimipour-Fard P, Hossain S, Bhadra CM, Bandyopadhyay A, Banerjee A, Basu B. Development, processing and characterization of polycaprolactone/nano-hydroxyapatite/chitin-nano-whisker nanocomposite filaments for additive manufacturing of bone tissue scaffolds. J Mech Behav Biomed Mater. 2021;120:104580.
- 6. Turnbull G, Clarke J, Picard F, Riches P, Jia L, Han F, et al. 3D bioactive composite scaffolds for bone tissue engineering. Bioact Mater. 2018;3(3):278-314.

- 7. Mystiridou E, Patsidis AC, Bouropoulos N. Development and characterization of 3D printed multifunctional bioscaffolds based on PLA/PCL/HAp/BaTiO3 composites. Appl Sci. 2021;11(14):6643.
- 8. Kim CG, Lee JS, Kim HJ, Rhee SH, Kim YH, Shin US, et al. Fabrication of biocompatible polycaprolactone—hydroxyapatite composite filaments for the FDM 3D printing of bone scaffolds. Appl Sci. 2021;11(10):4630.
- Pierantozzi D, Scalzone A, Jindal S, Trombetta M, Rainer A. 3D printed Sr-containing composite scaffolds: effect of structural design and material formulation towards new strategies for bone tissue engineering. Compos Sci Technol. 2020;191:108069.
- 10. Ahmadova I, et al. Microwave-assisted ring-opening polymerization of ε-caprolactone using organic acids. Polymers (Basel). 2023;15(12):2597.
- 11. Nyberg E, Rindone A, Dorafshar A, Grayson WL. Comparison of 3D-printed poly-ε-caprolactone scaffolds functionalized with tricalcium phosphate, hydroxyapatite, bio-oss, or decellularized bone matrix. Tissue Eng Part A. 2017;23(11-12):503-514.
- 12. Kong L, Gao Y, Lu G, Gong Y, Zhao N, Zhang X. A study on the bioactivity of chitosan/nano-hydroxyapatite composite scaffolds for bone tissue engineering. Eur Polym J. 2006;42(12):3171-3179.
- 13. Degirmenbasi N, Kalyon DM, Birinci E. Biocomposites of nanohydroxyapatite with collagen and poly(vinyl alcohol). Colloids Surf B Biointerfaces. 2006;48(1):42-49.
- 14. Akhoundi B, Taghipour Lahijani Y, Modanloo V. Optimizing compressive mechanical properties and water absorption of polycaprolactone/nanohydroxyapatite composite scaffolds by 3D printing based on fused deposition modeling. Proc Inst Mech Eng N J Nanomater Nanoeng Nanosyst. 2023;23977914231205639.

Produced Water Treatment: A Bibliometric Review of Strategies and Technologies

Emilly Perrone Ramos^{1*}, Lilian Lefol Nani Guarieiro¹, Tatiana Oliveira do Vale¹

"SENAI CIMATEC University; Salvador, Bahia, Brazil

Produced Water (PW) contains chemical compounds and heavy metals that make it toxic and harmful to ecosystems and human health. The inadequate disposal of this byproduct, which is the largest in the oil industry, can pollute water bodies, impact biodiversity, and harm communities that depend on water for consumption and agriculture. This work analyzed the most widely used technologies and strategies for PW treatment. The bibliometric research was based on the Web of Science platform. It mapped the main approaches in the last five years, identifying three essential groups of treatment: physical, chemical, and biological, with increasing interest in the latter. The study emphasizes the importance of enhancing PW management to mitigate environmental impacts and promote more sustainable solutions.

Keywords: Bibliometric Analysis. Produced Water. Treatment. Technologies.

The unit operations related to oil production and extraction processes generate, in addition to the central processing objective, byproducts and effluents that, unlike crude oil, do not have high added value and must be disposed of in a way that does not affect or minimally impacts the environment [1].

Produced Water (PW) is the water that reaches the surface along with crude oil and is considered the most significant byproduct of the oil industry. It is generated in large volumes, with a global ratio of 3 barrels of PW for 1 barrel of oil. The composition of PW varies according to the maturity and region of the producing well. It is complex, containing dissolved and dispersed oil compounds, production chemicals, dissolved gases. dissolved formation minerals. production solids, which include formation solids, corrosion, scaling products, asphaltenes, waxes, and bacteria. Due to its high salinity and toxicity, the reuse and disposal of this material without prior treatment are prohibited [1,2].

In this context, physical, chemical, and biological treatments are adopted to reduce the Received on 13 May 2025; revised 24 July 2025.

Address for correspondence: Emilly Perrone Ramos. SENAI CIMATEC University. Avenida Orlando Gomes, 1845.

Zincode: 41650-010, Salvador, Bahia Brazil, E-mail: emilly

Zipcode: 41650-010. Salvador, Bahia, Brazil. E-mail: emilly. ramos@fbter.org.br. Original extended abstract presented at SAPCT 2025.

J Bioeng. Tech. Health 2025;8(4):389-392 © 2025 by SENAI CIMATEC University. All rights reserved.

level of hazard associated with this byproduct. The choice of the ideal technology depends on the intended destination of the PW (disposal and reinjection are the most common), production base location, equipment and infrastructure availability, technical feasibility, costs, and legislation [1]. In Brazil, CONAMA Resolution 393/2007 specifies the required standards for managing this byproduct. The objective of this work was to map, through a bibliometric review, the main treatments applied to produced water, in addition to presenting the microbial pathway as a sustainable treatment possibility that may enable safe reuse.

Materials and Methods

The study was conducted through bibliometric analysis to map the main techniques and strategies used in the last 5 years to treat Produced Water. The database used was Web of Science, with the keywords "produced water" in the title and "treatment" and "technologies" in the abstract. The Boolean operator AND was used to delimit the results obtained.

The results were subjected to a primary evaluation of the titles to verify their correlation with the proposed theme. After reading the titles, the conclusions were analyzed to understand the treatment specifications. Open-access filters were not applied, and the focus consisted of articles, regardless of whether they were reviews or not.

The retrieved documents from the search were analyzed using VOSviewer software version 1.6.20, which involved keyword co-occurrence and the removal of non-related terms, resulting in a network of clusters. A chart was also created to succinctly highlight the treatments and facilitate the understanding of the bibliometric review.

Results and Discussion

The search through the Web of Science database yielded 113 documents analyzed using VOSviewer software, with a minimum of four co-occurrences. From the 61 results obtained, non-related keywords were removed. The software displayed 3 clusters, illustrated in Figure 1, showing the intrinsic correlation among studies published in various countries. This demonstrates that advancements in the development of more sustainable and effective technologies and strategies are of global interest.

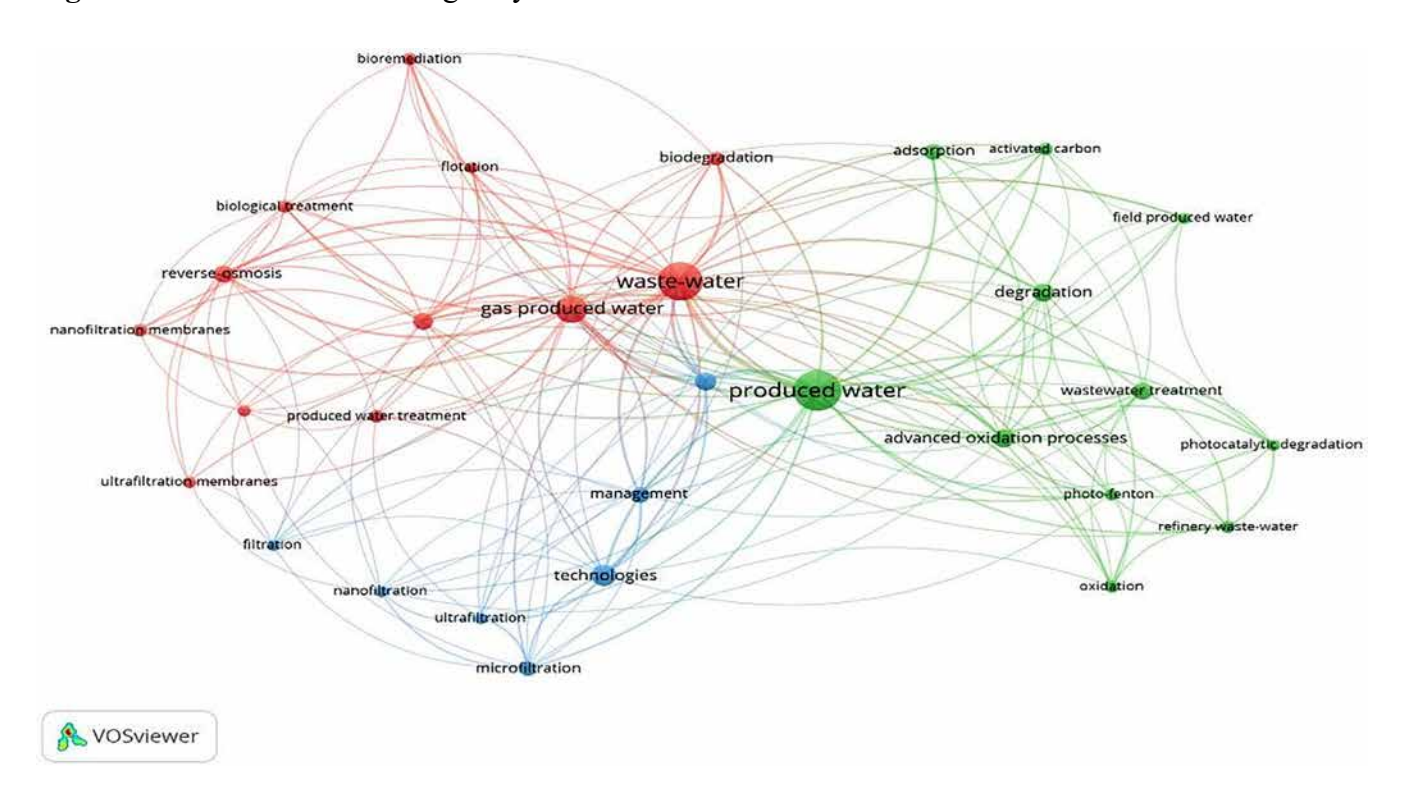
The blue cluster exhibits 7 correspondences to physical treatments, with a particular emphasis on filtration. The red cluster, comprising 12 items, highlights the predominance of physical treatments and the growth of biological processes.

The green cluster attributes greater relevance to chemical treatment processes, with emphasis on oxidation and adsorption. Box 1 presents the most studied treatments, highlighting their key features, nature, and limitations.

Membrane systems demonstrated significant competence in the primary treatment of PW, removing suspended solid contaminants in a compact design; however, it is necessary to overcome the challenges of membrane fouling to enable large-scale use [3]. Secondary treatment aims to remove emulsified oil, and flotation stands out by minimizing the environmental impacts of chemical compounds. Efficiency depends on pH and the probabilities of collision, adhesion, and stabilization of oil droplet bubbles. Future research is needed to analyze intervening factors to optimize this process [4].

Hydrocyclones are an efficient, compact, and durable technology with good cost-effectiveness. Their principle is the separation of layers according

Figure 1. Cluster network through keywords.



Box 1. Summary of treatments applied to produced water.

| Treatment Types | Examples | Removal Efficiency | Limitation | References |
|--------------------|------------------|--|---|------------|
| | Membranes | Suspended solids | Easy membrane fouling | [3] |
| Physical | Flotation | Oil droplets | Long retention period | [4] |
| 1 ilysicai | Hydrocyclones | Up to 98% of oil without pre-treatment | Unstable flow in single-entry models | [5] |
| Chemical | Oxidation | Dissolved oil at low concentrations | Requires intensive monitoring | [6] |
| | Adsorption | Dispersed and dissolved oil | Reduced efficiency at high contaminant concentrations | [6] |
| Biological | Bioremediation | Organic compounds by bacteria | Adjustment of C, N, and nutrient sources | [7] |
| | Phytoremediation | Organic compounds by microalgae | Requires pre-treatment | [8] |

to density, and their effectiveness in oil-water separation depends on inlet flow rate, velocity, and oil droplet size. Dual-entry models are more efficient, but the impact of turbulence on particles requires further study [5].

Oxidation facilitates the removal of organic and inorganic compounds, necessitating periodic calibration. Adsorption is effective in PW treatment, as it reduces BTEX and up to 80% of heavy metals. Both are independent of total dissolved solids concentrations and salinity; however, a disposal system is necessary for the waste generated by adsorbent consumption [6].

PW contains nutrients that favor the development of degrading microalgae, as well as indigenous microorganisms that act in the bioremediation of alkanes and aromatic hydrocarbons. Biological processes aim to safely reuse PW and require monitoring and pre-treatment, particularly in the case of phytoremediation [7,8].

Conclusion

The increase in oil production and growing environmental concerns reinforce the need to improve PW management. Treatments can be applied individually or in an integrated manner, the latter being highlighted in the literature as more efficient, since it removes degrees of distinct compounds. Physical processes, such as membranes, flotation, and hydrocyclones, are widely used in primary treatment. In contrast, chemical processes, including oxidation and adsorption, perform better when integrated with physical treatments, as they require coupled waste disposal systems. Biological processes are emerging as promising alternatives, which may utilize native or induced microorganisms, in the case of phytoremediation, to reduce the hazardous level of this effluent, while also enabling its safe reuse, including as an input for the industrial sector. Besides contributing to environmental preservation, these strategies drive the circular economy and sustainable development.

Acknowledgments

We thank the financial support of the Human Resources Program of the National Agency of Petroleum, Natural Gas and Biofuels (PRH/ANP–PRH27.1/SENAI CIMATEC), supported by resources from the investment of qualified oil companies in the R&D Clause of ANP Resolution No. 50/2015 and from the São Paulo Research Foundation (FAPESP), process No. 2024/10433-6; my advisors and all who contributed to the success of this work.

References

- Fakhrul-Razi A, et al. Review of technologies for oil and gas produced water treatment. J Hazard Mater. 2009;170:530-51.
- 2. Amini S, et al. Mathematical modelling of a hydrocyclone for the down-hole oil—water separation (DOWS). Chem Eng Res Des. 2012;90:2186-95.

- 3. Ibrahim M, et al. Advances in produced water treatment technologies: an in-depth exploration with an emphasis on membrane-based systems and future perspectives. Water. 2023;15.
- 4. Wang C, et al. Separation of emulsified crude oil from produced water by gas flotation: a review. Sci Total Environ. 2022:845.
- Ekechukwu OM, Assim T, Hawez HK. Recent developments in hydrocyclone technology for oil-inwater separation from produced water. Energies. 2024;17.
- Igunnu ET, Chen GZ. Produced water treatment technologies. Int J Low Carbon Technol. 2014;9:157-77.
- 7. Xie K, et al. Contrasting distribution of microbial communities, functional genes, and antibiotic resistance genes in produced water treatment plants with different treatment technologies. Water. 2024;16.
- 8. Alsarayreh M, et al. Biological-based produced water treatment using microalgae: challenges and efficiency. Sustainability. 2022;14.

A Review of the Most Well-Known Aggregation Algorithms for Federated Learning Applied to Large Language Models (LLMS)

Ygor Vieira^{1*}, Oberdan Rocha¹, Davidson Martins¹
¹SENAI CIMATEC University Center; Salvador, Bahia, Brazil

Research on federated learning has grown due to its ability to perform local training on distributed devices, especially in the context of artificial intelligence. However, there are still a few studies focused on the aggregation algorithms used in this type of learning, and even fewer addressing their application in large language models (LLMs). This article reviews the literature on federated learning with an emphasis on aggregation techniques applied to LLM training. A scarcity of specific studies was observed, along with the predominance of three algorithms: FedAvg, FedProx, and SCAFFOLD. Each was analyzed in terms of its strengths and weaknesses, including accuracy under data heterogeneity, convergence speed, and aspects of security and privacy. It is concluded that the future of aggregation algorithms in LLM training involves developing solutions that balance these aspects in an integrated manner.

Keywords: Federated Learning. Aggregation Algorithms. Large Language Models.

Federated Learning (FL) has gained significant popularity in research and real-world applications over the past few years [1]. This popularity stems from the fact that this type of machine learning is distributed; that is, participants train local models with local data, aggregating and sharing only the weights with a global model, unlike the traditional model, where all data had to be collected and stored on a central server for training [2]. This aggregation of weights between models is based on an aggregation algorithm, such as the well-known Federated Averaging (FedAvg) [1,3].

In the context of FL applied to large language models (LLMs), which involve challenges such as models with billions of parameters, data security and privacy, vast amounts of non-independent and identically distributed (non-IID) data, the choice of aggregation methods is crucial, as they directly influence the efficiency of distributed training and the convergence of the global model [3–7].

This article discusses methodologies involving the most widely used aggregation algorithms currently employed in LLM training. Another Received on 10 May 2025; revised 22 July 2025. Address for correspondence: Ygor Vieira. SENAI CIMATEC University. Avenida Orlando Gomes, 1845. Zipcode: 41650-010. Salvador, Bahia, Brazil. E-mail: ygor.vieira@fbter.org.

J Bioeng. Tech. Health 2025;8(4):393-395 © 2025 by SENAI CIMATEC University. All rights reserved.

br. Original extended abstract presented at SAPCT 2025.

important aspect verified in this work is how FL associated with LLMs generates positive impacts on their training. The articles were compared, and it was noticeable that among the best-known aggregation algorithms, SCAFFOLD presented the best results, with strengths including the correction of statistical drifts, improved convergence in non-IID scenarios, and stable performance across multiple local iterations. Its weakness, however, was a higher communication cost, doubling the communication overhead compared to FedAvg [8–11].

Materials and Methods

An academic search was carried out with the assistance of the Consensus AI tool [12] (a peer-reviewed scientific article search engine that provides access to articles from major publishers such as Elsevier, IEEE, SciELO, Atena, among others).

The search parameters used were: Publishers such as Elsevier, IEEE, Atena, among others; Peer-reviewed scientific articles; Publication period (2019–2024).

To classify the articles, the number of citations was taken into consideration. Five main aspects were defined to meet the objective of this review:

(a) the article needed to be directly related to

Federated Learning; (b) the article had to discuss and explore aggregation methods; (c) the article needed to cite aggregation algorithms; and (d) the algorithms had to be related to Large Language Models (LLMs) and the challenges faced by Federated Learning.

Through the Consensus search, 60 articles were identified, tracked, mapped, and extracted. A subsequent review and contextual evaluation of these 60 articles was carried out to determine their relevance. Considering the four aspects defined above, 23 relevant articles were obtained.

Theoretical Framework

Of the 60 articles initially found, 23 were considered relevant, as they met the purpose of addressing three key research questions for this study:

Research Question 1: What are the most widely used Federated Learning algorithms for training LLMs?

Research Question 2: What are the strengths and weaknesses of the most widely used Federated Learning algorithms for training LLMs?

Research Question 3: What is the future of Federated Learning algorithms in the context of LLM training?

After this screening, the 23 selected articles were categorized based on the aggregation algorithms they addressed: FedAvg, FedProx, and SCAFFOLD. This categorization was structured into subsections, each presenting a brief introduction of the selected aggregation algorithm, along with an analysis and discussion of the article's contribution.

For Research Question 1, FedAvg, despite being a more straightforward and basic algorithm, is widely known and popularly used, including in LLM training. FedProx, in turn, remains widely used due to its effectiveness in handling data heterogeneity, even as more robust algorithms are being developed. SCAFFOLD, considering the LLM context, proved to be robust and effective, outperforming FedAvg and FedProx, particularly in domains that require specialized knowledge, such as finance and medicine.

For Research Question 2, subsections were created to present the strengths and weaknesses of FedAvg, FedProx, and SCAFFOLD.

Finally, based on the study carried out and the references analyzed, it was concluded that combining techniques to increase robustness in aggregation algorithms is necessary to mitigate the challenges faced by federated learning applied to LLMs. FedAvg shows sensitivity to non-IID data, resulting in slower convergence or suboptimal solutions, and its performance varies with the increase in the number of participating devices. FedProx incurs a higher computational cost compared to FedAvg, and in some cases, model accuracy may degrade when the number of local iterations is increased. SCAFFOLD has the highest computational cost among them, being approximately double that of FedAvg [9–12].

Furthermore, none of the three algorithms incorporates security techniques to reinforce data privacy in FL. Therefore, merging techniques to overcome these weaknesses, either by optimizing existing algorithms or developing new ones, represents the future of aggregation algorithms in FL.

Conclusion

Given the lack of comprehensive research on aggregation algorithms applied to LLM training, this article aimed to provide an analysis of the most widely used algorithms for this purpose.

The review identified that FedAvg, FedProx, and SCAFFOLD have been widely applied in several cases. However, the application and development of these algorithms still require more in-depth research, specifically for LLM training. This review contributes to the field by consolidating the most recent studies on aggregation algorithms

applied to LLMs, offering a broad overview of current trends and areas requiring further attention.

Despite significant advances, important gaps remain, such as enhancing security and data privacy in federated learning aggregation without sacrificing model efficiency, as no aggregation algorithms applied to LLMs have been found to address this issue. Another gap concerns how to handle data heterogeneity while reducing computational resource demands.

Additionally, other aggregation algorithms, such as FedNova, have not yet been implemented or tested in LLM training and should also be addressed in future studies.

In summary, this review highlights the importance of aggregation algorithms in the field of LLMs and lays a solid foundation for future research, which may lead to significant advances.

Acknowledgements

This work was carried out with support from the São Paulo Research Foundation (FAPESP) - process n°. 2020/09770-7.

References

- 1. Gu X, Sabrina F, Fan Z, Sohail S. A review of privacy enhancement methods for federated learning in healthcare systems. Int J Environ Res Public Health. 2023;20(15):6539.
- 2. Aledhari M, Razzak R, Parizi R, Saeed F. Federated learning: a survey on enabling technologies, protocols, and applications. IEEE Access [Internet]. 2020 [cited 2025 Feb 10];8:1-1. Available from: https://doi.org/10.1109/ACCESS.2020.3013541.
- 3. Allan MS. Lab-09 MO809 Aprendizado de máquina e reconhecimento de padrões [Internet]. Instituto de

- Computação, UNICAMP; 2025 [cited 2025 Feb 10]. Available from: https://ic.unicamp.br/~allanms/mo809/labs/Lab-09/.
- 4. Neto HNC, Mattos DMF, Fernandes NC. Privacidade do usuário em aprendizado colaborativo: federated learning, da teoria à prática. In: Segurança em Redes de Computadores e Sistemas Distribuídos (Cap. 3). Anais do SBSEG 2020; 2020 [cited 2025 Feb 10]. Available from: https://sbseg.sbc.org.br/2020/capitulos/ capitulo%203.pdf.
- The Shift. Futuro do treinamento de LLMs é federado [Internet]. 2024 Mar 14 [cited 2025 Feb 10]. Available from: https://theshift.info/hot/futuro-do-treinamentode-llms-e-federado/.
- Santos LEB. Middleware baseado em aprendizado federado para aplicações de smart campus [Internet]. Instituto Federal de Educação, Ciência e Tecnologia da Paraíba; 2022 [cited 2025 Feb 10]. Available from: https://repositorio.ifpb.edu.br/handle/177683/4052
- Autor desconhecido. Aprendizado federado: uma abordagem de aprendizado de máquina descentralizada para privacidade e segurança de dados [Internet]. ICHI. PRO; [cited 2025 Feb 10]. Available from: https:// ichi.pro/pt/aprendizado-federado-uma-abordagemde-aprendizado-de-maquina-descentralizada-paraprivacidade-e-seguranca-de-dados-197608543778676
- 8. Gao Y. Federated learning: impact of different algorithms and models on prediction results based on fashion-MNIST data set. Appl Comput Eng. 2024;86:204-12.
- 9. Dai J. Comparative analysis of federated learning algorithms under non-IID data. Appl Comput Eng. 2024;86:91-100.
- Li Q, Diao Y, Chen Q. Federated learning on non-IID data silos: an experimental study [Internet]. arXiv. 2021 [cited 2025 Feb 15]. Available from: https://arxiv.org/abs/2102.02079
- 11. Zheng W. Comparative analysis of federated learning algorithms under extreme non-IID conditions for computer vision. Appl Comput Eng. 2024;86:168-76.
- 12. Consensus. Consensus: AI-powered research search engine [Internet]. [cited 2025 Feb 10]. Available from: https://consensus.app/search/.

The Importance of Data and Metadata Management for Scientific Research

Daniel Cerqueira Rodrigues¹, Julia Maria Araujo Vianna¹, Rosana Vieira Albuquerque¹*

'SENAI CIMATEC University; Salvador, Bahia, Brazil

The approach presented in this review seeks to demonstrate how the impact of data quality and integration can be directly influenced by metadata standardization, ensuring greater reliability and accessibility in the modeling and analysis of complex networks. This study is ongoing, and data collection was conducted in the SciELO, Google Scholar, and ScienceDirect databases, focusing on publications from 2020 to 2025. Based on the literature review, it is expected to demonstrate the relevance of data management for conducting scientific research, highlighting how a well-defined structure can ensure reliability and accessibility of information over time. At the conclusion of this ongoing research, the results may serve as a basis for developing a data and metadata management framework to support the structuring and retrieval of data necessary for scientific research in the field of complex networks.

Keywords: Data Management. Metadata. Complex Networks. Social Networks.

The digital era has exponentially expanded the volume of data generated, particularly in research involving complex social networks. This exponential growth in information production poses increasing challenges for data and metadata management in scientific research. However, the absence of consolidated practices for managing data and metadata compromises the integrity, reuse, and interoperability of this information [1,2].

The lack of well-defined standards for organizing, storing, and sharing data can compromise its interpretation and reuse, hindering scientific progress. The exponential increase in data also requires new computational structures to store and process it, ensuring that information can be accessed efficiently.

The reliability and accessibility of this information are crucial for building robust analytical models, particularly in complex networks where multiple elements interact dynamically. This study aims to demonstrate the importance of data management in scientific

Received on 14 May 2025; revised 28 July 2025.

Address for correspondence: Rosana Vieira Albuquerque. Avenida Orlando Gomes, 1845, Piatã. Salvador, Bahia, Brazil Zipcode: 41650-010. E-mail: rosana.albuquerque@fieb.org.br. Original extended abstract presented at SAPCT 2025.

J Bioeng. Tech. Health 2025;8(4):396-398 © 2025 by SENAI CIMATEC University. All rights reserved.

research, highlighting how a well-defined structure can ensure the reliability and accessibility of information over time, particularly for the data required in complex network research.

Materials and Methods

This study is ongoing, and the research is exploratory in nature. It is being carried out through a literature review, utilizing a qualitative bibliographic approach.

For the bibliographic survey, the following keywords were used: "Gestão," "Dados," "Metadados," "Redes Complexas," and their English equivalents in the databases SciELO and Google Scholar, as well as with English terms: "management," "data and metadata," and "complex networks." Articles and books directly addressing the topic were selected, ensuring a diverse range of perspectives on the subject.

The inclusion criteria were based on the relevance of the works for understanding the challenges and solutions related to data and metadata management. The following inclusion criteria were applied: articles published between 2020 and 2025 addressing only data management, metadata, and complex networks. Exclusion criteria included articles published before 2020 and those not directly related to the theme.

Theoretical Framework

The analyzed literature highlights that the lack of data standardization is a significant obstacle to interoperability and reuse. Sawadogo and Darmont (2021) [3] discuss the architecture of data lakes and metadata management as an emerging solution. Mattos and Oliveira (2022) [4] analyze tools for data management plans, while Fernandes and Ribeiro (2022) [5] address metadata standards for digital preservation.

In addition, the study by Pellen and colleagues (2025) [6] emphasizes the importance of data governance and ethical sharing in scientific research, aligning with the FAIR principles. These principles, widely accepted since their proposal, have been adapted and applied in recent works, such as that of Terra and colleagues (2023) [7], to guide best practices in organizing, accessing, and reusing scientific data.

The research revealed that the lack of data standardization is one of the most significant obstacles for researchers, making access to and the reuse of information difficult. Data dispersion and technological obsolescence increase the risk of data loss and compromise the continuity of studies.

The analysis showed that each stage of the management process—search, control, organization, storage, and availability—is crucial to the quality and reliability of information. Interoperability between systems and metadata standardization are essential to facilitate data sharing and reuse. The application of FAIR principles (Findable, Accessible, Interoperable, and Reusable) is essential to maintaining an open and collaborative data environment.

Despite some progress, the consistent implementation of data management practices remains a challenge, especially in complex networks. The development of specific management models is crucial for enhancing the efficiency and reproducibility of scientific research.

Conclusion

The findings of this ongoing research underscore the importance of efficient data and metadata management as a crucial factor in ensuring the transparency, reproducibility, and reliability of scientific research. The analyzed literature confirms that challenges such as the absence of standardization, the lack of interoperability between systems, and the shortage of robust digital preservation structures persist. Despite some advances, the lack of standardization in data management remains a significant challenge for researchers, particularly in the analysis of complex networks.

The analysis also reveals that the adoption of structured metadata, aligned with frameworks such as the OAIS model, combined with the use of artificial intelligence and complex networks, can significantly improve data retrieval and reuse. An effective model for data and metadata management is fundamental for the advancement of science, as it promotes transparency and reproducibility of research, while facilitating the integration of different data sources.

Therefore, data management should be treated as a priority in academic and scientific institutions, and it is indispensable to propose a comprehensive framework to support the standardization and integration of processes for organizing, preserving, and sharing information. As a continuation of this research, it is suggested that the use of innovative technologies be further developed and a framework be created to assist researchers in managing the data required for scientific research.

Acknowledgements

We thank SENAI CIMATEC and FAPESB for their support of this research.

References

 Felipe CBM, Santos RF. Avaliação de metadados em repositórios de dados de pesquisa sobre biodiversidade. Em Questão [Internet]. 2022 [cited 2025 Apr

- 17];28(3):1-25. Available from: https://www.scielo.br/j/emquestao/a/q5dXB3wjnQ9KdJtpZ6NrVVj/
- Corrêa FC. Gestão de dados científicos para pesquisadores. Rev Dig Bibliotecon Ciênc Inf [Internet]. 2021 [cited 2025 Apr 17];19(2):1-15. Available from: https://www.scielo.br/j/rdbci/a/ kYbvbjVQPp5nFkZkxvs8Mzj/
- 3. Sawadogo P, Darmont J. On data lake architectures and metadata management. arXiv [Internet]. 2021 [cited 2025 Apr 17]. Available from: https://arxiv.org/abs/2107.11152
- Mattos R, Oliveira J. Ferramentas para elaboração de planos de gestão de dados: visão geral e análise. Transinformação [Internet]. 2022 [cited 2025 Apr 17];32(2):1-12. Available from: https://www.scielo. br/j/tinf/a/hrf99WdTqJmLnNv594tgQPb/
- Fernandes L, Ribeiro AP. Padrões de metadados no arquivamento da Web: recursos essenciais para a preservação digital. Rev Dig Bibliotecon Ciênc Inf [Internet]. 2022 [cited 2025 Apr 17];19(3):1-14. Available from: https://www.scielo.br/j/rdbci/a/ vGFMKmfHBFcxYthcsPy4f7v/
- Pellen C, et al. Data management and sharing. J Clin Epidemiol [Internet]. 2025 [cited 2025 Apr 17];151:1-10. Available from: https://doi.org/10.1016/j. jclinepi.2025.111680
- 7. Terra AL, Carneiro JL, Silva AS. Abordagem à gestão de dados científicos num plano de estudos de graduação: resultados de uma experiência didática. Encontros Bibli [Internet]. 2023 [cited 2025 Apr 17];28(1):1-17. Available from: https://www.scielo.br/j/eb/a/SNdSnyTLCBb8n4yvh85tymN/

Bibliometric Analysis on the Joint Application of Core-Shell Catalysts and Atomic Layer Deposition in Solide Oxide Fuel Cells

Iuri Dantas Passos da Mota^{1*}, Marcos Makoto Toyama¹, Gerhard Ett¹, Lilian Lefol Nani Guarieiro¹

**ISENAI CIMATEC University, Salvador, Bahia, Brazil

This study presents a bibliometric analysis of the scientific output between 2010 and 2025 related to solid oxide fuel cells (SOFC), atomic layer deposition (ALD), and core-shell catalysts. Based on Scopus database records processed using the Bibliometrix R tool, various combinations of these themes were evaluated to map publications, authors, institutions, collaboration networks, geographic distribution, gaps, and emerging trends. The results indicate that the association between ALD and core-shell structures already constitutes a consolidated field, with the highest volume of publications. At the same time, approaches directly involving SOFCs remain in an emerging stage. Although no studies were found that integrate ALD, core-shell catalysts, and SOFC simultaneously, the qualitative indicators observed in the individual analyses suggest a significant gap and a promising, specialized research niche. The predominance of Asian and North American countries, such as China, South Korea, and the United States, was also observed, underscoring the strategic role of these nations in leading the development of advanced energy technologies. Overall, combining these approaches may drive significant advances in the development of more efficient and sustainable energy systems.

Keywords: SOFC. Core-Shell. ALD. Sustainability. Solid Oxide Fuel Cells. Atomic Layer Deposition. Bibliometric Analysis.

This work presents a bibliometric analysis of publications related to solid oxide fuel cells (SOFC), with emphasis on the use of core-shell catalysts and atomic layer deposition (ALD) techniques. Bibliometrics is a widely employed tool to map the development of a scientific area, identifying publication patterns, emerging trends, and connections among different fields of study [1].

Fuel cells are electrochemical devices that directly convert chemical energy into electrical energy through redox reactions, representing a clean and sustainable alternative for power generation. The first functional fuel cell was demonstrated in 1839 by William Robert Grove, who used platinum electrodes in sulfuric acid with hydrogen and oxygen gases as reactants [2]. Over time, important advances boosted the development

Received on 28 May 2025; revised 25 July 2025. Address for correspondence: Iuri Dantas Passos da Mota. SENAI CIMATEC University. Avenida Orlando Gomes, 1845. Zipcode: 41650-010. Salvador, Bahia, Brazil. E-mail: iuri.mota@fbter.org.br. Original extended abstract presented at SAPCT 2025.

J Bioeng. Tech. Health 2025;8(4):399-407 © 2025 by SENAI CIMATEC University. All rights reserved.

of this technology. In 1889, Ludwig Mond and Carl Langer coined the term "fuel cell" and presented a functional prototype. Later, in 1892, Nernst discovered solid oxide electrolytes, enabling the emergence of high-temperature ceramic cells. This progress culminated in 1936, when Baur and Preis created the first ceramic cell operating at 1000 °C [3].

SOFCs are electrochemical devices that convert chemical energy into electrical energy through redox reactions, utilizing solid ceramic materials as both electrolytes and electrodes. They operate at high temperatures, between 800 and 1,000 °C, which favors reaction kinetics, eliminates the need for precious metal catalysts, and allows high energy efficiency, as well as flexibility regarding the type of fuel used [4,5]. SOFCs stand out compared to other fuel cells due to their substantial construction, high operating temperature, and greater flexibility in structural configuration [6]. The basic structure of SOFCs comprises two porous electrodes, the anode and the cathode, separated by a solid electrolyte that conducts oxygen ions (O2-). At the anode, the fuel undergoes oxidation, releasing electrons that travel through an external circuit to the cathode. At this electrode, oxygen reduction

occurs, completing the electrochemical cycle and generating electricity [6]

Core-shell nanoparticles are structures consisting of a central core surrounded by one or more external layers of different composition. These configurations may range from simple shapes to more complex structures, such as multiple shells or hollow cores [7,8]. Such particles have attracted interest in various fields, including batteries [8], biomedicine [9,10], heterogeneous catalysis [11], fuel cells [12,13], and photocatalysis [14,15]. They can be classified according to their constituent materials — inorganic-inorganic, inorganicorganic, organic-inorganic, and organic-organic — depending on the intended application, which allows tuning their physicochemical properties [7]. Another classification considers the morphology of the outer layer, which may be hollow, porous, or composed of multiple layers, features that directly influence their functionalities and applications [16].

The ALD technique began in the 1970s and gained widespread popularity in the 2000s, replacing the term ALE (Atomic Layer Epitaxy), as most deposited films did not present epitaxial structure but rather amorphous forms, suitable for dielectrics and diffusion barriers [17,18]. ALD consists of sequential, self-limiting gas-phase reactions that allow thickness control at the atomic level, ensuring high uniformity and conformality even on complex surfaces, with thicknesses typically below 20 nm [19,20]. Compared to traditional methods, such as PVD (Physical Vapor Deposition) and CVD (Chemical Vapor Deposition), ALD operates at lower temperatures and ensures the formation of continuous films with precise thickness control [21]. Among its main advantages are exceptional conformality, high film quality, the ability to operate at reduced temperatures, and the capability to form multilayered structures [21–23].

ALD can be carried out through two main variants: thermal ALD (ThALD) and plasma-enhanced ALD (PEALD). In ThALD, the energy required for surface reactions is provided by substrate heating, generally above 200 °C,

using water vapor as a co-reactant. In PEALD, highly reactive species are generated by plasma, using gases such as oxygen and nitrogen with purity above 99.999%, allowing film growth at near-room temperatures. This feature makes PEALD suitable for coatings on heat-sensitive substrates, such as polymers. However, the conformality of films obtained by PEALD is usually lower than that of ThALD [17–19,24,25]. Considering the relevance of this field, this study analyzes Scopus-indexed documents using the Bibliometrix R tool. The aim is to map the most impactful publications, identify research gaps, and highlight advances in the application of core-shell catalysts and ALD in SOFC.

Materials and Methods

The technological prospecting was conducted by collecting academic data from the Scopus database and using the Bibliometrix tool for analysis. The main indicators extracted from the processed data are organized in Table 1, which synthesizes the results obtained. The survey was conducted in March 2025, encompassing scientific publications from 2010 to 2025. The year 2010 was adopted as the starting point as it corresponds to the publication of the most relevant identified article, with this criterion maintained up to the year of research.

Three different keyword combinations were applied to the title, abstract, and keyword fields of the records:

- "Solid Oxide Fuel Cell" AND "Atomic Layer Deposition",
- "Solid Oxide Fuel Cell" AND "core-shell",
- "Atomic Layer Deposition" AND "core-shell".

These searches yielded 118, 113, and 498 documents, respectively, all of which were subjected to bibliometric analysis.

No studies were identified addressing ALD, core-shell catalysts, and SOFC simultaneously. This absence highlights a significant gap in the scientific literature, demonstrating that the integration of these topics has not yet been consolidated. This

Table 1. Main information on the data generated by bibliometrix.

| Description | "Solid Oxide Fuel Cell" AND "Atomic layer deposition" | "Solid Oxide Fuel Cell" AND "core-shell" | "Atomic layer deposition" AND "core-shell" | |
|--------------------------------|---|---|--|--|
| Time interval | 2010–2025 | 2010–2025 | 2010–2025 | |
| Sources | 51 | 51 | 175 | |
| Documents | 118 | 113 | 498 | |
| Annual growth rate | -7.06% | -8.83% | -2.67% | |
| Authors | 309 | 468 | 2026 | |
| Single-authored documents | 1 | 0 | 2 | |
| International co-authorship | 33.05% | 37.17% | 26.51% | |
| Co-authors per document | 6.15 | 6.21 | 6.44 | |
| Author keywords – DE | 235 | 313 | 1063 | |
| References | 4041 | 5083 | 21721 | |
| Average document age | 7.41 | 6.89 | 7.42 | |
| Average citations per document | 29.67 | 28.42 | 40.22 | |

scenario highlights the relevance and opportunity for research that combines these technologies, given the potential of their integration for developing innovative and efficient solutions for SOFC.

Results and Discussion

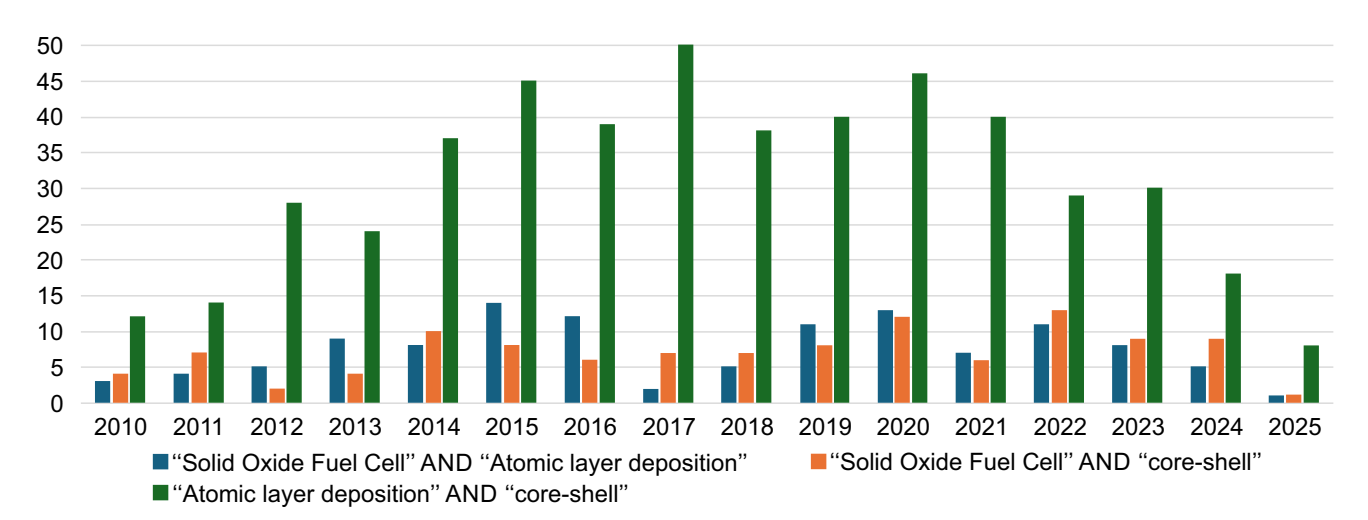
Figure 1 shows the annual evolution of scientific production between 2010 and 2025 related to the topics "Solid Oxide Fuel Cell," "core-shell," and "Atomic Layer Deposition," considering different combinations of these terms. Among the analyzed sets, it is observed that the association between "Atomic Layer Deposition" and "coreshell" presents the highest number of publications throughout the period, reaching its peak in 2017 with 50 articles. This high and relatively constant volume over the years indicates an already consolidated interest in research on core-shell structures obtained through ALD, whether by the formation of these structures during the process or by the direct deposition of materials already

configured in this format. This interest is likely due to the broad applicability of these structures in various technological areas, beyond solid oxide fuel cells.

In contrast, the combinations that directly involve SOFCs show a significantly lower volume of publications. The combination of "Solid Oxide Fuel Cell" and "Atomic Layer Deposition" exhibits an irregular trend, with two notable peaks of activity recorded in 2015 and 2020, corresponding to 14 and 13 publications, respectively. From 2022 onward, however, there is a sharp decline in this number, reaching only one article published in 2025. Similarly, the combination of "Solid Oxide Fuel Cell" and "core-shell" also shows a modest evolution, with the most expressive values observed in 2020 (12) and 2022 (13).

Figure 2 highlights the countries with the highest number of scientific publications related to the different combinations of the terms "Solid Oxide Fuel Cell," "Atomic Layer Deposition," and "core-shell." The data show a significant

Figure 1. Annual evolution of the number of scientific publications between 2010 and 2025, considering the combinations between the terms "Solid Oxide Fuel Cell," "Atomic Layer Deposition," and "core-shell."



concentration of production in Asia and North America, with China, South Korea, and the United States occupying prominent positions. In the analysis of the combination between "Atomic Layer Deposition" and "core-shell" [Figure 2A], the highest absolute volumes among the four analyzed categories are noted. China leads with 1018 publications, followed by the United States (523) and South Korea (490). This distribution suggests that, regardless of the application system, there is already a consolidated interest in these countries in exploring the ALD technique for fabricating coreshell structures, as demonstrated by the quantitative expressiveness of the publications.

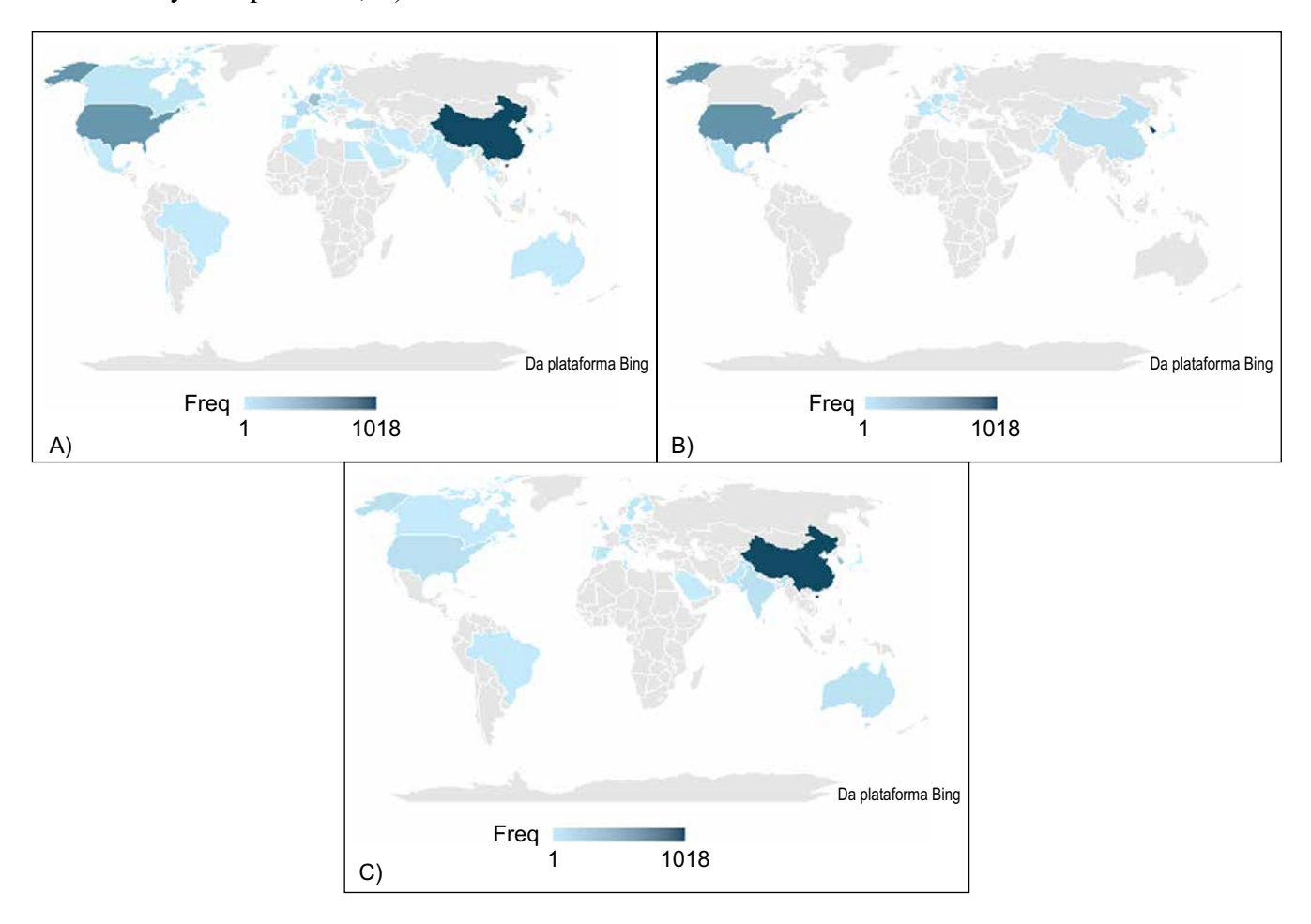
In the case of the combination between "Solid Oxide Fuel Cell" and "Atomic Layer Deposition" (Figure 2B), South Korea appears in the lead, accounting for 403 publications. Next are the United States, with 218, and China, with 28. These numbers indicate that studies involving the application of ALD in solid oxide fuel cells have gained greater prominence in the South Korean context, as revealed by the volume of identified works. When observing the combination of "Solid Oxide Fuel Cell" and "core-shell" (Figure 2C), China takes the lead, with 397 publications. South Korea comes in second, with 100, followed by the United States, with 28. These data point to greater

activity by Chinese institutions in investigations exploring the use of core-shell structures in the context of SOFCs.

The analysis of Brazilian participation in the thematic combinations reveals that the country is present only once in the association between "Atomic Layer Deposition" and "core-shell," and in four instances in the combination between "Solid Oxide Fuel Cell" and "core-shell." On the other hand, there are no records of national publications relating to "Solid Oxide Fuel Cell" and "Atomic Layer Deposition." This scenario highlights a relevant gap in Brazil's scientific production on the topic, while also signaling a strategic opportunity for the formation of new research groups and for strengthening the national presence in this field.

The pattern observed in the three categories suggests a higher density of publications in countries with significant activity in science and technology, particularly in research areas related to advanced materials and alternative energy sources. The consistent presence of China, South Korea, and the United States in the different sets, associated with the absolute values of publications, justifies identifying these countries as the primary centers of scientific production on the addressed topics. Overall, the data identified in the four categories indicate a greater concentration of publications

Figure 2. Geographic distribution of scientific production by country, according to different combinations of research terms: A) "Atomic Layer Deposition" AND "core-shell"; B) "Solid Oxide Fuel Cell" AND "Atomic Layer Deposition"; C) "Solid Oxide Fuel Cell" AND "core-shell."



in countries with prominent roles in science and technology, especially in areas focused on materials and alternative energy sources. The constant presence of China, South Korea, and the United States in various combinations, along with the high absolute numbers of publications, confirms the importance of these countries as the main centers of scientific production related to the topics in question. Other countries, such as Germany, France, India, Australia, and Singapore, occasionally make significant contributions in specific areas within the research field.

Table 2 presents the five institutions with the highest number of publications for each combination of the terms "Solid Oxide Fuel Cell," "Atomic Layer Deposition," and "core-shell," revealing significant patterns in the institutional distribution of scientific production.

In the combination of "Solid Oxide Fuel Cell" and "Atomic Layer Deposition," Seoul National University occupies first place, with 94 publications. Next are Seoul National University of Science and Technology, with 60 publications, and Stanford University, with 53. Completing the group are Korea University (43) and West Virginia University (38). In this group, there is a notable concentration in South Korean institutions, which account for three of the top five positions and more than half of the total articles, evidencing South Korea's leadership in ALD applications in SOFC.

In the case of the combination of "Solid Oxide Fuel Cell" and "core-shell," the five most

Table 2. The five central institutions with the highest number of publications.

| "Solid Oxide Fuel Cell" AND "Atomic Layer Deposition" | | | "Solid Oxide Fuel Cell" AND "core-shell" | | | "Atomic Layer Deposition" AND "core-shell" | | |
|--|------------------|----------|--|---------|----------|--|------------------|----------|
| Affiliation | Country | Articles | Affiliation | Country | Articles | Affiliation | Country | Articles |
| Seoul National University | South Korea | 94 | Hubei University | China | 44 | Fudan University | China | 120 |
| Seoul National University of Science and Technology | South Korea | 60 | Huazhong University of Science and Technology | China | 28 | University of North Carolina at Chapel Hill | United States | 84 |
| Stanford University | United States | 53 | Shenzhen University | China | 23 | Hanyang University | South Korea | 81 |
| Korea University | South Korea | 43 | Tianjin University | China | 18 | Inha University | South Korea | 70 |
| West Virginia University | United States | 38 | University of Science and Technology of China | China | 18 | Nanyang Technological University | Singapore | 43 |

productive institutions are all located in China. Leadership is attributed to Hubei University, with 44 publications, followed by Huazhong University of Science and Technology (28), Shenzhen University (23), Tianjin University (18), and the University of Science and Technology of China (18). The geographic concentration of the data reveals a strong institutional focus of the Chinese scientific community on the study of core-shell structures applied to solid oxide fuel cells.

For the combination of "Atomic Layer Deposition" and "core-shell," Fudan University (China) leads with 120 publications. Next are the University of North Carolina at Chapel Hill (United States), with 84, and three Asian institutions: Hanyang University (South Korea), with 81, Inha University (South Korea), with 70, and Nanyang Technological University (Singapore), with 43. This combination presents a more balanced institutional distribution between North America and Asia, indicating a relatively more diversified scientific interest in this field.

The institutional analysis reveals a pronounced concentration of scientific production in Asian universities, particularly those in South Korea and China. Institutions in North America and Singapore are also present, reflecting the leadership of the most productive countries and the strategic role of research centers that stand out in advancing technologies such as ALD, SOFC, and core-shell structures. "Solid Oxide Fuel Cell" AND "Atomic Layer Deposition" Solid Oxide Fuel Cell" AND "core-shell" AND "core-shell"

Table 3 brings together the five most productive authors in each of the analyzed term combinations. The data reveal significant variations in individual productivity, depending on the thematic focus, highlighting the prominence of certain researchers in specific areas.

In the combination "Solid Oxide Fuel Cell" with "Atomic Layer Deposition," author AN J leads with 29 publications, followed by CHA SW (23), JI S (17), LEE S (17), and PRINZ FB (17). These results indicate production concentrated in a small number of authors, with a clear highlight for AN J, whose contribution significantly surpasses that of the others.

In the combination of "Solid Oxide Fuel Cell" and "core-shell," a different scenario is observed.

| T 11 3 | D 1 1 1 | C .1 C | • | .1 |
|----------|--------------|----------------|---------|-------------|
| Table 3. | Distribution | of the five | nrimary | authors. |
| I the co | Dibuioution | OI UIIO II I O | priming | continuity. |

| "Solid Oxide Fuel Cell" AND "Atomic Layer Deposition" | | | Fuel Cell" AND -shell" | "Atomic Layer Deposition" AND "core-shell" | |
|---|----------|--------|---------------------------|--|----------|
| Author | Articles | Author | Articles | Author | Articles |
| AN J | 29 | LI J | 10 | LU H-L | 18 |
| CHA SW | 23 | ZHU B | 9 | LEE C | 15 |
| JI S | 17 | CHI B | 6 | WANG X | 15 |
| LEE S | 17 | JIA L | 6 | KIM H | 14 |
| PRINZ FB | 17 | LIU W | 6 | KIM SS | 12 |

LI J appears at the top with 10 publications, followed by ZHU B (9), CHI B (6), JIA L (6), and LIU W (6). In this case, the values are lower and relatively balanced among the authors, which suggests a more dispersed distribution of scientific production and a possibly less consolidated stage of the topic.

When considering the combination between "Atomic Layer Deposition" and "core-shell," LU H-L leads with 16 publications, followed by LEE C (15), WANG X (15), KIM H (14), and KIM SS (12). The data show a distribution concentrated among authors with similar productivity, indicating the active involvement of several research groups in this thematic area.

Overall, the data reveal variations in productivity among authors depending on the thematic combination analyzed. In some approaches, there is a greater balance among researchers, while in others, specific authors stand out. This scenario may reflect different levels of maturity and specialization within the research field.

Challenges and Opportunities

No publications were found addressing the simultaneous use of core-shell catalysts, and ALD applied to SOFC. However, relevant studies addressing these themes separately were identified. The combinations among "Solid Oxide"

Fuel Cell" and "Atomic Layer Deposition," "Solid Oxide Fuel Cell" and "core-shell," and "Atomic Layer Deposition" and "core-shell" provide important insights for identifying challenges and opportunities regarding their possible integration.

Literature indicates that both core-shell structures and ALD are widely applied in other technological contexts. However, their joint application in SOFC still presents significant gaps. From the data analysis, several challenges stand out: the limited number of studies addressing the convergence of the three themes, the operational instability of certain structures, restricted access to specific ALD equipment, and difficulties in thermal compatibility among materials used.

On the other hand, the results also indicate promising opportunities, such as the potential for increasing catalytic activity in anodes and cathodes, mitigating structural degradation, enabling operation at intermediate temperatures, and compatibility with alternative fuels, as well as the ability of ALD to form ultrathin, selective, and uniform layers.

Additionally, core-shell structures may contribute to improving the thermal and chemical stability of materials. The presence of international co-authorship in the publications further suggests a favorable environment for global collaborations.

Thus, despite the absence of studies integrating these three elements, the technical and bibliometric indicators analyzed point to a promising research field. Recognizing current limitations, along with identified opportunities, suggests that this line of investigation has the potential to generate significant contributions to the development of more efficient energy technologies, especially in the context of transitioning to sustainable sources.

Conclusion

The bibliometric analysis carried out in this study, based on data from the Scopus database and processed with Bibliometrix R, enabled a detailed mapping of the scientific output between 2010 and 2025, focusing on the combinations among the terms "Solid Oxide Fuel Cell," "Atomic Layer Deposition," and "core-shell." The results indicate that while the association between ALD and core-shell structures shows the highest volume of publications and a more regular evolution over time, combinations directly involving SOFC still represent less developed niches, reflected in a lower frequency of studies during the analyzed period.

The combination of "Atomic Layer Deposition" and "core-shell" stood out for both the highest absolute number of publications and the temporal stability observed, indicating a consolidated field with applications spanning several knowledge areas. In contrast, approaches directly involving SOFC showed lower quantitative expressiveness, with more pronounced variations in publication numbers and no clear growth pattern.

No publications were found that simultaneously integrate core-shell catalysts and ALD in SOFC. However, analyses based on isolated studies of these approaches allowed identifying technical and operational challenges, as well as revealing promising opportunities for developing advanced solutions in the SOFC context. These results indicate that integrating these technologies represents both a significant gap and an opportunity for progress in the field.

Geographically, scientific research is concentrated in Asian and North American countries, notably China, South Korea, and the United States. These same countries gather the most productive institutions, reinforcing their central role in investigations related to ALD, SOFC, and core-shell structures. The analysis of authors and institutions shows a thematic distribution consistent with the different focuses of the term combinations, highlighting specific leaderships according to each research line.

Although no studies integrating ALD, coreshell catalysts, and SOFC simultaneously were found, the results indicate the presence of active collaborative networks, high-quality publications, and promising indicators in the individual analyses of these combinations. In this scenario, the gradual approximation of these approaches may pave the way for an innovative and strategic research line, with the potential to make significant contributions to improving SOFC. The integration of these topics presents a significant opportunity for the development of more efficient and durable energy technologies that align with the demands of the global energy transition.

References

- Dereli T, Baykasoglu A, Altun K, Durmusoglu A, Türksen IB. Industrial applications of type-2 fuzzy sets and systems: a concise review. Comput Ind. 2011;62:125-37.
- Grove WR. XXIV. On voltaic series and the combination of gases by platinum. Lond Edinb Dubl Philos Mag J Sci. 1839;14:127-30.
- 3. Möbius H-H. On the history of solid electrolyte fuel cells. J Solid State Electrochem. 1997;1:2-16.
- Singhal SC, Kendall K. High-temperature solid oxide fuel cells: fundamentals, design and applications. Elsevier; 2003. p. 1-18.
- 5. Minh NQ. Ceramic fuel cells. J Am Ceram Soc. 1993;76:563-88.
- 6. Stambouli AB, Traversa E. Solid oxide fuel cells (SOFCs): a review of an environmentally clean and efficient source of energy. Renew Sustain Energy Rev. 2002;6:433-55.
- 7. Ghosh Chaudhuri R, Paria S. Core/shell nanoparticles: classes, properties, synthesis mechanisms, characterization, and applications. Chem Rev. 2012;112(4):2373-433.
- 8. Lu W, Guo X, Luo Y, Li Q, Zhu R, Pang H. Coreshell materials for advanced batteries. Chem Eng J. 2019;355:208-37.
- 9. Chatterjee K, Sarkar S, Rao KJ, Paria S. Core/shell nanoparticles in biomedical applications. Adv Colloid Interface Sci. 2014;209:8-39

- Esquivel-Castro TA, Ibarra-Alonso MC, Oliva J, Martínez-Luévanos A. Porous aerogel and core/shell nanoparticles for controlled drug delivery: a review. Mater Sci Eng C. 2019;96:915-40.
- 11. Zheng X, Tan S, Dong L, Li S, Chen H. LaNiO3@ SiO² core–shell nanoparticles for the dry reforming of CH4 in the dielectric barrier discharge plasma. Int J Hydrogen Energy. 2014;39(22):11360-7.
- 12. Muthuswamy N, De La Fuente JL, Tran DT, Walmsley J, Tsypkin M, Raaen S, et al. Ru@Pt core–shell nanoparticles for methanol fuel cell catalyst: control and effects of shell composition. Int J Hydrogen Energy. 2013;38(36):16631-41.
- 13. Wang Z, Lu C, Kong W, Zhang Y, Li J. Platinum nanoparticles supported on core–shell nickel–carbon as catalyst for methanol oxidation reaction. J Alloys Compd. 2017;690:95-100.
- 14. Li N, Zhang J, Tian Y, Zhao J, Zhang J, Zuo W. Precisely controlled fabrication of magnetic 3D γ-Fe2O3@ ZnO core-shell photocatalyst with enhanced activity: ciprofloxacin degradation and mechanism insight. Chem Eng J. 2017;308:377-85.
- 15. Sun G, Zhu C, Zheng J, Jiang B, Yin H, Wang H, et al. Preparation of spherical and dendritic CdS@TiO2 hollow double-shelled nanoparticles for photocatalysis. Mater Lett. 2016;166:113-5.
- 16. Gawande MB, Goswami A, Asefa T, Guo H, Biradar AV, Peng DL, et al. Core–shell nanoparticles: synthesis

- and applications in catalysis and electrocatalysis. Chem Soc Rev. 2015;44(21):7540-90.
- 17. George SM. Atomic layer deposition: an overview. Chem Rev. 2010;110(1):111-31.
- 18. Knoops HC, Potts SE, Bol AA, Kessels WMM. Atomic layer deposition. In: Handbook of crystal growth. North-Holland; 2015. p. 1101-34.
- Hashmi MSJ. Comprehensive materials processing. Newnes; 2014.
- Shahmohammadi M, Mukherjee R, Sukotjo C, Diwekar UM, Takoudis CG. Recent advances in theoretical development of thermal atomic layer deposition: a review. Nanomaterials. 2022;12(5):831.
- 21. French P, Krijnen G, Roozeboom F. Precision in harsh environments. Microsyst Nanoeng. 2016;2(1):1-12.
- Nguyen MT, Yonezawa T. Sputtering onto a liquid: interesting physical preparation method for multimetallic nanoparticles. Sci Technol Adv Mater. 2018;19(1):883-98.
- Yabu H. Fabrication of honeycomb films by the breath figure technique and their applications. Sci Technol Adv Mater. 2018;19(1):802-22.
- Kim H, Oh IK. Review of plasma-enhanced atomic layer deposition: technical enabler of nanoscale device fabrication. Jpn J Appl Phys. 2014;53(3S2):03DA01.
- Mallick BC, Hsieh CT, Yin KM, Gandomi YA, Huang KT.
 On atomic layer deposition: current progress and future challenges. ECS J Solid State Sci Technol. 2019;8(4):N55.

Instructions for Authors

The Authors must indicate in a cover letter the address, telephone number and e-mail of the corresponding author. The corresponding author will be asked to make a statement confirming that the content of the manuscript represents the views of the co-authors, that neither the corresponding author nor the co-authors have submitted duplicate or overlapping manuscripts elsewhere, and that the items indicated as personal communications in the text are supported by the referenced person. Also, the protocol letter with the number should be included in the submission article, as well as the name of sponsors (if applicable).

Manuscripts may be submitted within designated categories of communication, including:

- Original basic or clinical investigation (original articles on topics of broad interest in the field of bioengineering and biotechnology applied to health). We particularly welcome papers that discuss epidemiological aspects of international health, clinical reports, clinical trials and reports of laboratory investigations.
- Case presentation and discussion (case reports must be carefully documented and must be of importance because they illustrate or describe unusual features or have important practice implications).
- Brief reports of new methods or observations (short communications brief reports of unusual or preliminary findings).

- State-of-the-art presentations (reviews on protocols of importance to readers in diverse geographic areas. These should be comprehensive and fully referenced).
- Review articles (reviews on topics of importance with a new approach in the discussion). However, review articles only will be accepted after an invitation of the Editors.
- Letters to the editor or editorials concerning previous publications (correspondence relating to papers recently published in the Journal, or containing brief reports of unusual or preliminary findings).
- Editor's corner, containing ideas, hypotheses and comments (papers that advance a hypothesis or represent an opinion relating to a topic of current interest).
- Innovative medical products (description of new biotechnology and innovative products applied to health).
- Health innovation initiatives articles (innovative articles
 of technological production in Brazil and worldwide,
 national policies and directives related to technology
 applied to health in our country and abroad).

The authors should checklist comparing the text with the template of the Journal.

Supplements to the JBTH include articles under a unifying theme, such as those summarizing presentations of symposia or focusing on a specific subject. These will be added to the regular publication of the Journal as appropriate, and will be peer reviewed in the same manner as submitted manuscripts.

Statement of Editorial Policy

The editors of the Journal reserve the right to edit manuscripts for clarity, grammar and style. Authors will have an opportunity to review these changes prior to creation of galley proofs. Changes in content after galley proofs will be sent for reviewing and could be required charges to the author. The JBTH does not accept articles which duplicate or overlap publications elsewhere.

Peer-Review Process

All manuscripts are assigned to an Associate Editor by the Editor-in-Chief and Deputy

Editor, and sent to outside experts for peer review. The Associate Editor, aided by the reviewers' comments, makes a recommendation to the Editor-in-Chief regarding the merits of the manuscript. The Editor-in-Chief makes a final decision to accept, reject, or request revision of the manuscript. A request for revision does not guarantee ultimate acceptance of the revised manuscript.

Manuscripts may also be sent out for statistical review ou *ad hoc* reviewers. The average time from submission to first decision is three weeks.

Revisions

Manuscripts that are sent back to authors for revision must be returned to the editorial office by 15 days after the date of the revision request. Unless the decision letter specifically indicates otherwise, it is important not to increase the text length of the manuscript in responding to the comments. The cover letter must include a point-by-point response to the reviewers and Editors comments, and should indicate any additional changes made. Any alteration in authorship, including a change in order of authors, must be agreed upon by all authors, and a statement signed by all authors must be submitted to the editorial office.

Style

Manuscripts may be submitted only in electronic form by www.jbth.com.br. Each manuscript will be assigned a registration number, and the author notified that the manuscript is complete and appropriate to begin the review process. The submission file is in OpenOffice, Microsoft Word, or RTF document file format for texts and JPG (300dpi) for figures.

Authors must indicate in a cover letter the address, telephone number, fax number, and e-mail of the corresponding author. The corresponding author will be asked to make a statement confirming that the content of the manuscript represents the views of the co-authors, that neither the corresponding author nor the co-authors have submitted duplicate or overlapping manuscripts elsewhere, and that the items indicated as personal communications in the text are supported by the referenced person.

Manuscripts are to be typed as indicated in Guide for Authors, as well as text, tables, references, legends. All pages are to be numbered with the order of presentation as follows: title page, abstract, text, acknowledgements, references, tables, figure legends and figures. A running title of not more than 40 characters should be at the top of each page. References should be listed consecutively in the text and recorded as follows in the reference list, and must follow the format of the National

Library of Medicine as in Index Medicus and "Uniform Requirements for Manuscripts Submitted to Biomedical Journals" or in "Vancouver Citation Style". Titles of journals not listed in Index Medicus should be spelled out in full.

Manuscript style will follow accepted standards. Please refer to the JBTH for guidance. The final style will be determined by the Editor-in-Chief as reviewed and accepted by the manuscript's corresponding author.

Approval of the Ethics Committee

The JBTH will only accept articles that are approved by the ethics committees of the respective institutions (protocol number and/or approval certification should be sent after the references). The protocol number should be included in the end of the Introduction section of the article.

Publication Ethics

Authors should observe high standards with respect to publication ethics as set out by the International Committee of Medical Journal Editors (ICMJE). Falsification or fabrication of data, plagiarism, including duplicate publication of the authors' own work without proper citation, and misappropriation of the work are all unacceptable practices. Any cases of ethical misconduct are treated very seriously and will be dealt with in accordance with the JBTH guidelines.

Conflicts of Interest

At the point of submission, each author should reveal any financial interests or connections, direct or indirect, or other situations that might raise the question of bias in the work reported or the conclusions, implications, or opinions stated - including pertinent commercial or other sources of funding for the individual author(s) or for the associated department(s) or organizations(s), and personal relationships. There is a potential conflict of interest when anyone involved in the publication process has a financial or other beneficial interest in

the products or concepts mentioned in a submitted manuscript or in competing products that might bias his or her judgment.

Material Disclaimer

The opinions expressed in JBTH are those of the authors and contributors, and do not necessarily reflect those of the SENAI CIMATEC, the editors, the editorial board, or the organization with which the authors are affiliated.

Privacy Statement

The names and email addresses entered in this Journal site will be used exclusively for the stated purposes of this journal and will not be made available for any other purpose or to any other party.

Brief Policies of Style

| Manuscript | Original | Review | Birief Comunication | Case Report | Editorial ; Letter to the Editor; Editor's Corner | Innovative Medical Products | State-of-the-Art | Health Innovation Initiatives |
|---|---|---|---|---|---|---|---|---|
| Font Type | Times or Arial | Times or Arial | Times or Arial | Times or Arial |
| Number of Words – Title | 120 | 90 | 95 | 85 | 70 | 60 | 120 | 90 |
| Font Size/Space- Title | 12; double space | 12; double space | 12; double space | 12; double space |
| Font Size/Space- Abstracts/Key Words and Abbreviations | 10; single space | 10; single space | 10; single space | 10; single space | - | - | 10; single space | 10; single space |
| Number of Words – Abstracts/Key Words | 300/5 | 300/5 | 200/5 | 250/5 | - | - | 300/5 | 300/5 |
| Font Size/Space- Text | 12; Double space | 12; Double space | 12; Double space | 12; Double space |
| Number of Words – Text | 5,000 including spaces | 5,500 including spaces | 2,500 including spaces | 1,000 including spaces | 1,000 including spaces | 550 including spaces | 5,000 including spaces | 5,500 including spaces |
| Number of Figures | 8 (title font size 12, double space) | 3 (title font size 12, double space) | 2 (title font size 12, double space) | 2 (title font size 12, double space) | - | 2 (title font size 12, double space) | 8 (title font size 12, double space) | 8 (title font size 12, double space) |
| Number of Tables/Graphic | 7 title font size 12, double space | 2 title font size 12, double space | 2(title font size 12, double space) | 1(title font size 12, double space) | - | - | 7 title font size 12, double space | 4 title font size 12, double space |
| Number of Authors and Co- authors* | 15 | 10 | 5 | 10 | 3 | 3 | 15 | 10 |
| References | 20 (font size 10,single space | 30(font size 10,single space | 15 (font size 10,single space) | 10 (font size 10,single space) | 10 (font size 10,single space | 5(font size 10,single space | 20 (font size 10,single space | 20 |

^{*}First and last name with a sequencing overwritten number. Corresponding author(s) should be identified with an asterisk; Type 10, Times or Arial, single space. Running title of not more than 40 characters should be at the top of each page. References should be listed consecutively in the text. References must be cited on (not above) the line of text and in brackets instead of parentheses, e.g., [7,8]. References must be numbered in the order in which they appear in the text. References not cited in the text cannot appear in the reference section. References only or first cited in a table or figures are numbered according to where the table or figure is cited in the text. For instance, if a table is placed after reference 8, a new reference cited in table 1 would be reference 9.1 would be reference 9.

Checklist for Submitted Manuscripts

| 1 . | Please provide a cover letter with your submission specifying the corresponding author as well as an address, telephone number and e-mail. |
|--------------|---|
| 1 2. | Submit your paper using our website www.jbth.com.br. Use Word Perfect/Word for Windows, each with a complete set of original illustrations. |
| □ 3. | The entire manuscript (including tables and references) must be typed according to the guidelines instructions. |
| 1 4. | The order of appearance of material in all manuscripts should be as follows: title page, abstract, text, acknowledgements, references, tables, figures/graphics/diagrams with the respective legends. |
| □ 5. | The title page must include a title of not more than three printed lines (please check the guidelines of each specific manuscript), authors (no titles or degrees), institutional affiliations, a running headline of not more than 40 letters with spaces. |
| □ 6. | Acknowledgements of persons who assisted the authors should be included on the page preceding the references. |
| 1 7. | References must begin on a separate page. |
| □8. | References must be cited on (not above) the line of text and in brackets instead of parentheses, e.g., [7,8]. |
| □ 9. | References must be numbered in the order in which they appear in the text. References not cited in the text cannot appear in the reference section. References only or first cited in a table or figures are numbered according to where the table or figure is cited in the text. For instance, if a table is placed after reference 8, a new reference cited in table 1 would be reference 9. |
| □ 10. | Reference citations must follow the format established by the "Uniform Requirements for Manuscripts Submitted to Biomedical Journals" or in "Vancouver Citation Style". |
| □ 11. | If you reference your own unpublished work (i.e., an "in press" article) in the manuscript that you are submitting, you must attach a file of the "in press" article and an acceptance letter from the journal. |
| □ 12. | If you cite unpublished data that are not your own, you must provide a letter of permission from the author of that publication. |
| □ 13. | Please provide each figure in high quality (minimum 300 dpi: JPG or TIF). Figure must be on a separate file. |
| □ 14. | If the study received a financial support, the name of the sponsors must be included in the cover letter and in the text, after the author's affiliations. |
| □ 15. | Provide the number of the Ethics Committees (please check the guidelines for authors). |